School of Chemical and Petroleum Engineering

Department of Chemical Engineering

Synthesis of layered carbonaceous materials for degradation of water contaminants

Shizhen Liu

This thesis is presented for Degree of

Doctor of Philosophy

of

Curtin University

June 2016

Declaration

To the best of my knowledge and belief this thesis contains no material previously published by any other person except where due acknowledgment has been made. This thesis contains no material which has been accepted for the award of any other degree or diploma in any university.

Shizhen Liu

Acknowledgement

My enthusiastic gratitude must be presented to my supervisor, Professor Shaobin Wang, who supports me with extremely worthy instruction, patience and rigorous attitudes to complete this research work. His intelligence brings me into an absolutely novel realm with passions and supervision.

My deepest gratitude must also go to my co-supervisor, Associate Professor Hongqi Sun, whose knowledge always gives me inspiration. I really thank him for always paying such attention on my study and life in Australia to support me finishing my Master degree.

I also want to thank Professor Shaomin Liu. I must say, without the help from him, I cannot have this precious opportunity to study as a researcher and such an achievement in my work.

I am also thankful to all laboratory technical staff, Anja Werner, Roshanak Doroushi, Karen Haynes, Jason Wright and Ann Carroll for their technical supports.

Finally, I specially thank my parents for anything they give to me, thank them to give me infinite encouragement and financial support for so many years, and thank them to give me a life to see this beautiful world by my eyes.

Abstract

In the past decades, more and more researchers have paid much interest to the development of environmentally friendly energy, because of the pressure to control and prevent a variety of environmental pollutants which were caused by fossil fuel combustion. Carbon dioxide emission control becomes a hot topic of research. In 2015, Plenary lecture in Paris Climate Change Conference (COP21) indicates, during 1990 to 2012, CO_2 emission was dramatically increased around the world [1] and the total CO_2 in the atmosphere comparing with one century before is 30 times higher[2]. At the same time, some waste organic compounds are considered as serious pollutants in the ecosystem. Organic contamination mainly comes from large number of industrial, agricultural and domestic wastes to be discharged into the water. Organic pollutants play an important role in water pollution; they take up more than 50% of water pollutants. The major paths of this kind of pollutants are involved in the pigment, solvent synthesis, paints, pesticides, food additives, industry of plastics, synthetic fibres, synthetic rubber, detergents, pharmaceuticals and other organic compounds. They are considered as toxics or a contributor to human chronic diseases including the human hepatic dysfunction, carcinogenics, hindering human body development and endangering body endocrine system [3-5].

In the last decades, many studies have been paid attention to solar energy conversion development. Although photochemical methods in water treatment has been found at the end of 20^{th} century, photocatalysis supplies a promising strategy to decompose organic contaminants directly into carbon dioxide and water without any extensive energy consuming and it is totally environmentally friendly. It also provides a new path for novel technology. Numerous studies have been reported to use nano-particles as photocatalysts for water splitting

into hydrogen fuel, degradation of environmental pollutants and wastewater treatment, carbon dioxide remediation, self-cleaning activity and air purification[6-8].

TiO_2 has been studied extensively because it is considered as one of the most effective photocatalysts for the degradation of organic pollutants[9]. This reputation is also by its relative nontoxicity and outstanding thermodynamic stability. Today, many research groups manage to enhance the photocatalytic properties and optimize the process to degrade various organic and inorganic pollutants[10]. The overall efficiency of photon utilization by TiO_2 is limited by electron–hole recombination, which transforms the radiation into thermal energy. Indeed photon scattering and the intrinsic physical properties of TiO_2 limit the absorption of photons with UV-A or greater wavelength energy[11]. Because of the issues, new photosensitive semiconductor development has been considered as the key technology toward future photo-chemistry.

Since the single atomic layer graphene appeared, the graphene-liked single layer lattice compounds stimulated the intensive studying. Graphitic carbon nitride ($g-C_3N_4$, GCN) is a stable, metal-free photocatalyst showing visible light response. The $g-C_3N_4$ possesses dislocation in π states, different from graphene. The band gap is 2.7 eV with the conduction band at -1.4 eV and the valence band at 1.3 eV[16], which supports $g-C_3N_4$ to absorb visible light, and the chemical stability endows the organic $g-C_3N_4$ totally environmentally friendliness.

In this thesis, firstly we report a metal-free heterojunction photocatalyst consisted of melem and $g-C_3N_4$, which was prepared by a hydrothermal method at mild temperatures. The melem/$g-C_3N_4$ heterojunction materials exhibited strong photocatalytic activities and high stability toward decomposition of methylene blue solution under artificial solar radiation. The study suggests melem composites can weaken the electronic pair recombination by dislocating

photo-generated electrons from $g-C_3N_4$. Then oxygen modification was achieved via a hydrothermal treatment of $g-C_3N_4$ with H_2O_2 solutions. Compared to the reported study, the effects of hydrothermal temperature on the characteristics such as crystalline structure, surface area, chemical states, optical property, band structure, recombination rate of carriers and photoelectrochemical properties were comprehensively investigated. The enhanced photocatalysis was confirmed by photodegradation of methylene blue and the related mechanism was studied. Later, oxygen doped GCN (GCNO) catalysts sensitized by several cooperative asymmetric organophotoredox organic dyes, Eosin-Y, Perylene, Nile Red and Coumarin, were then prepared and found to exhibit high activities in methylene blue (MB) and phenol photodegradation under visible light irradiations. Finally, the controlled uniform size carbon sphere (CS) has been successfully synthesised through varying surfactants and impregnated on GCN. The effects of CS on the electronic and optical properties as well as photocatalytic behaviour of the GCN materials were evaluated and discussed.

Current publications

S. Liu, D. Li, H. Sun, H.M. Ang, M.O. Tadé, S. Wang, Oxygen functional groups in graphitic carbon nitride for enhanced photocatalysis, Journal of Colloid and Interface Science, 468 (2016) 176-182

S. Liu, H. Sun, K. O'Donnell, H.M. Ang, M.O. Tade, S. Wang, Metal-free melem/$g-C_3N_4$ hybrid photocatalysts for water treatment, Journal of Colloid and Interface Science, 464 (2016) 10-17.

H. Sun, S. Liu, S. Liu, S. Wang, A comparative study of reduced graphene oxide modified TiO_2, ZnO and Ta_2O_2 in visible light photocatalytic/photochemical oxidation of methylene blue, Applied Catalysis B: Environmental, 146 (2014) 162-168.

S. Liu, H. Sun, H. Ang, M.O. Tade, S. Wang, Integrated oxygen-doping and dye sensitization of graphitic carbon nitride for enhanced visible light photodegradation, Journal of Colloid and Interface Science, 476 (2016) 193-199.

S. Liu, Jun, Ke, H. Sun, Jian, Liu, H. Ang, M.O. Tade, S. Wang, Uniformed carbon spheres for promoting graphitic carbon nitride toward enhanced photocatalysis, Applied Catalysis B: Environmental, in revision.

References

[1] W. Obergassel, C. Arens, L. Hermwille, N. Kreibich, F. Mersmann, H.E. Ott, H. Wang-Helmreich, Phoenix from the Ashes–An Analysis of the Paris Agreement to the United Nations Framework Convention on Climate Change, Wuppertal: Wuppertal Institute. wupperinst., (2016).

[2] R.E. Zeebe, J.C. Zachos, K. Caldeira, T. Tyrrell, Carbon emissions and acidification, SCIENCE-NEW YORK THEN WASHINGTON-, 321 (2008) 51.

[3] I. Arslan, I. Balcioglu, T. Tuhkanen, D. Bahnemann, H_2O_2/UV-C and Fe_2+/H_2O_2/UV-C versus TiO_2/UV-A Treatment for Reactive Dye Wastewater, Journal of Environmental Engineering, 126 (2000) 903-911.

[4] M. Rani, N. Gupta, B. Pal, Superior photodecomposition of pyrene by metal ion-loaded TiO_2 catalyst under UV light irradiation, Environmental Science and Pollution Research, 19 (2012) 2305-2312.

[5] E. Forgacs, T. Cserháti, G. Oros, Removal of synthetic dyes from wastewaters: A review, Environment International, 30 (2004) 953-971.

[6] F.B. Li, The enhancement of photodegradation efficiency using Pt-TiO_2 catalyst, Chemosphere, 48 (2002) 1103.

[7] F. Wang, K. Zhang, Reduced graphene oxide–TiO_2 nanocomposite with high photocatalystic activity for the degradation of rhodamine B, Journal of Molecular Catalysis A: Chemical, 345 (2011) 101-107.

[8] H. Sun, R. Ullah, S. Chong, H.M. Ang, M.O. Tadé, S. Wang, Room-light-induced indoor air purification using an efficient Pt/N-TiO_2 photocatalyst, Applied Catalysis B: Environmental, 108–109 (2011) 127-133.

[9] S. Klosek, D. Raftery, Visible Light Driven V-Doped TiO_2 Photocatalyst and Its Photooxidation of Ethanol, The Journal of Physical Chemistry B, 105 (2001) 2815-2819.

[10] K. Woan, Pyrgiotakis, G. and Sigmund, W., Photocatalytic Carbon-Nanotube–TiO_2 Composites, Advanced Materials, (2009) 2233–2239.

[11] B. Gao, G.Z. Chen, G. Li Puma, Carbon nanotubes/titanium dioxide (CNTs/TiO_2) nanocomposites prepared by conventional and novel surfactant wrapping sol-gel methods exhibiting enhanced photocatalytic activity, Applied Catalysis B: Environmental, 89 (2009) 503-509.

Contents

Figure List

1 Introduction and overview

1.1 Background of environmental issues

Human history is a story of how people understanding to use nature energies and resource. In the world, our development totally relies on abundant natural resources. Today we are living in an age dominated by thermal engine, however most of thermal energy depends on chemical reactions which would create pollutants into the environment. So many researchers strive on developing cheap, high efficient, environmentally friendly energies. On the other hand, the environment pollution problems today attract more and more attention. In 2015, Paris Climate Change Conference (COP21) disclosed an environment statistic report. Between 1990 to 2012, carbon dioxide emission was dramatically increased in a global sight, and the increasing tendency in developing countries, China, India, and Brazil, is incredibly high as four times as before [1]. The total CO_2 in the atmosphere compared with the past one century is 30 times higher[2]. A consequent has been presented in front of us, that excessive CO_2 emission will lead to global warming and environment pollution. The fuel combustion will literally influence people life, civilization development and biological ecosystem safety.

At the same time carbon based pollutants in water system are a serious threat to people. Organic water contamination mainly comes from various chemical industries, agricultural leaching and domestic wastes discharged into the water. At present, more than 4200 billion cubic meters of sewage water were discharged into rivers of the world annually, and about 5.5 trillion cubic meters of sewage leached into lakes, polluting fresh water, which is equivalent to more than 14% of the total global fresh water storage. Organic pollutants play an important role in water pollution; they take up more than 50% of water pollutants. The major paths of this kind of pollutants are involved in the pigment, solvents synthesis, paints, pesticides, food additives, industry of plastics, synthetic fibres, synthetic rubber, detergents, pharmaceuticals and other

organic compounds. Those industries on the one hand are improving the quality of human life and on the other hand they endanger human health. They are considered as toxics or a contributor to human chronic diseases including the human hepatic dysfunction, carcinogenics, hindering human body development and endangering body endocrine system [3, 4].

As new type energy, solar energy has been considered as the feasible candidate to substitute fossil fuels, which is in a widely global distribution and low-cost. To extract solar energy it is depended on photovoltaic derives, many photo-sensitive semiconductors have been found to be the key, to convert the light radiation into electrical energy. Meanwhile the other application of photocatalytic technology is used for hydrogen generation by water splitting, this photocatalytic mechanism also supplies a strategy to decompose organic contaminants directly into carbon dioxide and water without any extensive energy supply. Photocatalytic technology is totally environmentally friendly, which can be used for environmental pollutants degradation, wastewater purification, carbon dioxide remediation, self-cleaning activity and air purification [5-7].

1.2 Photocatalysts

In 1970, a photocatalytic reaction was firstly reported by Professors Fujishima and Honda at the University of Tokyo in Japan [8]. TiO_2 has been discovered the photocatalytic water decomposition (water photolysis) when he exposed a titanium dioxide electrode to strong light, this phenomenon revealed the possibility to produce hydrogen gas from solar radiation energy, and it was widely acknowledged as the Honda-Fujishima Effect [8]. When the surface of a rutile TiO_2 electrode was irradiated by light constantly at wavelengths shorter than 415 nm (3.1 eV), a photocurrent from the platinum electrode to the TiO_2 electrode through an external redox circuit occurred. Water can be decomposed by UV radiation without the additional voltage according to the following scheme.

$$TiO_2 + hv \rightarrow e^- + h^+$$

$$2H_2O + 4h^+ \rightarrow O_2 + 4H^+$$

$$2H^+ + e^- \rightarrow H_2$$

The overall reaction is:

$$2H_2O + hv \rightarrow O_2 + 2H_2$$

Today, it is well known that TiO_2 semiconductors and their modified particles can be adopted in photovoltaic devices because they are considered as the most effective photocatalysts for the degradation of organic pollutants[9]. Kim et al. employed TiO_2 with anatase crystal for sterilization of food-borne pathogenic bacteria[10]. TiO_2 nanoparticles with near ultraviolet radiation (UV-A) can produce electronic holes (h^+) in its valence band, it reinforced production of hydroxyl radicals (OH^-) which can decompose the bio-cell efficiently and eliminate bacteria.. However, this photocatalytic function limited by electron–hole recombination of semiconductor itself, and TiO_2 has wide band gap energy which limited the absorption of photons within UV-A wavelength[11]. Until now, there is no photo-sensitive material that can balance the economic cost, high radiation harvest, high efficiency, chemical/physical stability and environmental friendliness[12]. There is an eager desire for new type of photosensitive semiconductors.

With the knowledge of semiconductors, more and more semiconductor materials have been adopted in photocatalyst family. ZnO occurs as white hexagonal crystal or white powder known as zinc white. ZnO has a direct and wide band gap in the near-UV spectral region, strong oxidation ability, good photocatalytic property, and a large free-exciton binding energy[13, 14]. Tin dioxide is another popular photocatalyst. It has unique optical and electrical properties.

SnO_2 is a n-type transparent semiconductor with a rutile structure. It has found many practical applications, mainly as gas sensor material, electrode in dye-sensitized solar cells, catalysts, and electrodes for lithium batteries[15]. Zirconium dioxide (ZrO_2 , zirconia), a widely used heterogeneous catalyst, is a n-type semiconductor with bandgap energy of 5.0 eV, conductance and valence band potentials of −1.0 and + 4.0 V versus NHE, respectively, allowing its use as a photocatalyst in the production of hydrogen through water decomposition[16]. CdS also has been extensively studied because of its excellent properties with the band gap (2.3 eV) corresponding well with the spectrum of sunlight and the conduction band edge is more negative than the H_2O/H_2 redox potential[17]. Recent studies inventively report a new organic photosensitive semiconductor, graphitic carbon nitride, which has been considered as a rising star in photocatalyst studying.

1.3 Graphitic carbon nitride photocatalyst.

Melem was constructed by carbon and nitrogen element, which was referred as linear polymers of connected tri-s-triazines via secondary nitrogen. The first record of synthesizing a polymeric nanostructured carbon nitrides (CN, melon) was reported by Berzelius and Liebig in 1834, which is one of the oldest synthetic polymers[18, 19]. Owing by Melem backbones, these potential CNx precursors certainly implicate for the structure and formation of graphitic carbon nitride ($g - C_3N_4$). Stacked two dimensional structure, polymeric compounds are known to be consisted of carbon and nitrogen[20] and other nearby elements were in the periodic lotic film, which was composed of aromatic triazine rings connected to each other by secondary amine[19, 21].

Unsaturated structural variants may suggest CNs with different structures possess intriguing properties including high hardness [20, 22, 23]. The calculation indicated that the Mohs scale

of the Melem is therefore between 7 and 9 which is superior to diamond[24]. The hardness of the particle could be explained by the existence of the C–N single bond (287.9 eV in ESCA C1s spectrum) in the material[21] and the graphitic structure is indeed more stable than the isolated melem chains by 63 kJ mol^{-1} [25]. The distribution of electronic rich and π-π* CN possesses low friction coefficient, and reliable chemical inertness, but also a great potential for energy conversion and storage, and environmental applications including direct methanol fuel cells, catalysis, photocatalysis and CO_2 capture.

$g - C_3N_4$ is delineated as a photo sensitive semiconductor, also a slight yellow colour conferred this semiconductor to have activity under visible radiation[26]. $g - C_3N_4$ possesses an experimental band gap of 2.7 eV. The 2p state of N mainly supports a valence band for +1.4 eV and C element contributes the conductive band for -1.3eV[27], which is suitable for serving as a highly efficient, low-cost photocatalyst for water splitting[28]. In a research of Ram[29], Nitrogen atoms in the Melem matrix would be the preferable oxidation sites for H_2O to O_2, whereas the carbon atoms provide the reduction sites for H^+ converting into H_2[29]. However, it is as the same as other catalysts, introduction of porosity and high surface area can enhance the catalytic performance of $g - C_3N_4$ to a large extension [18, 30, 31] which enhance the light quantum harvesting and multiple scattering effects[32]. The ratio of N & C will obviously affect the band gap and properties of $g - C_3N_4$ bulk[33]. However graphitic carbon nitride has limited light absorption in the visible region, which imposes a fundamental limitation on overall photocatalytic efficiency.

1.4 Scope and objectives of this thesis

The main goals of this study are to investigate and engineering graphitic carbon nitride based photocatalysts. Some photocatalyst modification methods were adopted to enhance the photocatalytic performance, such as surface dedication, surface extension, heterogeneous atomic doping, polarity functional group grafting, organic dye photosensitising, high capacitance carbonaceous materials coating, and so on. Multiple modification methods are helpful to further understand the optical and photovoltaic properties of graphitic carbon nitride.

In this thesis, photocatalysis evaluation was preceded in water treatment. Organic pollutants such as Methylene Blue, Phenol, and SCP were decomposed by $g-C_3N_4$ based photocatalysts.

1.5 Structure of the thesis

In this thesis, metal-free photosensitive semiconductor, graphitic carbon nitride, has been synthesised, and a series of modification methods have been adopted to enhance photocatalysis activity on degradation of organic pollutants in aqueous systems under visible radiation or artificial solar radiation. There are seven chapters in this thesis. In the introduction section, the background of photocatalysis technologies and photovoltaic adoption devices will be narrated. In chapter two, the physical principles of photosensitive semiconductors is presented, and the basic knowledge of band gap, semiconductor energy levels, the photoelectron drifting and how electronic pair splitting and reaction with radicals in solution are explained. In chapter three, melem/$g-C_3N_4$heterojunction photocatalysts (MGCN) had been generated by hydrothermal treatment of $g-C_3N_4$ in DI water between 130-200 ℃. Photocatalytic methylene blue degradation on the samples indicated MGCN-180 presented much better photocatalytic

performance comparing with other $g-C_3N_4$ catalysts under artificial solar radiation. Melem fibre was identified by XRD and SEM. Optical properties of Melem/ $g-C_3N_4$ hybrid show a synergistic effect of heterojunction. Melem in $g-C_3N_4$catalyst support provides a new energy level to $g-C_3N_4$ for effectively weaken recombination by electron dislocation from $g-C_3N_4$ into melem cocatalyst therefore increasing photo generated electron to reaction. In chapter four, oxygen modified graphitic carbon nitride photocatalysts were prepared by hydrothermal treatment of $g-C_3N_4$ and hydrogen peroxide at controlled temperatures. The oxygen functional groups incorporated into $g-C_3N_4$ structure have induced a positive photoelectronic effect in dye degradation procedure. UV-vis DRS and Mott–Schottky plots suggested the band gap energies and band gap positions were manipulated by the oxygen functional groups. All modified $g-C_3N_4$ performed better degradation of methylene blue under visible light (wavelength more than 420 nm) and sunlight irradiations than pristine $g-C_3N_4$. The electrochemical study reveals the multiple roles of oxygen functional groups on $g-C_3N_4$ in electrocatalysis for increased electron and hole activities. In chapter five, four cooperative asymmetric organophotoredox organic dyes, Eosin-Y, Perylene, Nile Red and Coumarin, were adopted to sensitize the oxygen-doped $g-C_3N_4$. O-doping can promote dye sensitization on $g-C_3N_4$ and the dyes presented different effects on photocatalytic activity. Eosin-Y and Nile Red produced a better synergistic effect on photocatalysis. Nile-red effectively extends the light absorption and hence giving a good activity in methylene blue degradation. Eosin-Y could balance the absorption and the electron/hole pair recombination, leading to the best activity in phenol decomposition. In chapter six, uniformed carbon sphere with varying particle sizes as an electron tunnel were prepared and used for tailoring graphitic carbon nitride to be a new metal-free photocatalyst. Different size carbon spheres possess ability of electron capture, which could contribute to the separation of electron-hole pairs on the surface of $g-C_3N_4$. The $g-C_3N_4$ with 200 nm carbon sphere sample exhibits enhanced

photocatalytic activity two times higher than that of the pristine $g-C_3N_4$ over MB. In final section, this thesis concludes all research achievements on graphitic carbon nitride, which systemically reveal the engineering method toward $g-C_3N_4$ in future.

1.6 References

[1] W. Obergassel, C. Arens, L. Hermwille, N. Kreibich, F. Mersmann, H.E. Ott, H. Wang-Helmreich, Phoenix from the Ashes–An Analysis of the Paris Agreement to the United Nations Framework Convention on Climate Change, Wuppertal: Wuppertal Institute. wupperinst. org/uploads/tx_wupperinst/Paris_Results. pdf (accessed February 18, 2016), (2016).

[2] R.E. Zeebe, J.C. Zachos, K. Caldeira, T. Tyrrell, Carbon emissions and acidification, SCIENCE-NEW YORK THEN WASHINGTON-, 321 (2008) 51.

[3] M. Rani, N. Gupta, B. Pal, Superior photodecomposition of pyrene by metal ion-loaded TiO_2 catalyst under UV light irradiation, Environmental Science and Pollution Research, 19 (2012) 2305-2312.

[4] E. Forgacs, T. Cserháti, G. Oros, Removal of synthetic dyes from wastewaters: A review, Environment International, 30 (2004) 953-971.

[5] F.B. Li, The enhancement of photodegradation efficiency using Pt-TiO_2 catalyst, Chemosphere, 48 (2002) 1103.

[6] F. Wang, K. Zhang, Reduced graphene oxide–TiO_2 nanocomposite with high photocatalystic activity for the degradation of rhodamine B, Journal of Molecular Catalysis A: Chemical, 345 (2011) 101-107.

[7] H. Sun, R. Ullah, S. Chong, H.M. Ang, M.O. Tadé, S. Wang, Room-light-induced indoor air purification using an efficient Pt/N-TiO_2 photocatalyst, Applied Catalysis B: Environmental, 108–109 (2011) 127-133.

[8] A. Fujishima, K. Honda, Electrochemical Photolysis of Water at a Semiconductor Electrode, Nature, 238 (1972) 37-38.

[9] S. Klosek, D. Raftery, Visible Light Driven V-Doped TiO_2 Photocatalyst and Its Photooxidation of Ethanol, The Journal of Physical Chemistry B, 105 (2001) 2815-2819.

[10] B. Kim, D. Kim, D. Cho, S. Cho, Bactericidal effect of TiO_2 photocatalyst on selected food-borne pathogenic bacteria, Chemosphere, 52 (2003) 277-281.

[11] B. Gao, G.Z. Chen, G. Li Puma, Carbon nanotubes/titanium dioxide ($CNTs/TiO_2$) nanocomposites prepared by conventional and novel surfactant wrapping sol-gel methods exhibiting enhanced photocatalytic activity, Applied Catalysis B: Environmental, 89 (2009) 503-509.

[12] A.R. Bhatti, Z. Salam, M.J.B.A. Aziz, K.P. Yee, R.H. Ashique, Electric vehicles charging using photovoltaic: Status and technological review, Renewable and Sustainable Energy Reviews, 54 (2016) 34-47.

[13] Ü. Özgür, Y.I. Alivov, C. Liu, A. Teke, M. Reshchikov, S. Doğan, V. Avrutin, S.-J. Cho, H. Morkoc, A comprehensive review of ZnO materials and devices, Journal of applied physics, 98 (2005) 041301.

[14] K.M. Lee, C.W. Lai, K.S. Ngai, J.C. Juan, Recent developments of zinc oxide based photocatalyst in water treatment technology: A review, Water Research, 88 (2016) 428-448.

[15] D. Solís-Casados, E. Vigueras-Santiago, S. Hernández-López, M.A. Camacho-López, Characterization and Photocatalytic Performance of Tin Oxide, Industrial & Engineering Chemistry Research, 48 (2009) 1249-1252.

[16] C. Karunakaran, S. Senthilvelan, Photocatalysis with ZrO_2: oxidation of aniline, Journal of Molecular Catalysis A: Chemical, 233 (2005) 1-8.

[17] M. Matsumura, Y. Saho, H. Tsubomura, Photocatalytic hydrogen production from solutions of sulfite using platinized cadmium sulfide powder, The Journal of Physical Chemistry, 87 (1983) 3807-3808.

[18] Y. Zheng, J. Liu, J. Liang, M. Jaroniec, S.Z. Qiao, Graphitic carbon nitride materials: controllable synthesis and applications in fuel cells and photocatalysis, Energy & Environmental Science, 5 (2012) 6717-6731.

[19] B.V. Lotsch, W. Schnick, New light on an old story: Formation of melam during thermal condensation of melamine, Chemistry-a European Journal, 13 (2007) 4956-4968.

[20] E. Kroke, M. Schwarz, Novel group 14 nitrides, Coordination Chemistry Reviews, 248 (2004) 493-532.

[21] M. Kawaguchi, S. Yagi, H. Enomoto, Chemical preparation and characterization of nitrogen-rich carbon nitride powders, Carbon, 42 (2004) 345-350.

[22] A.Y. Liu, M.L. Cohen, Prediction of new low compressibility solids, Science, 245 (1989) 841-842.

[23] J. Wang, J. Lei, R. Wang, Diffraction-pattern calculation and phase identification of hypothetical crystalline C_3N_4, Physical Review B, 58 (1998) 11890-11895.

[24] A.Y. Liu, M.L. Cohen, Structural properties and electronic structure of low-compressibility materials: β-Si_3N_4 and hypothetical β-C_3N_4, Physical Review B, 41 (1990) 10727.

[25] A. Thomas, A. Fischer, F. Goettmann, M. Antonietti, J.-O. Müller, R. Schlögl, J.M. Carlsson, Graphitic carbon nitride materials: variation of structure and morphology and their use as metal-free catalysts, Journal of Materials Chemistry, 18 (2008) 4893-4908.

[26] K. Hashimoto, H. Irie, A. Fujishima, TiO_2 Photocatalysis: A Historical Overview and Future Prospects, Japenese Journal Of Applied Physics Part 1 Regular Papers Short Notes And Review Papers, 44 (2005) 8269.

[27] X. Ma, Y. Lv, J. Xu, Y. Liu, R. Zhang, Y. Zhu, A Strategy of Enhancing the Photoactivity of g-C_3N_4 via Doping of Nonmetal Elements: A First-Principles Study, The Journal of Physical Chemistry C, 116 (2012) 23485-23493.

[28] X. Wang, K. Maeda, A. Thomas, K. Takanabe, G. Xin, J.M. Carlsson, K. Domen, M. Antonietti, A metal-free polymeric photocatalyst for hydrogen production from water under visible light, Nature materials, 8 (2009) 76-80.

[29] S.R.G. Naraharisetty, V.M. Kasyanenko, J. Zimmermann, M.C. Thielges, F.E. Romesberg, I.V. Rubtsov, C−D Modes of Deuterated Side Chain of Leucine as Structural Reporters via Dual-frequency Two-dimensional Infrared Spectroscopy, The Journal of Physical Chemistry B, 113 (2009) 4940-4946.

[30] A. Thomas, A. Fischer, F. Goettmann, M. Antonietti, J.-O. Muller, R. Schlogl, J.M. Carlsson, Graphitic carbon nitride materials: variation of structure and morphology and their use as metal-free catalysts, Journal of Materials Chemistry, 18 (2008) 4893-4908.

[31] Q. Yu, S. Guo, X. Li, M. Zhang, Template free fabrication of porous g-C_3N_4/graphene hybrid with enhanced photocatalytic capability under visible light, Materials Technology: Advanced Performance Materials, (2014).

[32] X. Wang, K. Maeda, X. Chen, K. Takanabe, K. Domen, Y. Hou, X. Fu, M. Antonietti, Polymer semiconductors for artificial photosynthesis: hydrogen evolution by mesoporous graphitic carbon nitride with visible light, Journal of the American Chemical Society, 131 (2009) 1680-1681.

[33] X. Li, J. Zhang, L. Shen, Y. Ma, W. Lei, Q. Cui, G. Zou, Preparation and characterization of graphitic carbon nitride through pyrolysis of melamine, Applied Physics A, 94 (2009) 387-392.

Ever reasonable effort has been made to acknowledge the owner of copyright material. I would be pleased to hear from any copyright owner who has been omitted or incorrectly acknowledged.

2

2 Literature review of $g - C_3N_4$ based photocatalysts

2.1 Introduction

Civilization developments rely on natural energies. We are living in a thermal engine age however, the fossil energy is limited and the energy crisis is gradually upon to our life. To develop cheap, high efficient, environmentally friendly energies interests many researchers in all walks of life. Hydrogen fuel is considered as one of ideal candidate because hydrogen fuel can be produced from clean and renewable energy sources and its life cycle is clean and recyclable. Solar energy as well is one major source of renewable energy resources; at the same time it is the promising source for hydrogen production. But today renewable energy contributes only about 5% of the commercial hydrogen production primarily through water electrolysis, while other 95% hydrogen is mainly derived from by production in refining fossil fuels. Current hydrogen fuel production is cost-intensive and is infeasible to many developing countries. Photovoltaic water electrolysis may become a more competitive selection toward most sections on the earth, with the new technology development. However, the considerable small band gap semiconducting materials may cause serious environmental problems, and many of them are expensive. Alternatively, photocatalytic water-splitting using graphitic carbon nitride for hydrogen production offers a bright view for clean, low-cost and environmentally friendly procedure of hydrogen generation by solar energy.

On the other hand, during the long-time irreversible consuming development, today the environment is threaten by civilization developing, pollutions coming from human activities are now conversely restricted a country development. For example, different industries such as textile, paper, cosmetic, hair colour, leather good, food and consumer electronic manufacturing [1] are easily releasing the toxic pollutants into fresh water system, which dramatically decreases water resource. Today, water pollution is a major environmental problem affecting many countries. In developing countries, 70 percent of industrial wastes are dumped untreated

into waters, polluting the usable water supply. On average, 99 million pounds (45 million kilograms) of fertilizers and chemicals are used each year[2]. Every day, 2 million tons of sewage and industrial and agricultural waste are discharged into the world’s water, the equivalent of the weight of the entire human population of 6.8 billion people. The UN estimates that the amount of wastewater produced annually is about 1,500 km^3 , six times more than the water exists in all the rivers of the world. Lacking of adequate sanitation, contaminated water is one of the most significant forms of water pollution. Worldwide, 2.5 billion people live without improved sanitation. Over 70% of these people who lack sanitation, or 1.8 billion people, live in Asia[3]. As the terminal of food chain pyramid on earth, our planet's lakes, rivers, streams, and groundwater are often a chemical cocktail to us.

Recently, photocatalysis technology has been found not only potential in water splitting but also utilization in water pollutant treatment, the active radicals generated by photosensitive semiconductor possess strong redox potential toward pollutant degradation into nontoxic compounds, which supports a feasible way for economic water treatment. Metal free graphitic carbon nitride ($g - C_3N_4$) with a band gap of 2.7 eV is studied as a nonmetallic photocatalyst for H_2 or O_2 evolution from water under ultraviolet (UV) and visible light. The $g - C_3N_4$ catalyst exhibits activities in pollutant degradation in both air and water.

2.2 Basic knowledge of photocatalyst

Radiation is the most common energy resource on the earth. Electromagnetic radiation (EM radiation, EMR, or light) is a form of energy released by solar nuclear fusion process. On the earth surface, solar radiation spectrum, visible light, ultraviolet, and infrared take about 42.5%, 13.8% and 3.1%, respectively[15]; only minority part radiation has high energy.

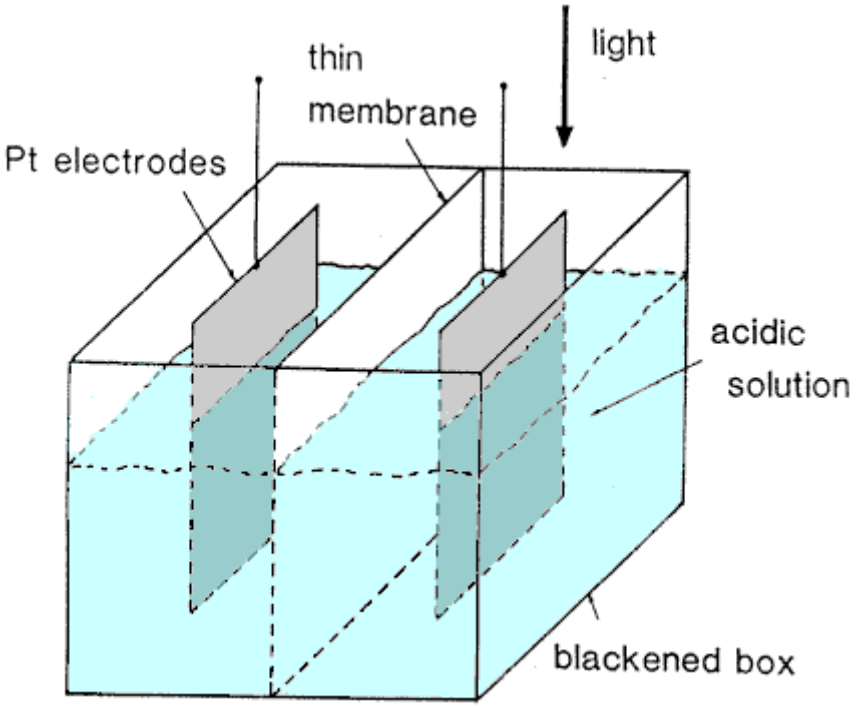

Fig. 1 Diagram of apparatus described by Becquerel (1839) [4]

The history of development of radiation energy into electronic energy began in 1839 by a French physicist, Alexandre-Edmond Becquerel[4], who first discovered the photovoltaic phenomenon. An electric current could be detected when two plates of platinum (or gold) are diving in an acid (neutral or alkaline) solution and exposed in an uneven way to solar radiation. This is the first time that photoelectric conversion was exhibited in front of scientists. In the following years, Photoelectric Effect was found by a German physicist, Heinrich Hertz in 1887 [5]. It has been proved that electron could escape from metal surface under ultraviolet illumination[6]. In a photovoltaic device, a photosensitive semiconductor usually plays the key role in conversion of the radiation into electronic energy.

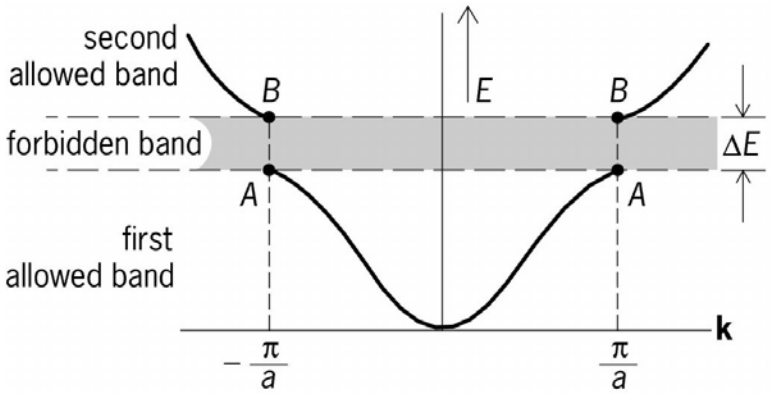

Fig. 2. Brillouin zone for electron in a lattice system[7].

Semiconductors are crystalline or amorphous solids with distinct electrical characteristics. They are high current resistance, but much lower resistance than insulators[8]. Brillouin zone for electron in a lattice system (Fig.2) can be used to explain semiconductor phenomenon. When two atom orbits with the same energy level are approaching to each other, the internal effects between them will separate one energy orbit to two energy states based on Pauli exclusion principle[9]. However, when many atoms with the same electron orbits have closely direct in a special arrangement (for example crystal skeleton), the same energy level is well separated as sub- continuous energy band, which has an ability to accommodate electrons, those bands in a semiconductor have been referred as Energy band. This identification of energy band is the fundamental knowledge of semiconductor materials, at the same time it supports a good explanation to electronic resistance, crystal conductor and electrical/ thermal properties, which also constructs modern technology of solar energy application.

A photocatalyst is a branch of photovoltaic semiconductor. The history of photocatalyst started since 1967, titanium oxide was found to be able to split water into oxygen and hydrogen gases when it was exposed under ultraviolet radiation, this phenome is named as "The multi-Fujishima effect"[10]. Titanium oxide is a semiconductor; band gap energy is about 3.7 eV,

which has a flexible function in a variety of applications. For example, it can be employed in paint, sunscreen or food colouring, because it is significantly compatible and non-toxic. For TiO_2 as a semiconductor, two energy bands have been confirmed: valence band (VB) and conductive band (CB). When photo-generated electron transits between VB and CB, the electron and residue electronic hole possess potential to split H_2O into H_2 and O_2. In this process, TiO_2 semiconductor plays a role as electron pump or converter between radiation energy to electronic energy. The "multi-Fujishima effect" presents a bright future of solar energy applications; unfortunately this application has bottlenecks because it only works under ultraviolet light with limited efficiency. Totally speaking, ionic crystal compounds usually possess wide band gap energy which is equal to certain electronic voltage. An ideal monocrystalline material with a high band gap could not absorb the radiation energy from visible light and infrared light range, in other words, these particles are transparent.

2.3 Photocatalytic reaction mechanism

More and more semiconductor materials have been tested in photocatalytic reactions. At the same time the classical transition metal oxide materials (like titanium dioxide[11], zinc oxide[12], cadmium sulphide[13] and so on) have been widely studied and adopted in many applications.

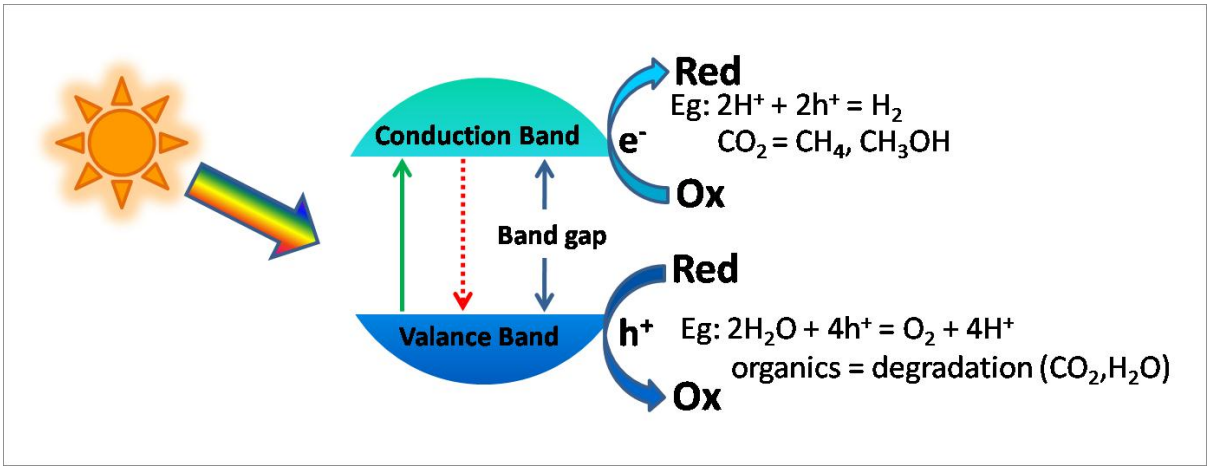

Fig. 3. Photocatalytic process on $\boldsymbol{TiO_2}$ [14]

The electronic properties of an organic polymeric substance are different from classical semiconductors because the energy levels of an organic semiconductor are usually composed of large delocalized π orbits or anti- π orbits. However the major initial steps of photocatalytic mechanism under irradiation[15] for both photocatalysts are similar. For example, for photocatalytic steps occur on TiO_2 are summarized in following (Fig. 3):

$$T_iO_2 + hv \rightarrow h^+_{vb} + e^-_{cb}$$

$$h^+_{vb} + OH^- \rightarrow {}^{\cdot}OH$$

$$e^-_{cb} + Ti^{+4}OH \leftrightarrow Ti^{+3}OH$$

$$Ti^{+3} + O_{2\,ads} \rightarrow Ti^{+4} + O_2^-$$

$${}^{\cdot}OH + R_{pollutant} \rightarrow CO_2 + H_2O \text{ or Actived Radical}$$

$$h^+_{vb} + e^-_{cb} \rightarrow \text{Thermal energy or Luminescence}$$

In above reaction steps, three chemical reaction rates dominate the whole progress: excess carrier generation; photo generated electron/hole reaction with catalyst substrate and excess carrier Devoid (recombination). Those three reaction steps collaborate and compete with each other. But obviously if in order to elevate the photocatalytic efficiency, the excess carrier generation and catalyst reacting with the subject are benefits.

When environment temperature is higher than absolute zero, the conductive band and valance band are filled by electron or hole which could be ascribed by thermal reasons. Although electronic carrier is not fixed in energy band, but those carrier hardly react with subject because it should be balanced for positive and negative charge in a particle. The really electronic charges for photoreaction or light-emitting diodes are excess carrier (non-equilibrium carrier), which are injected in photo sensitive device by external action such that a particle is exposed under feasible radiation or particle is placed in a closed electronic circuit with feasible voltage. Their energy levels are the highest occupied molecular orbital (HOMO) and lowest unoccupied molecular orbital (LUMO) in valence band and conductive band, respectively.

When photo generated electron/hole recombines, there is an energy transfer procedure. The potential energy of electron in high energy level will convert into thermal energy as Lattice vibrations (phonon) or emit a photon. The energy transfer depends on catalyst crystal. Most of crystals contain many crystal facets, and the characteristics in different crystal facets are different [16, 17]. The recombination process occurs between electron/hole in the lowest point of LUMO and the highest point of HOMO. When excess electron recombines with hole, the lowest energy will directly be accepted by electronic hole and emitting a photon, at the same time the extra potential will become phonon and accept by lattice as thermal energy[18]. This semiconductor is referred as indirect semiconductor. For a photovoltaic device, indirect semiconductors are good candidates as a photocatalyst because the recombination process does not undergo directly and this will decrease the chance of electron/hole devoid but increase the chance to contact with subjects. In contrast, direct semiconductor has the same or similar energy level in different crystal facets, this structure endows electron ability to recombine electronic hole directly. So direct semiconductor has be widely applied in light emitting material, because it can transfer electronic energy into light efficiently without thermal wasting and mitigate device heating. But direct semiconductors are not to be photocatalysts because of

very high recombination rate [19-21]. Graphitic carbon nitride is a direct semiconductor, and only has one face in its graphene like structure[22]. Now many researches are focusing on how to modify its recombination rate.

2.4 Optical properties of photocatalysts

Totally speaking, improving the photocatalytic reaction efficiency in the kinetic view could be generally in two ways: firstly increasing photo generated carrier creation, secondly increasing the rate of contact chance between pollutants and carrier and weak recombination.

If a photocatalyst is used in an aqueous media, the light absorbance could be explained by the Beer–Lambert law[23]:

$$\mathrm{A} = -log_{10}\left(\frac{I_t}{I_0}\right) = K \cdot l \cdot c$$

In above equation "A" represents light absorbance, "*K*" is molar extinction coefficient which depends on the system and environmental conditions, "*l*" represents thickness of light penetration, and "c" is the concentration of the system. When a photocatalyst is in a solution, the high concentration could help the catalyst absorb more radiation but if the subjects for degradation also possess high light absorption, it will affect the behavior [24-27].

When electromagnetic wave is absorbed by semiconductor bandgap structure and photo generated electron/electronic hole existed in a particle, the transport of those charge carrier toward the surface of particles become a question. There are two kinds of mobility function for carrier in a photocatalyst (semiconductor), carrier drift and carrier diffusion. When a semiconductor (photocatalyst) is located in an electronic field, the electron in conductive band will move to the opposite electric field direction and electronic hole will move to electric field direction with a limited velocity:

$$v_d = \mu \cdot E$$

Here, "v_d "represents carrier (electron or electronic hole) migration velocity, "E " represents electric field strength and "μ" is electron/hole mobility which is character of carrier mobility in a material in ($\frac{cm^2}{V \cdot s}$). Single layer graphite (graphene) has been studied since 2008[28]. Graphene has a theoretical electron mobility of 15.000 ($\frac{cm^2}{V \cdot s}$) [29], very close to superconductor and its resistivity is 1×10^{-6} similar to silver 1.59×10^{-6} . The electron and electronic hole dedicate to electron drift in the material, but the electron mobility of electron is usually bigger than hole. When a carrier moves in crystal lattice, its mobilization will be affected by phonon and impurity atom in crystal skeleton, and finally the carrier will be devoid by combination. It should be mentioned that "μ" value is not only dependent on crystal lattice but also it has an inverse relationship with temperature. When temperature is arising, the electron mobility will be going down[30].

2.5 Photoelectron drifting in photocatalysts

In a crystal, the drift current density could be presented in the following equation:

$$J_{drf} = (e \cdot \rho) \cdot \mu \cdot \mathrm{E}$$

Here "e" is single electric charge $(1.602 \times 10^{-19}, Coulomb)$, "$\rho$" is concentration in unit volume. So the total drift current density (electron drift and electronic hole drift) could be revealed as:

$$J_{drf_a} = e \cdot (\rho_e \cdot \mu_e + \rho_h \cdot \mu_h) \cdot E = \delta \cdot E = \frac{1}{p} \cdot E$$

Here, "δ" represents the resistivity and "p" represents conductivity. This equation also demonstrated the relationship between carrier mobility and resistivity. Usually a material has

lower resistivity when it is placed in higher temperature. Papageorgiou and his co-workers[31] found the open-circuit voltage of solar cells decreased linearly with increasing temperature. High working temperature will negatively affect the solar cell peaking power[32].

Although drifting plays a significant role of carrier mobility, most of photocatalysts (photo sensitive semiconductor) are operated in a non-electronic field, at this time carrier diffusion is more important:

$$J_d = e \cdot v_{th} \cdot l \cdot \frac{dn}{dx} = e \cdot D_n \cdot \frac{dn}{dx}$$

The above equation is carrier diffusion current density. In it, "e" is single electric charge, "v_{th}" is thermal motion speed, "l" is carrier mean free path, "D_n" is referred as carrier diffusion coefficient and "$\frac{dn}{dx}$" is carrier concentration gradient. So it could be indicated that the diffusion distance is a key factor for carrier exposing to material surface. High temperature is beneficial for carrier diffusion, and it is widely accepted that photocatalytic reaction has higher efficiency at higher temperature, which could be contributed by lower binding energy between subject and photo generated electron/hole[33-35]. The "μ" is electron/hole mobility and "D_n" carrier diffusion coefficient is not depended, the relationship could be referred as Einstein relation (also known as Einstein–Smoluchowski relation)[36, 37]:

$$\frac{D_n}{\mu} = k_B \cdot T$$

Here, "k_B" is Boltzmann's constant and "T" is absolute temperature.

2.6 Electronic pair recombination in photocatalysts

The principle of recombination could be simply understood as follows: when carriers are drifting or diffusing in crystal lattice, they will collide and reflect with atom in lattice or impurity. When two contrary charges move into a certain distance, those two particles will recombine and release energy. The understanding of recombination is coming from Shockley-read-hall (SRH) conception. The hypothesis assumed there is an energy level between LUMO and HOMO, the photo generated electron and electric hole could jump or rebound in to this energy level with the same probability, which means this energy is properly located at Fermi level ($1/2$ probability of occurrence). At this time this energy level plays a role as a trap. When electron/hole is trapped in this energy level, recombination will happen. When semiconductor composition is closer to instinct semiconductor, the lifespan of excess carrier is longer. It is mentioned above, defects and impurities could build up a new energy level in band gap and on the surface of particles, so recombination process could be classified in three types: (1) direct recombination which depends on direct semiconductor with high recombination rate; (2) indirect recombination where electron and hole could direct contact with each other unless there is a process of energy transfer with phonon or lattice atom, this kind of recombination is harder than direct recombination and it is not favourite material for LED device; and (3) surface recombination, electric properties of photocatalysts (semiconductor) are complicated. The excess carrier concentration on surface is smaller than that in inner section of semiconductors. The carrier could diffuse to the surface but the recombination rate on surface could be big, and seriously impact the photovoltaic device efficiency. This is why in solar cell production procedure the surface cleaning progress is the key for successful production of solar cell[38]. Ohno has a statement about carrier transport between different subjects[39]. Oxygen gas is easy to receive electron from Anatase TiO_2 but Fe^{+3} is easy to receive electron from rutile TiO_2.

Lachheb et al. [40] tested dyes: Alizarin S, Crocein Orange G, Methyl Red, Congo Red and Methylene Blue to be degraded by a titania photocatalyst under ultraviolet radiation. The photocatalytic reactor was preceded at 293 K by a water cycling system, under the same radiation source in the same reactor. Finally the initial rates of disappearance in $mol/l\ min^{-1}$ are in the order: MR > MB > OG > AS > CR. This result not only counts on the absorption function between dye and particle but also resulted by carrier exposing from TiO_2. Similarly, there are also some researches of a graphitic carbon nitride for different organic decomposition. Yan and his co-workers[41] fabricated boron doped graphitic carbon nitride for two different dye degradation, Rhodamine B and Methyl Orange. As he stated that photo generated electronic hole dominated all reactions so it is a reduction reaction. The photo reaction rate constant in methyl orange is higher than Rhodamine B and boron oxide doped graphitic carbon nitride could increase the reaction rate constant in 1.5 times in all reaction.

In a solution, photocatalytic process of a subject could be attributed into a cycle: the subject molecules contact the surface of particles, accept the positive/negative charge and have a reaction, the products detach from the particle surface [42, 43]. Increasing the surface area of photocatalysts or the activated centre on particle surface is critically helpful to photo reaction. Currently, there are two methodologies toward increasing the surface of particles: reducing the volume of particle and increasing the porous structure. When the pore size is smaller than some or too much porosity of particle surface is, the porous structure will become defects and this kind of defects could accelerate surface recombination and negatively affect the carrier exposing.

2.7 Surface properties of photocatalysts

The surface of a semiconductor is a kind of defects, because the periodic arrangement of atoms on the particle surface has been broken by particle edge, which will cause recombination. The

surface of particles has a main function to contact with external environment which will affect electronic cloud distribution of a particle or catalyst. The Shockley-read-hall (SRH) generation-recombination process[44] indicates that the existence of defects in a photovoltaic device will accelerate excess carrier (non-equilibrium carrier, Exciton) devoid, the recombination progress between photo generated electron and hole. Particularly recombination progress has an impact on photocatalytic reaction[45] [46, 47].

Adsorption over particle surface can be classified as physical adsorption and chemisorption; both are beneficial for catalytic reaction. Physical adsorption usually presents as multilayer absorption. But chemisorption is involved in new bonding, as covalent, coordinative and ionic bond. Chemisorption is very strong and usually appears as single layer structure. Before some chemical being absorbed over the material surface it would be ionized, and the ion group could be absorbed by material. Some chemicals with unshared pair electrons (lone pair electrons) or covalence bond could be chemisorbed via rehybridization of the unsaturation bond in molecules then will bind with the material. The adjustment to surface potentials of semiconductor could be useful for chemisorption.

2.8 The common strategies to engineer photocatalysts

In order to increase the efficiency of photocatalytic reaction three majority strategies could be implemented: enhancing the rate of photo carrier generation; accelerating the combination between carries and subject; weakening recombination progress. Apart from electromagnetic wave absorption, carrier generation progress and properties of photocatalyst surface are very important. The electronic characters of catalysts are crucial. Many modification strategies of photocatalyst are available to convert semiconductor electronic properties.

Downgrade the band gap energy of photosensitive semiconductor is usually considered, because the electromagnetic wave absorption is dependent on the band gap energy. When the excitation wavelength match with absorption thresholds (band gap), the semiconductor could transform radiation into electronic potential. Doping of TiO_2 is a promising route to extend the optical absorption of this material to the visible spectral region. Titanium dioxide is a good photocatalyst, because it is no-toxic, environmentally friendly and chemical stability. However, it has a big band gap energy (3.2 eV), which restricts titanium dioxide to absorb electromagnetic wave in ultraviolet spectral range. In a research of Sakthivel et al. [48], nitrogen atom has been doped into TiO_2 skeleton by hydrolysis of titanium tetrachloride with a nitrogen-containing base, such as ammonia, ammonium carbonate, or ammonium bicarbonate to obtain TiO_2-N/1, TiO_2-N/2, TiO_2-N/3, respectively. After calcination in air at 400℃, the slightly yellow materials contained 0.08 ± 0.13 wt% of nitrogen element. The diffuse reflectance spectra analysis demonstrated that as the nitrogen content increasing, the radiation absorption edge has a red shift, thus the requirement for exciting energy is lower. As a result, nitrogen doped TiO_2 photocatalyze the mineralization of 4-chlorophenol with artificial visible light (455 nm). About 50% conversion was observed after 6 h, whereas less than 1% of mineralization occurred in unmodified titanium dioxide. The initial rates of degradation were about ten to 20 times larger. Carbon doping could also reconstruct energy level in titanium dioxide, which could weaken the exciting radiation energy requirement, some investigations indicate carbon doped TiO_2 could be more efficient than nitrogen doped particle[49].

In order to increase carrier exposure some researchers studied the effect of shape, polymorphs and crystalline surface, because crystalline properties could seriously affect photocatalytic efficiency. Titanium dioxide has three types of polymorphs: rutile, anatase and brookie. The lattice structure of rutile and anatase are octahedral, however rutile has orthorhombic distortion. Rutile TiO_2 is stacked with ten cells but anatase is only stacked with eight cells in crystal[50].

Typically, anatase TiO_2 has a higher activity than rutile because the band gap energy of anatase is lower than rutile, and it is easier to be excited. At the same time the valence band of anatase TiO_2 is lower than rutile valence band, which contributes stronger oxidizing to anatase TiO_2. In addition, anatase has stronger chemisorption toward anion radical and lone pair of electrons[51, 52]. Brookie is not adopted for photocatalysis because it could support defect energy level and accelerate carrier recombination. Nakabayashi[53] investigated the correlation between the OH radical formation and oxygen production by photoelectron chemical properties of three rutile TiO_2 (100), (110), and (001) faces. It was found that the current efficiency of OH radical formation on TiO_2 rutile surfaces increased in the order of (001) < (110) < (100). The difference could be explained by the difference in the strength of Ti−O bond of the peroxo intermediate Ti−O−O−Ti against the hole attack.

The migration velocity of carrier in material could also be adjusted by coating technology. Some materials with a high migration velocity (such as graphene single sheet and sliver nanoparticle) could be attached on the surface of photocatalysts. When excess electron has ability to inject carrier in to those composite, they could shorten the time for carrier transition from inside of particle to outside surface. This could forbear the electronic pair prematurely recombination. Zhang and his research team[54] has researched on graphene coated commercial titanium dioxide (P25). In the research graphene oxide was synthesised by oxidation method (Hummers' method[55]), then the graphene oxide was mixed with P25. The spectral absorption of graphene coated TiO_2 photocatalyst has a red shift comparing with P25, thus it could degrade methylene blue solution under visible light (wavelength >400 nm). The formed hydroxyl radical and superoxide radical species in P25-0.5% GR is much stronger than that of P25 under radiation, The graphene coated TiO_2 photocatalysts were analysed by photoluminescence (PL) spectroscopy [56]. The emission peak of TiO_2 at around 510 nm was

slightly broadened and quenched in intensity indicating carrier transfer from the conduction band of TiO_2 to the graphene; weakening the recombination in the photocatalyst.

Impurity doping technology has multifunctions to semiconductor modification, for examples carbon impurity not only increases the absorption spectrum range of TiO_2; accelerate photo generated electron/electronic hole migration but also weaken the recombination for excess carrier[57]. This can be contributed by impurity level from carbon atom, [41]. Impurity dopant could appear in semiconductor lattice in two circumstances: it could substitute the atom in original lattice or it could imbed between crystalline structures. But the impurity atom should have a similar atomic radius with the replaced element. Because of the different bond length and electronegativity, the impurity has potential to become carrier trap, which limits the carrier mobility and affect ionization energy of donor/acceptor. Frequently the electronegativity of the non-metal dopant must be lower than substituted element, so the dopant states can be involved into formation of a new valence band[58].

Hybrid semiconductor is other way to weaken recombination of excess carrier. This will introduce a new energy level from outside particle, photogenerated electron/hole could drift and inject into this new energy level, instead of recombination directly. PN-junction is usually applied which could unidirectionally transfer positive charge (electronic hole) or negative charge (electron) in one.

2.9 Graphitic carbon nitride as a photocatalyst

Currently, organic photo sensitive particles are attracting more and more attentions for photovoltaic device, such as graphitic carbon nitride (GCN)[59-62], the latest found organic photocatalyst. Organic semiconductor material could be adopted in transparent electrode film[63], flat heater[64], antistatic film[65] and selective light film[66]. The advantages of

organic semiconductor could be concluded by: low production cost with uncomplicated production process; soft, highly compatible and flexible processing; the band gap in organic semiconductor is adjustable by verifying the molecular length or the grafting function groups. Photosensitive organic semiconductor possess high molar extinction coefficient, thus a small amount of organic material can absorb a large amount of light[67]. Typically, organic semiconductors contain several conjugated double bonds, which could bind delocalized π orbital in whole molecule. In an organic semiconductor, π orbital plays a role as HOMO but anti- π orbital (π^*) attributes to LUMO which is totally different from crystalline semiconductor[68]. Graphitic carbon nitride possessed those characters[69].

The carbon nitride compound has been reported in 1830s. Berzelius and Liebig discovered the general formula$(C_3N_3H)_n$, namely referred as "melem"[70]. In 1989, Liu and his co-worker[71] theoretically indicated a super hard β-polymorph of hydrogen-free C_3N_4, Since then, polyamory carbon nitride composites have attracted much attention.

Graphitic carbon nitride (C_3N_4) is an organic photo sensitive semiconductor, comparing with graphite which has strong covalent C–N bonds in each layer by van der Waals forces. Graphitic carbon nitride is a defect-rich semiconductor. The tri-s-triazine ring structure and the high degree of condensation (up to 600 °C in air) provide the polymer with high stability with resistance toward thermal and chemical decomposition.

Graphitic carbon nitride could absorb radiation in visible light spectral range, however, it is a direct semiconductor and has multiple defects, and thus the recombination rate in graphitic carbon nitride is fast. Coating graphene particle on graphitic carbon nitride could enhance the mobility of carrier and weaken the carrier recombination. It is easily prepared from the condensation of simple nitrogen-rich precursors such as cyanamide[72], dicyandiamide[72] and melamine[73]. Xiang et al.[74] prepared graphene coated graphitic carbon nitride particles

(GC) from calcination of a precursor (melamine) and commercial graphene nanosheet. As a result, the light absorption edge of GC photocatalyst has merely no shift than C_3N_4 but in the photoluminescence spectra, graphene coating could significantly decrease the fluorescence intensity. The optimal graphene coating was found to be 1.0 wt%, and the corresponding H_2-production rate was 451 μmol $\cdot\ h^{-1} \cdot g^{-1}$, which exceeded that of pure C_3N_4 by more than 3.07 times.

As a typical organic semiconductor, $g - C_3N_4$ possess enormous delocalized orbitals. Nitrogen atom P_z orbitals and P_Z in carbon orbitals construct the anti-π orbital (π*) of the VB and CB, in which the photogenerated e^- and H^+ are easily separated in the nitrogen atom and carbon atom. $g - C_3N_4$ with a 2D surface also provides a larger adsorption scaffold[75].

$g - C_3N_4$ was first used as a photocaralyst for catalyzing Friedel–Crafts reaction in 2006 [76]. It was revealed $g - C_3N_4$ can be a metal-free polymeric photocatalysts for hydrogen evolution by water splitting in 2009[77]. Until now, more than 1900 publications could be found on the catalytic, electrocatalytic, and photocatalytic performance of graphitic carbon nitride, such as photocatalytic H_2 evolution[78], photodegradation of organic pollutants[78], photoelectric conversion[78], CO_2 activation[79], and other important catalytic reactions.

2.10 Morphological properties of graphitic carbon nitride

In the past years, researchers attempted different techniques on synthesis of graphitic carbon nitride, thus micro-/nanostructures and morphologies of $g - C_3N_4$ appeared. Morphologies of $g - C_3N_4$ strongly relates to its properties and applications. Bulk $g - C_3N_4$ usually is prepared through the thermal condensation with carbon-nitrogen beared precursors such as cyanamide, dicyandiamide, melamine, thiourea, urea, or mixtures[80]. Such bulk materials have a very low surface area (lower than 10 m^2/g). “Topotactic transformations” has been applied to make

melamine pre-organize in a supramolecular complex and cyanuric acid condensation to the surface area of 60–80 m^2/g [81].

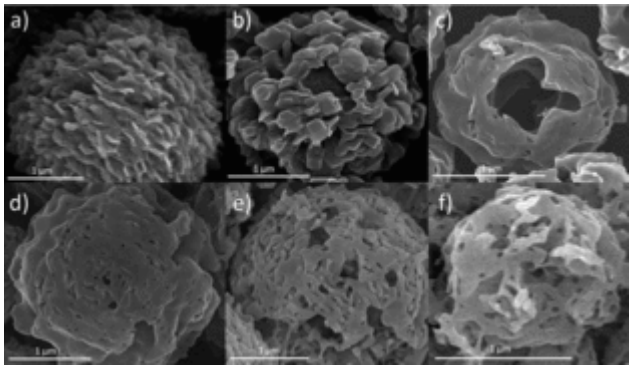

Fig. 4 SEM images of MCA heated at different temperatures; a) as-synthesized and heated at b) 350, c) 400, d) 450, e) 500, and f) 550 ℃[81].

Mesoporous $g-C_3N_4$ has been prepared by nanocasting/replication of silica spheres or mesoporous silica templates. In a typical preparation, commercially available silica sol and cyanamide are mixed in aqueous solutions. After the complete removal of water, the complex polymeric carbon nitride/silica has been proceeded in thermal condensation and the template was removed in ammonia hydrogen difluoride [82, 83]. Mesoporous $g-C_3N_4$ surface area could reach 350 m^2/g.

Two dimension, single layer molecular structure has been considered as the best catalyst material, such as graphene, graphene oxide or graphene-liked material[84]. Graphene has a theoretical surface area of $2600 m^2/g$, making graphene highly attractive as a high-surface area 2D photocatalyst supporter. Furthermore, high quality graphene sheets induce ballistic transport, which means that electrons can travel without scattering at motilities exceeding 15.000 $m^2\ V^{-1}\ ss^{-1}$ at room temperature. Graphitic carbon nitride possesses multiply layer stack structure, two dimensions $g-C_3N_4$ have been considered as super photocatalyst has been studied for long time. A sonication-assisted liquid-exfoliation top-down method has been

reported to prepare nanosheet $g-C_3N_4$ which could exfoliated in solvent media with surface energy matching with the materials with highly stabilization[85, 86]. Exfoliated thin layer from the dicyandiamide-derived bulky $g-C_3N_4$ could be with a high surface area of 300 m^2/g [87]. Liu et al. engineered a "nanoconfinement" procedure to merge thin films $g-C_3N_4$ on conductive substrates[88]. A cyanamide aqueous solution infiltrated anodic aluminium oxide (AAO) stamp is found to be capable of "ink-jetting" carbon nitride films featuring regular microstructures of the stamp onto the substrates via chemical vapor deposition (CVD).

For one dimensional $g-C_3N_4$ (nanowires/nanorods/nanotubes), Li et al. reported a successful synthesis of inter-rod hexagonal nanorods $g-C_3N_4$ by template interfere[89]. Cyanamide could be condensed inside the template channels, thereby hierarchical carbon nitride nanorod could be obtained via removing the template[90]. Crystal growth has been reported to obtain $g-C_3N_4$ nanowires[91]. Recently one dimension $g-C_3N_4$ (graphitic carbon nitride quantum dots) also has been report be synthesised by Groenewolt et al by employing silica host matrices. The 5 nm size production showed blueshifted photoluminescence comparing bulky $g-C_3N_4$ [92]. As a metal-free polymeric material, $g-C_3N_4$ QDs have the advantages of bright fluorescence, good stability, water-solubility, biocompatibility, and nontoxicity, making them good candidates in place of traditional QDs[93, 94].

2.11 Graphitic carbon nitride based photocatalysts

The heterojunction semiconductor photocatalysts were widely researched now, there are many successful hybrid semiconductors with C_3N_4, such as TiO_2[86, 95-97], CdS[98], BiOBr[99], MoS_2[100] and so on. Wang and his co-workers[86] prepared a heterojunction of TiO_2 and C_3N_4 to enhance the decomposing Rhodamine B under visible light. The photocatalytic mechanism could be explained by excess carrier drifting and limited recombination. N-TiO_2

and C_3N_4 could absorb electromagnetic waves in visible light spectral range, the LUMO in C_3N_4 (-1.2 eV) is more negative than that of N-TiO_2 (-0.34 eV) under standard hydrogen electrode scale (SHE), indicating that the excess electron in C_3N_4 could transfer in to the LUMO of N-TiO_2. Those trapped excess electron could reduce O_2 into $\cdot O^{-1}$ (-0.28 vs SHE) and weaken the recombination progress in C_3N_4.

Surface attaching with chemical groups could shift band gap energy or band energy location in organic semiconductors. There are two types of function groups: the electron - donating groups (for example: $(CH_3)_3C- > (CH_3)_2CH- > CH_3CCH_2- > CH_3- > H-$, ; and the electron-withdrawing groups (for example: $NO_2- > CN- > F- > COOH- > Cl- > Br- > I- > C\equiv C- > OCH_3- > OH- > C_6H_5- > C=C- > H-$,) . Usually when electron - donating groups bind with a delocalized π orbital compound, electrons of the compound will be easier to ionized, as a result the energy of HOMO will increase and its Fermi level will increase too. In contrast when electron withdrawing groups collaborate with organic compound, the energy of LUMO and HOMO will reduce[101, 102]. In Price's research[103], organic photovoltaic material PBnDT-HTAZ had been modified by fluorine (Fig. 15).

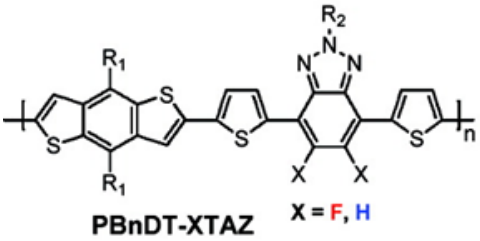

. PBnDT-HTAZ had be modified by fluorine [103]

Fluorine possesses magnificent electronegativity and the F- function group is a strange electron accepter. In the research, after substitution the intensity of PBnDT-FTAZ in UV-vis absorption spectra have a significant increasing and the electronic hole mobility has increased 2 times comparing with PBnDT-HTAZ. In a consequent, the PBnDT-FTAZ solar cell has a peak device

efficiency of 7.1% which is higher than PBnDT-HTAZ solar cell. There are some researches about fluorinated Polymeric Carbon Nitride photocatalyst (CNF) [104]. When the C_3N_4 particle and ammonium fluoride are thermally treated at 550℃, F- groups could replace the ammonia function groups of C_3N_4. As a result, the band gap energy of fluorinated C_3N_4 decreased with the LUMO and MOMO level increased at the same time. CNF photocatalyst could well dispersed in water and degrade benzene under visible light but C_3N_4 unlikely did.

2.12 Graphitic carbon nitride for organic pollutant photodegradation

Wastewater treatment and water resource reuse became utmost requirements for many countries. To develop efficient and economical technologies which are able to meet an increasing safe quality demand is a big challenge in global wide. Photocatalytic technology is a potential selection for future. Today, many reports disclose the successful results for photocatalytic degradation of biological wastewater, such as endocrine disrupting compounds, pharmaceutical drugs including antibiotics, disinfection by-products, personal care products, metabolites, transformation products, pesticides, surfactants and biocides. Photocatalytic water treatment technology is a great attention from the scientific community. Thereby, $g - C_3N_4$ has been widely adopted in various pollutant remediation systems.

The textile industry is one of the largest pollution industries in the world. The World Bank estimates that almost 20% of global industrial water pollution comes from the treatment and dyeing of textiles. Dye containing waste water usually has aromatic amines (benzamine and toluidine), heavy metals, ammonia, alkali salts, toxic solids and large amounts of pigments and chlorine.

In the past decays, many researchers investigated the photodegradation of dye compounds by $g-C_3N_4$ based particles. Rhodamine B (RhB) is widely utilized in printing, textile and photographic industries and is also a well-known water tracer fluorescent. It is harmful to animal tissues. In addition, the toxicity, carcinogenicity, neurotoxicity and chronic toxicity are demonstrated [105-107]. BiOBr/ $g-C_3N_4$ heterojunction for the RhB degradation in the presence of visible and indoor lights have been reported. The optimum photoactivity of the 0.5BiOBr/ $g-C_3N_4$ heterojunction could reach about 4.9 and 17.2 times higher than BiOBr and $g-C_3N_4$ under indoor light irradiation. [99]. Heterojunction posed intimately contacted interfaces and well-matched straddling band structures, which efficiently transfer and separate electronic pairs, imped the recombination. Heterojunction ZnS/ $g-C_3N_4$ particle has been studied to decompose RhB[108]. The photocatalytic activity of ZnS/ $g-C_3N_4$ is obviously higher than TiO_2. In addition, many other $g-C_3N_4$ based heterojunction particles have been showed an enhanced photocatalytic performance for RhB degradation under visible illumination, such as $MoS_2/\ g-C_3N_4$ [109], $Ag_3PO_4/\ g-C_3N_4$ [110], $MoS_2/\ g-C_3N_4$ [109], $In_2S_3/\ g-C_3N_4$ [111], $BiIO_4/\ g-C_3N_4$ [112], $InVO_4/\ g-C_3N_4$ [113], $ZrO_2/\ g-C_3N_4$ [114], $SmVO_4/\ g-C_3N_4$ [115], $V_2O_5/\ g-C_3N_4$ [116], $SrTiO_3/\ g-C_3N_4$ [117], CdS/ $g-C_3N_4$ [118].

Methylene Blue (MB) is another dye pollutant, which is usually used in textile pigment, wool and hair colouring. However, it is a thiazine dye, which threats human health and environment[119, 120]. $g-C_3N_4$ based photocatalysts have be found to decompose MB from water. $TiO_2/\ g-C_3N_4$ nanosheet exhibited superior photocatalytic performance under both UV and visible light irradiation, $g-C_3N_4$ as a sensitized medium could inject electrons into TiO_2 [121, 122]. Zhou et al. claimed 7 wt% loaded ZnO/ $g-C_3N_4$ composites for photocatalytic degradation of 95% MB in 180 min[123]. Microporous $g-C_3N_4$ based core–shell structure of ZnO/mp $g-C_3N_4$ heterojunction could raise the photocatalytic activity by

surface hybridization of π–π* stacking chemisorption of MB molecules[124]. $WO_3/\ g-C_3N_4$ photocatalyst fabricated via ball milling and heat treatment technique is greatly effective and stable for visible light-driven photodegradation of MB, dependent on the ratio between $WO_3\ and\ g-C_3N_4$ [125]. CdS/ $g-C_3N_4$ catalysts have been applied toward the MB degradation under the exposure of visible light irradiation. The efficiency has an obvious increase than single CdS and $g-C_3N_4$ [126]. Besides above composites, many other $g-C_3N_4$ based photocatalysts were studied in MB degradation evaluation with an outstanding efficiency, such as $MoO_3/\ g-C_3N_4$ [127], $Bi_2O_3/\ g-C_3N_4$.[128] $Ag_3VO_4/\ g-C_3N_4$[129] and so on.

Methyl orange (MO) released from the manufacturing industries into water bodies can cause numerous deleterious health effects, owing to its mutagenic and carcinogenic properties [130, 131]. Recently, $g-C_3N_4$ based photocatalysts have widely been studied in removing MO from water. Optimised $Bi_2WO_6/\ g-C_3N_4$ prepared via a hydrothermal method. was almost 3 and 155 times higher than those of pure $g-C_3N_4$ and Bi_2WO_6, respectively under the visible light, because of the well-matched overlapping band structures and charge separation efficiency[75]. Xu et al. [132] also reported that the visible light degradation of MO by AgBr and AgI was significantly improved after the hybrid with $g-C_3N_4$. The Cu_2O and $g-C_3N_4$in the heterojunction could extend visible light spectral response. Comparing with $g-C_3N_4$ the visible light photoactivity was improved significantly[133]. A feasibility study on CdS/ $g-C_3N_4$ has been presented by Fu et al. [134]. MO could be decomposed under visible light irradiation. The activities were much higher than those of $TiO_2/\ g-C_3N_4$, and CdS/TiO_2 composites. $Co_3O_4\ /\ g-C_3N_4$ composites for MO degradation under the visible light irradiation also has been proved a great improvement[135].

Wang and co-workers [163] synthesized Ag_3VO_4 anchored on $g-C_3N_4$ sheets and utilized for degradation of triphenylmethane dyes (basic fuchsin (BF), malachite green (MG) and crystal violet (CV)) under the visible light. The photocatalytic activities were in the order of MG>BF>CV. The mineralization of these three dyes was also observed with TOC removal of 45% (BF), 53% (MG) and 34% (CV) in 150 min[136].

Zhao et al. fabricated a $Ag/AgVO_3/\ g-C_3N_4$ ternary plasmonic photocatalyst through a one-step in-situ hydrothermal treatment[137]. New particle showed the highest apparent rate constant of 0.0701 min^{-1} for the basic fuchsin (BF) photodegradation, about 12.5 times higher than $g-C_3N_4$ [137].

The study about Acid Orange-II (AO-II) photodegradation by $Cu_2O/\ g-C_3N_4$ heterojunction cpmposite was presented by Peng et al. [138]. As reported, the degradation efficiency could reach ~95% within 180 min. Lei et al. demonstrated the $TiO_2/\ g-C_3N_4$ photocatalysts can remove Acid Orange 7 (AO7) dye under UV and visible illumination. $g-C_3N_4$ loading could significantly increase the light absorption range of TiO_2 [139].

In recent studies, phenolic compounds could also be degraded by $g-C_3N_4$ based photocatalysts. Zhang et al. prepared carbon dot (CD) loading $g-C_3N_4$ through condensation of cyanamide and calcination of $g-C_3N_4$ /CD mixture at 300℃. CD/ $g-C_3N_4$ was able remove about 98% phenol from water in 200 min. Upconversion photoluminescence spectra and photocurrent experiments indicated CD could induce extra electron into $g-C_3N_4$ and the recombination rate was slow when CD appeared[140].

2D porous $g-C_3N_4$ /Ag_3PO_4 could degrade 4-chlorophenol under visible radiation, and the photocatalytic reaction rate constant could reach 0.018min^{-1} , much higher than naked $g-C_3N_4$ (0.000061min^{-1}). $g-C_3N_4$ /Ag_3PO_4 heterojunction effectively weakens the electronic pair recombination and enlarges the absorption spectrum[141].

BiOBr / $g-C_3N_4$ heterojunction photocatalyst was obtained via solvothermal with enhanced visible-light response. The evaluation experiment of bisphenol A (BPA) photodegradation showed an enhance photoactivity of the heterojunction material than pure BiOBr, which can be contributed by the extra photoelectron from $g-C_3N_4$ and swift chargers drifting between the interface [142].

Wu et al. [143] revealed that, after a hydrothermal treatment with 10% hydrochloric acid, the surface area of $g-C_3N_4$ increased from 11.5 m^2/g to 115 m^2/g. Meanwhile, the photocatalytic activity of $g-C_3N_4$ was significantly improved after treatment toward degradation of 4-nitrophenol under visible light irradiation. Activity constant of the new particle is 5.7 times of that of bulk $g-C_3N_4$.

A pharmaceuticals pollutant, ciprofloxacin, has also been reported to be remediated by a ternary ZnO-Ag_2O/porous $g-C_3N_4$ photocatalyst under visible-light radiation. $g-C_3N_4$ enlarged the light absorption of ZnO-Ag_2O, at the same time $g-C_3N_4$ could impede the charger recombination of ZnO-Ag_2O. The reaction rate constant of ZnO-Ag_2O/ $g-C_3N_4$ heterojunction is 0.057 min^{-1}, which is much higher than single ZnO, $g-C_3N_4$ and Ag_2O [144]. Au/Pt/ $g-C_3N_4$ has been found to successfully remove tetracycline from water with visible light [145]. Au and Pt NPs codecorated g-C_3N_4 nanocomposites were prepared through a photodeposition procedure with hole scavenger (PH) method, and a suspension was photoirradiated for 3h by a mercury light with stirring. The co-decorated Au (III) and Pt (II) salt sources were reduced by photogenerated electrons, and the novel metals were deposited on the surfaces of the $g-C_3N_4$. The degradation rate of TC-HCl follows an order of Au/Pt/ $g-C_3N_4$ (93.0%) > Au/ $g-C_3N_4$ (78.6%) > Pt/ $g-C_3N_4$ (67.2%) > $g-C_3N_4$ (52.8%) after the same irradiation time. CdS/ $g-C_3N_4$[146], Ag_2O/ $g-C_3N_4$ [147] have also been proved to have the photodegradation toward TC-HCl.

2.13 Other applications of graphitic carbon nitride

Chemical sensing relied on fluorescence to signal of a molecular recognition[148]. $g-C_3N_4$ is promising to be highly fluorescent metal-free nanomaterials with pronounced photostability and low toxicity, most important, $g-C_3N_4$ has photoluminescence to be against photobleaching. Lee et al. reported $g-C_3N_4$ can detect trace amounts of copper metal ions in aqueous solutions with high selection, detection limit was determined as 12.3 nM, which is due to a high surface volume ratio and exposed coordination points toward metal ions[149]. $g-C_3N_4$ based sensor has also been extended to Fe^{3+}, heparin, Pb^{2+}, Hg^{2+}, and Cr^{6+} [94, 150-152].

Graphitic carbon nitride could be adopted as a template agent. By using $g-C_3N_4$ as the soft template, SiO_2 -assisted synthesis of TaON over Ta_3N_5 nanoparticles with tailored composition through the calcination of Ta/urea mixture gels was obtained, which could be employed for alkene epoxidation[153]. Urea was converted into carbon nitride (CNx) species on the SiO_2-surface at mild temperature, which further slowly acted to release active nitrogen species for controlled nitridation. The electronic properties of Ta were tuned by the different nitridation levels in TaON and Ta_3N_5 NPs. This controlled nitridation significantly improved the activity for alkene epoxidation, as compared to Ta_2O_5 NPs. The simple synthetic process required neither catalyst nor solvent and was used to convert glucose directly into polycrystalline carbon sheets having a “patched” multidomain graphene structure with lateral domains 2–15 nm in size. The obtained carbon assemblies exhibit high conductivity, high specific surface area, and unexpectedly good solution processability. The authors also extended the synthesis strategy to incorporate boron and nitrogen into the graphene network, thus creating excellently selective catalysts for organic oxidation reactions[154].

2.14 Conclusions

Photocatalytic reaction has been considered to build up a new route toward cheap environment cleaning technology. However, currently developed photosensitive semiconductor could not be widely applied in industry because the bottleneck of the limited radiation energy utilization, un-constructible energy states and low photocatalytic efficiency. The strategies to improve photocatalyst or photovoltaic device efficiency could be concluded in following areas: (1) shrank particles size is good for photocatalytic reaction because small particles are easy to disperse, small particle has high surface area, and meanwhile the particles possess extinction coefficients for band semiconductor energy structure designing. (2) For electronic properties, photosensitive semiconductor should have a high carrier diffusion speed, the photogenerated carriers can be transport from inner of particle to the surface as soon as possible and react with pollutants instead carrier recombination with thermal energy wasting. (3) Defects or impurities in photosensitive semiconductor could disturb energy structure, rebuild the recombination centre. A reasonable distribution of defect is very important for a photocatalyst. (4) Photocatalyst hybridization is a very common technique in photocatalyst modification, which could enhance carrier mobility; also heterojunction is useful for carries exposure and weak recombination.

Graphitic carbon nitride is a metal-free photocatalyst, which could be easily prepared from nitrogen-rich organic compounds due thermal condensation treatment. The 2.7 eV band gap energy grants $g-C_3N_4$ an ability to absorb visible light. However, $g-C_3N_4$ is a direct semiconductor, the energy levels are builded up by π–π* stacking between nitrogen and carbon periodic units. Graphitic carbon nitride possesses very strong recombination, which make it hardly be applied as a good photocatalyst. Recently many studies are processing to modify the optical and electronic properties of $g-C_3N_4$. Such as morphological properties controlling,

crystalline renovation, atomic decoration, pore structure introduction, metallic (no-metallic) hybrid building and so on. At the same time, $g-C_3N_4$ based photaocatalysts have been found more and more utilization in pollutant remediation, such as dyes, phenolic compounds, pharmaceuticals, herbicides and so on. $g-C_3N_4$ based semiconductors have great potential for photocatalytic environment treatment.

2.15 References

[1] M. Solís, A. Solís, H.I. Pérez, N. Manjarrez, M. Flores, Microbial decolouration of azo dyes: a review, Process Biochemistry, 47 (2012) 1723-1748.

[2] E.G. Nielsen, L. Lee, The magnitude and costs of groundwater contamination from agricultural chemicals, Econ. Res. Ser. A National Perspective, ERS Staff Report, AGES, 870318 (1987).

[3] I.-I. Savin, R. Butnaru, Wastewater characteristics in textile finishing mills, Environmental engineering and management journal, 7 (2008) 859-864.

[4] A.-E. Becquerel, Mémoire sur les effets électriques produits sous l'influence des rayons solaires, Comptes Rendus, 9 (1839) 1839.

[5] H. Hertz, Ueber einen Einfluss des ultravioletten Lichtes auf die electrische Entladung, Annalen der Physik, 267 (1887) 983-1000.

[6] W. Heisenberg, Physics and beyond: Encounters and conversations, (1971).

[7] J.w. Yoo, Solid state physics in, UNIST.

[8] V. Mehta, Principles of Electronics, S. Chand, 2008.

[9] D.J. Griffiths, E.G. Harris, Introduction to quantum mechanics, Prentice Hall New Jersey, 1995.

[10] A. Fujishima, Discovery and applications of photocatalysis-Creating a comfortable future by making use of light energy, Japan Nanonet Bulletin, 44 (2005) 1-3.

[11] M. Ni, M.K. Leung, D.Y. Leung, K. Sumathy, A review and recent developments in photocatalytic water-splitting using TiO_2 for hydrogen production, Renewable and Sustainable Energy Reviews, 11 (2007) 401-425.

[12] Ü. Özgür, Y.I. Alivov, C. Liu, A. Teke, M. Reshchikov, S. Doğan, V. Avrutin, S.-J. Cho, H. Morkoc, A comprehensive review of ZnO materials and devices, Journal of applied physics, 98 (2005) 041301.

[13] N. Hullavarad, S. Hullavarad, P. Karulkar, Cadmium sulphide (CdS) nanotechnology: synthesis and applications, Journal of nanoscience and nanotechnology, 8 (2008) 3272-3299.

[14] T.P.K. Laboratory., Photocatalysis, in, University of Notre dame, U.S.A, 2012.

[15] C. Chen, X. Li, W. Ma, J. Zhao, H. Hidaka, N. Serpone, Effect of Transition Metal Ions on the TiO_2-Assisted Photodegradation of Dyes under Visible Irradiation: A Probe for the Interfacial Electron Transfer Process and Reaction Mechanism, The Journal of Physical Chemistry B, 106 (2001) 318-324.

[16] D.N. Spergel, L. Verde, H.V. Peiris, E. Komatsu, M. Nolta, C. Bennett, M. Halpern, G. Hinshaw, N. Jarosik, A. Kogut, First-year Wilkinson Microwave Anisotropy Probe (WMAP) observations: determination of cosmological parameters, The Astrophysical Journal Supplement Series, 148 (2003) 175.

[17] R.H. Blessing, An empirical correction for absorption anisotropy, Acta Crystallographica Section A: Foundations of Crystallography, 51 (1995) 33-38.

[18] W. Bludau, A. Onton, W. Heinke, Temperature dependence of the band gap of silicon, Journal of applied physics, 45 (1974) 1846-1848.

[19] H. Murata, C.D. Merritt, Z.H. Kafafi, Emission mechanism in rubrene-doped molecular organic light-emitting diodes: direct carrier recombination at luminescent centers, IEEE Journal, 4 (1998) 119-124.

[20] W. Choi, A. Termin, M.R. Hoffmann, The role of metal ion dopants in quantum-sized TiO2: correlation between photoreactivity and charge carrier recombination dynamics, The Journal of Physical Chemistry, 98 (1994) 13669-13679.

[21] L. Chen, C. Chen, S. Wei, D. Bhusari, K. Chen, Y. Chen, Y. Jong, Y. Huang, Crystalline silicon carbon nitride: A wide band gap semiconductor, Applied Physics Letters, 72 (1998) 2463-2465.

[22] A. Fischer, J.O. Müller, M. Antonietti, A. Thomas, Synthesis of ternary metal nitride nanoparticles using mesoporous carbon nitride as reactive template, Acs Nano, 2 (2008) 2489-2496.

[23] D.A. Skoog, D.M. West, Principles of instrumental analysis, Saunders College Philadelphia, 1980.

[24] P. Wang, S.M. Zakeeruddin, J.E. Moser, M.K. Nazeeruddin, T. Sekiguchi, M. Grätzel, A stable quasi-solid-state dye-sensitized solar cell with an amphiphilic ruthenium sensitizer and polymer gel electrolyte, Nature materials, 2 (2003) 402-407.

[25] X. Yan, T. Ohno, K. Nishijima, R. Abe, B. Ohtani, Is methylene blue an appropriate substrate for a photocatalytic activity test? A study with visible-light responsive titania, Chemical physics letters, 429 (2006) 606-610.

[26] S. Kurtz, T. Perry, A powder technique for the evaluation of nonlinear optical materials, Journal of applied physics, 39 (1968) 3798-3813.

[27] P.N. Prasad, D.J. Williams, Introduction to nonlinear optical effects in molecules and polymers, Wiley New York etc., 1991.

[28] A.K. Geim, P. Kim, Carbon wonderland, Scientific American, 298 (2008) 90-97.

[29] A.K. Geim, K.S. Novoselov, The rise of graphene, Nature materials, 6 (2007) 183-191.

[30] K.I. Bolotin, K. Sikes, Z. Jiang, M. Klima, G. Fudenberg, J. Hone, P. Kim, H. Stormer, Ultrahigh electron mobility in suspended graphene, Solid State Communications, 146 (2008) 351-355.

[31] N. Papageorgiou, Y. Athanassov, M. Armand, P. Bonho, H. Pettersson, A. Azam, M. Grätzel, The performance and stability of ambient temperature molten salts for solar cell applications, Journal of the Electrochemical Society, 143 (1996) 3099-3108.

[32] X. Ju, A. Vossier, Z. Wang, A. Dollet, G. Flamant, An improved temperature estimation method for solar cells operating at high concentrations, Solar energy, 93 (2013) 80-89.

[33] X. Bai, L. Wang, R. Zong, Y. Zhu, Photocatalytic Activity Enhanced via g-C_3N_4 Nanoplates to Nanorods, The Journal of Physical Chemistry C, 117 (2013) 9952-9961.

[34] L. Ge, F. Zuo, J. Liu, Q. Ma, C. Wang, D. Sun, L. Bartels, P. Feng, Synthesis and efficient visible light photocatalytic hydrogen evolution of polymeric g-C_3N_4 coupled with CdS quantum dots, The Journal of Physical Chemistry C, 116 (2012) 13708-13714.

[35] Y. Xie, G. Ali, S.H. Yoo, S.O. Cho, Sonication-assisted synthesis of CdS quantum-dot-sensitized TiO2 nanotube arrays with enhanced photoelectrochemical and photocatalytic activity, ACS Applied Materials & Interfaces, 2 (2010) 2910-2914.

[36] Y. Roichman, N. Tessler, Generalized Einstein relation for disordered semiconductors—implications for device performance, Applied Physics Letters, 80 (2002) 1948-1950.

[37] S. Lindsay, Introduction to nanoscience, Oxford University Press, 2009.

[38] M.A. Green, K. Emery, Y. Hishikawa, W. Warta, E.D. Dunlop, Solar cell efficiency tables (version 39), Progress in photovoltaics: research and applications, 20 (2012) 12-20.

[39] T. Ohno, K. Sarukawa, K. Tokieda, M. Matsumura, Morphology of a TiO_2 Photocatalyst (Degussa, P-25) Consisting of Anatase and Rutile Crystalline Phases, Journal of Catalysis, 203 (2001) 82-86.

[40] H. Lachheb, E. Puzenat, A. Houas, M. Ksibi, E. Elaloui, C. Guillard, J.-M. Herrmann, Photocatalytic degradation of various types of dyes (Alizarin S, Crocein Orange G, Methyl Red, Congo Red, Methylene Blue) in water by UV-irradiated titania, Applied Catalysis B: Environmental, 39 (2002) 75-90.

[41] J. Du, X. Lai, N. Yang, J. Zhai, D. Kisailus, F. Su, D. Wang, L. Jiang, Hierarchically ordered macro− mesoporous TiO2− graphene composite films: Improved mass transfer, reduced charge recombination, and their enhanced photocatalytic activities, Acs Nano, 5 (2010) 590-596.

[42] R. Sips, On the structure of a catalyst surface, The Journal of Chemical Physics, 16 (1948) 490-495.

[43] G.C. Bond, C. Louis, D.T. Thompson, Catalysis by gold, Gold Bulletin, 39 (2006) 3.

[44] A.G. Aberle, S. Glunz, W. Warta, Impact of illumination level and oxide parameters on Shockley–Read–Hall recombination at the Si-SiO_2 interface, Journal of applied physics, 71 (1992) 4422-4431.

[45] D. Lang, L. Kimerling, Observation of recombination-enhanced defect reactions in semiconductors, Physical Review Letters, 33 (1974) 489.

[46] A. Tsukazaki, A. Ohtomo, T. Onuma, M. Ohtani, T. Makino, M. Sumiya, K. Ohtani, S.F. Chichibu, S. Fuke, Y. Segawa, Repeated temperature modulation epitaxy for p-type doping and light-emitting diode based on ZnO, Nature materials, 4 (2004) 42-46.

[47] A.P. Kulkarni, C.J. Tonzola, A. Babel, S.A. Jenekhe, Electron transport materials for organic light-emitting diodes, Chemistry of materials, 16 (2004) 4556-4573.

[48] S. Sakthivel, H. Kisch, Photocatalytic and Photoelectrochemical Properties of Nitrogen-Doped Titanium Dioxide, ChemPhysChem, 4 (2003) 487-490.

[49] S. Sakthivel, H. Kisch, Daylight Photocatalysis by Carbon-Modified Titanium Dioxide, Angewandte Chemie International Edition, 42 (2003) 4908-4911.

[50] K. Tanaka, M.F. Capule, T. Hisanaga, Effect of crystallinity of TiO_2 on its photocatalytic action, Chemical physics letters, 187 (1991) 73-76.

[51] R.I. Bickley, T. Gonzalez-Carreno, J.S. Lees, L. Palmisano, R.J. Tilley, A structural investigation of titanium dioxide photocatalysts, Journal of Solid State Chemistry, 92 (1991) 178-190.

[52] S.-J. Tsai, S. Cheng, Effect of TiO2 crystalline structure in photocatalytic degradation of phenolic contaminants, Catalysis Today, 33 (1997) 227-237.

[53] Y. Nakabayashi, Y. Nosaka, OH Radical Formation at Distinct Faces of Rutile TiO_2 Crystal in the Procedure of Photoelectrochemical Water Oxidation, The Journal of Physical Chemistry C, 117 (2013) 23832-23839.

[54] Y. Zhang, Z.-R. Tang, X. Fu, Y.-J. Xu, TiO_2− graphene nanocomposites for gas-phase photocatalytic degradation of volatile aromatic pollutant: is TiO_2− graphene truly different from other TiO_2− carbon composite materials?, Acs Nano, 4 (2010) 7303-7314.

[55] W.S. Hummers Jr, R.E. Offeman, Preparation of graphitic oxide, Journal of the American Chemical Society, 80 (1958) 1339-1339.

[56] Z. Peining, A.S. Nair, P. Shengjie, Y. Shengyuan, S. Ramakrishna, Facile Fabrication of TiO2–Graphene Composite with Enhanced Photovoltaic and Photocatalytic Properties by Electrospinning, ACS Applied Materials & Interfaces, 4 (2012) 581-585.

[57] J.H. Park, S. Kim, A.J. Bard, Novel carbon-doped TiO2 nanotube arrays with high aspect ratios for efficient solar water splitting, Nano Letters, 6 (2006) 24-28.

[58] G. Liu, L. Wang, H.G. Yang, H.-M. Cheng, G.Q.M. Lu, Titania-based photocatalysts—crystal growth, doping and heterostructuring, Journal of Materials Chemistry, 20 (2010) 831-843.

[59] T. Sekine, H. Kanda, Y. Bando, M. Yokoyama, K. Hojou, A graphitic carbon nitride, Journal of Materials Science Letters, 9 (1990) 1376-1378.

[60] A. Rubio, J.L. Corkill, M.L. Cohen, Theory of graphitic boron nitride nanotubes, Physical Review B, 49 (1994) 5081.

[61] A. Thomas, A. Fischer, F. Goettmann, M. Antonietti, J.-O. Müller, R. Schlögl, J.M. Carlsson, Graphitic carbon nitride materials: variation of structure and morphology and their use as metal-free catalysts, Journal of Materials Chemistry, 18 (2008) 4893-4908.

[62] X. Wang, K. Maeda, A. Thomas, K. Takanabe, G. Xin, J.M. Carlsson, K. Domen, M. Antonietti, A metal-free polymeric photocatalyst for hydrogen production from water under visible light, Nature materials, 8 (2008) 76-80.

[63] T. Kobayashi, H. Yoneyama, H. Tamura, Polyaniline film-coated electrodes as electrochromic display devices, Journal of electroanalytical chemistry and interfacial electrochemistry, 161 (1984) 419-423.

[64] B.L. Laurin, Abrasion and antifog-resistant optical element, in, Google Patents, 1977.

[65] F. Jonas, W. Krafft, B. Muys, Poly (3, 4-ethylenedioxythiophene): Conductive coatings, technical applications and properties, in: Macromolecular Symposia, Wiley Online Library, 1995, pp. 169-173.

[66] Y. Yu, M. Nakano, T. Ikeda, Photomechanics: directed bending of a polymer film by light, Nature, 425 (2003) 145-145.

[67] C.D. Dimitrakopoulos, D.J. Mascaro, Organic thin-film transistors: A review of recent advances, IBM Journal of Research and Development, 45 (2001) 11-27.

[68] B.P. Rand, D.P. Burk, S.R. Forrest, Offset energies at organic semiconductor heterojunctions and their influence on the open-circuit voltage of thin-film solar cells, Physical Review B, 75 (2007) 115327.

[69] M. Deifallah, P.F. McMillan, F. Corà, Electronic and structural properties of two-dimensional carbon nitride graphenes, The Journal of Physical Chemistry C, 112 (2008) 5447-5453.

[70] L. Gmelin, Ueber einige Verbindungen des Melon's, Annalen der Pharmacie, 15 (1835) 252-258.

[71] A.Y. Liu, M.L. Cohen, Prediction of new low compressibility solids, Science, 245 (1989) 841-842.

[72] M. Groenewolt, M. Antonietti, Synthesis of g-C_3N_4 Nanoparticles in Mesoporous Silica Host Matrices, Advanced Materials, 17 (2005) 1789-1792.

[73] S. Yan, Z. Li, Z. Zou, Photodegradation performance of g-C_3N_4 fabricated by directly heating melamine, Langmuir, 25 (2009) 10397-10401.

[74] Q. Xiang, J. Yu, M. Jaroniec, Preparation and Enhanced Visible-Light Photocatalytic H_2-Production Activity of Graphene/C3N4 Composites, The Journal of Physical Chemistry C, 115 (2011) 7355-7363.

[75] Y. Tian, B. Chang, J. Lu, J. Fu, F. Xi, X. Dong, Hydrothermal synthesis of graphitic carbon nitride–Bi2WO6 heterojunctions with enhanced visible light photocatalytic activities, ACS Applied Materials & Interfaces, 5 (2013) 7079-7085.

[76] F. Goettmann, A. Fischer, M. Antonietti, A. Thomas, Chemical Synthesis of Mesoporous Carbon Nitrides Using Hard Templates and Their Use as a Metal-Free Catalyst for Friedel–Crafts Reaction of Benzene, Angewandte Chemie International Edition, 45 (2006) 4467-4471.

[77] X. Wang, K. Maeda, A. Thomas, K. Takanabe, G. Xin, J.M. Carlsson, K. Domen, M. Antonietti, A metal-free polymeric photocatalyst for hydrogen production from water under visible light, Nat Mater, 8 (2009) 76-80.

[78] Z.D. Gao, Y.F. Qu, X. Zhou, L. Wang, Y.Y. Song, P. Schmuki, Pt-Decorated g-C_3N_4/TiO_2 Nanotube Arrays with Enhanced Visible-Light Photocatalytic Activity for H_2 Evolution, ChemistryOpen, (2016).

[79] M. Seredych, S. Łoś, D.A. Giannakoudakis, E. Rodríguez-Castellón, T.J. Bandosz, Photoactivity of g-C3N4/S-Doped Porous Carbon Composite: Synergistic Effect of Composite Formation, ChemSusChem, 9 (2016) 795-799.

[80] Y. Zhang, J. Liu, G. Wu, W. Chen, Porous graphitic carbon nitride synthesized via direct polymerization of urea for efficient sunlight-driven photocatalytic hydrogen production, Nanoscale, 4 (2012) 5300-5303.

[81] Y.-S. Jun, E.Z. Lee, X. Wang, W.H. Hong, G.D. Stucky, A. Thomas, From Melamine-Cyanuric Acid Supramolecular Aggregates to Carbon Nitride Hollow Spheres, Advanced Functional Materials, 23 (2013) 3661-3667.

[82] J. Huang, M. Antonietti, J. Liu, Bio-inspired carbon nitride mesoporous spheres for artificial photosynthesis: photocatalytic cofactor regeneration for sustainable enzymatic synthesis, Journal of Materials Chemistry A, 2 (2014) 7686-7693.

[83] J. Zhang, M. Zhang, C. Yang, X. Wang, Nanospherical Carbon Nitride Frameworks with Sharp Edges Accelerating Charge Collection and Separation at a Soft Photocatalytic Interface, Advanced Materials, 26 (2014) 4121-4126.

[84] M. Diba, D.W. Fam, A.R. Boccaccini, M.S. Shaffer, Electrophoretic deposition of graphene-related materials: A review of the fundamentals, Progress in Materials Science, 82 (2016) 83-117.

[85] X. Zhang, X. Xie, H. Wang, J. Zhang, B. Pan, Y. Xie, Enhanced Photoresponsive Ultrathin Graphitic-Phase C3N4 Nanosheets for Bioimaging, Journal of the American Chemical Society, 135 (2013) 18-21.

[86] S. Yang, Y. Gong, J. Zhang, L. Zhan, L. Ma, Z. Fang, R. Vajtai, X. Wang, P.M. Ajayan, Exfoliated Graphitic Carbon Nitride Nanosheets as Efficient Catalysts for Hydrogen Evolution Under Visible Light, Advanced Materials, 25 (2013) 2452-2456.

[87] P. Niu, L. Zhang, G. Liu, H.-M. Cheng, Graphene-Like Carbon Nitride Nanosheets for Improved Photocatalytic Activities, Advanced Functional Materials, 22 (2012) 4763-4770.

[88] J. Liu, H. Wang, Z.P. Chen, H. Moehwald, S. Fiechter, R. van de Krol, L. Wen, L. Jiang, M. Antonietti, Microcontact-Printing-Assisted Access of Graphitic Carbon Nitride Films with Favorable Textures toward Photoelectrochemical Application, Advanced Materials, 27 (2015) 712-718.

[89] X.-H. Li, J. Zhang, X. Chen, A. Fischer, A. Thomas, M. Antonietti, X. Wang, Condensed Graphitic Carbon Nitride Nanorods by Nanoconfinement: Promotion of Crystallinity on Photocatalytic Conversion, Chemistry of materials, 23 (2011) 4344-4348.

[90] J. Liu, R. Cazelles, Z.P. Chen, H. Zhou, A. Galarneau, M. Antonietti, The bioinspired construction of an ordered carbon nitride array for photocatalytic mediated enzymatic reduction, Physical Chemistry Chemical Physics, 16 (2014) 14699-14705.

[91] J. Liu, J. Huang, D. Dontosova, M. Antonietti, Facile synthesis of carbon nitride micro-/nanoclusters with photocatalytic activity for hydrogen evolution, RSC Advances, 3 (2013) 22988-22993.

[92] M. Groenewolt, M. Antonietti, Synthesis of g-C3N4 Nanoparticles in Mesoporous Silica Host Matrices, Advanced Materials, 17 (2005) 1789-1792.

[93] S. Barman, M. Sadhukhan, Facile bulk production of highly blue fluorescent graphitic carbon nitride quantum dots and their application as highly selective and sensitive sensors for the detection of mercuric and iodide ions in aqueous media, Journal of Materials Chemistry, 22 (2012) 21832-21837.

[94] S. Zhang, J. Li, M. Zeng, J. Xu, X. Wang, W. Hu, Polymer nanodots of graphitic carbon nitride as effective fluorescent probes for the detection of Fe^{3+} and Cu^{2+} ions, Nanoscale, 6 (2014) 4157-4162.

[95] S. Zhao, S. Chen, H. Yu, X. Quan, g-C_3N_4/TiO_2 hybrid photocatalyst with wide absorption wavelength range and effective photogenerated charge separation, Separation and Purification Technology, 99 (2012) 50-54.

[96] X. Lu, Q. Wang, D. Cui, Preparation and Photocatalytic Properties of g-C_3N_4/TiO_2 Hybrid Composite, Journal of Materials Science & Technology, 26 (2010) 925-930.

[97] Q. Li, L. Zong, Y. Xing, X. Wang, L. Yu, J. Yang, Preparation of g-C3N4/TiO2 Nanocomposites and Investigation of Their Photocatalytic Activity, Science of Advanced Materials, 5 (2013) 1316-1322.

[98] J. Fu, B. Chang, Y. Tian, F. Xi, X. Dong, Novel C_3N_4–CdS composite photocatalysts with organic–inorganic heterojunctions: in situ synthesis, exceptional activity, high stability and photocatalytic mechanism, Journal of Materials Chemistry A, 1 (2013) 3083-3090.

[99] J. Fu, Y. Tian, B. Chang, F. Xi, X. Dong, BiOBr–carbon nitride heterojunctions: synthesis, enhanced activity and photocatalytic mechanism, Journal of Materials Chemistry, 22 (2012) 21159-21166.

[100] Q. Xiang, J. Yu, M. Jaroniec, Synergetic effect of MoS_2 and graphene as cocatalysts for enhanced photocatalytic H_2 production activity of TiO_2 nanoparticles, Journal of the American Chemical Society, 134 (2012) 6575-6578.

[101] A. Ajayaghosh, Donor–acceptor type low band gap polymers: polysquaraines and related systems, Chemical Society Reviews, 32 (2003) 181-191.

[102] J. Hou, H.-Y. Chen, S. Zhang, R.I. Chen, Y. Yang, Y. Wu, G. Li, Synthesis of a Low Band Gap Polymer and Its Application in Highly Efficient Polymer Solar Cells, Journal of the American Chemical Society, 131 (2009) 15586-15587.

[103] S.C. Price, A.C. Stuart, L. Yang, H. Zhou, W. You, Fluorine Substituted Conjugated Polymer of Medium Band Gap Yields 7% Efficiency in Polymer−Fullerene Solar Cells, Journal of the American Chemical Society, 133 (2011) 4625-4631.

[104] Y. Wang, Y. Di, M. Antonietti, H. Li, X. Chen, X. Wang, Excellent Visible-Light Photocatalysis of Fluorinated Polymeric Carbon Nitride Solids, Chemistry of materials, 22 (2010) 5119-5121.

[105] T. Shimada, H. Yamazaki, M. Mimura, Y. Inui, F.P. Guengerich, Interindividual variations in human liver cytochrome P-450 enzymes involved in the oxidation of drugs, carcinogens and toxic chemicals: studies with liver microsomes of 30 Japanese and 30 Caucasians, Journal of Pharmacology and Experimental Therapeutics, 270 (1994) 414-423.

[106] D.B. McGregor, A.G. Brown, S. Howgate, D. McBride, C. Riach, W.J. Caspary, J. Carver, Responses of the L5178Y mouse lymphoma cell forward mutation assay. V: 27 coded chemicals, Environmental and molecular mutagenesis, 17 (1991) 196-219.

[107] J.C. Mirsalis, C.K. Tyson, K.L. Steinmetz, E.K. Loh, C.M. Hamilton, J.P. Bakke, J.W. Spalding, Measurement of unscheduled DNA synthesis and S-phase synthesis in rodent hepatocytes following in vivo treatment: Testing of 24 compounds, Environmental and molecular mutagenesis, 14 (1989) 155-164.

[108] J. Wang, P. Guo, Q. Guo, P.G. Jönsson, Z. Zhao, Fabrication of novel g- C_3N_4/nanocage ZnS composites with enhanced photocatalytic activities under visible light irradiation, CrystEngComm, 16 (2014) 4485-4492.

[109] Q. Li, N. Zhang, Y. Yang, G. Wang, D.H. Ng, High efficiency photocatalysis for pollutant degradation with MoS_2/ C_3N_4 heterostructures, Langmuir, 30 (2014) 8965-8972.

[110] D. Jiang, J. Zhu, M. Chen, J. Xie, Highly efficient heterojunction photocatalyst based on nanoporous g-C_3N_4 sheets modified by Ag_3PO_4 nanoparticles: Synthesis and enhanced photocatalytic activity, Journal of Colloid and Interface Science, 417 (2014) 115-120.

[111] C. Xing, Z. Wu, D. Jiang, M. Chen, Hydrothermal synthesis of In_2S_3/g- C_3N_4 heterojunctions with enhanced photocatalytic activity, Journal of Colloid and Interface Science, 433 (2014) 9-15.

[112] N. Tian, H. Huang, Y. He, Y. Guo, Y. Zhang, Novel g- C_3N_4/$BiIO_4$ heterojunction photocatalysts: synthesis, characterization and enhanced visible-light-responsive photocatalytic activity, RSC Advances, 4 (2014) 42716-42722.

[113] W. Shi, F. Guo, J. Chen, G. Che, X. Lin, Hydrothermal synthesis of $InVO_4$/Graphitic carbon nitride heterojunctions and excellent visible-light-driven photocatalytic performance for rhodamine B, Journal of Alloys and Compounds, 612 (2014) 143-148.

[114] X. Wang, L. Zhang, H. Lin, Q. Nong, Y. Wu, T. Wu, Y. He, Synthesis and characterization of a ZrO_2/g- C_3N_4 composite with enhanced visible-light photoactivity for rhodamine degradation, RSC Advances, 4 (2014) 40029-40035.

[115] T. Li, L. Zhao, Y. He, J. Cai, M. Luo, J. Lin, Synthesis of g- C_3N_4/$SmVO_4$ composite photocatalyst with improved visible light photocatalytic activities in RhB degradation, Applied Catalysis B: Environmental, 129 (2013) 255-263.

[116] Y. Hong, Y. Jiang, C. Li, W. Fan, X. Yan, M. Yan, W. Shi, In-situ synthesis of direct solid-state Z-scheme V_2O_5/g- C_3N_4 heterojunctions with enhanced visible light efficiency in photocatalytic degradation of pollutants, Applied Catalysis B: Environmental, 180 (2016) 663-673.

[117] S. Kumar, S. Tonda, A. Baruah, B. Kumar, V. Shanker, Synthesis of novel and stable gC3N4/N-doped SrTiO 3 hybrid nanocomposites with improved photocurrent and photocatalytic activity under visible light irradiation, Dalton Transactions, 43 (2014) 16105-16114.

[118] W. Li, C. Feng, S. Dai, J. Yue, F. Hua, H. Hou, Fabrication of sulfur-doped g-C_3N_4/Au/CdS Z-scheme photocatalyst to improve the photocatalytic performance under visible light, Applied Catalysis B: Environmental, 168 (2015) 465-471.

[119] H. Ma, Q. Zhuo, B. Wang, Electro-catalytic degradation of methylene blue wastewater assisted by Fe 2 O 3-modified kaolin, Chemical Engineering Journal, 155 (2009) 248-253.

[120] A. Houas, H. Lachheb, M. Ksibi, E. Elaloui, C. Guillard, J.-M. Herrmann, Photocatalytic degradation pathway of methylene blue in water, Applied Catalysis B: Environmental, 31 (2001) 145-157.

[121] L. Gu, J. Wang, Z. Zou, X. Han, Graphitic- C_3N_4-hybridized TiO_2 nanosheets with reactive {001} facets to enhance the UV-and visible-light photocatalytic activity, Journal of hazardous materials, 268 (2014) 216-223.

[122] K. Sridharan, E. Jang, T.J. Park, Novel visible light active graphitic C_3N_4–TiO_2 composite photocatalyst: synergistic synthesis, growth and photocatalytic treatment of hazardous pollutants, Applied Catalysis B: Environmental, 142 (2013) 718-728.

[123] J. Zhou, M. Zhang, Y. Zhu, Preparation of visible light-driven g- C_3N_4@ ZnO hybrid photocatalyst via mechanochemistry, Physical Chemistry Chemical Physics, 16 (2014) 17627-17633.

[124] D. Chen, K. Wang, D. Xiang, R. Zong, W. Yao, Y. Zhu, Significantly enhancement of photocatalytic performances via core–shell structure of ZnO@ mpg- C_3N_4, Applied Catalysis B: Environmental, 147 (2014) 554-561.

[125] S. Chen, Y. Hu, S. Meng, X. Fu, Study on the separation mechanisms of photogenerated electrons and holes for composite photocatalysts g-C_3N_4-WO_3, Applied Catalysis B: Environmental, 150 (2014) 564-573.

[126] F. Jiang, T. Yan, H. Chen, A. Sun, C. Xu, X. Wang, Ag C_3N_4–CdS composite catalyst with high visible-light-driven catalytic activity and photostability for methylene blue degradation, Applied Surface Science, 295 (2014) 164-172.

[127] L. Huang, H. Xu, R. Zhang, X. Cheng, J. Xia, Y. Xu, H. Li, Synthesis and characterization of gC 3 N 4/MoO 3 photocatalyst with improved visible-light photoactivity, Applied Surface Science, 283 (2013) 25-32.

[128] X. Dang, X. Zhang, Y. Chen, X. Dong, G. Wang, C. Ma, X. Zhang, H. Ma, M. Xue, Preparation of β-Bi2O3/g-C3N4 nanosheet p–n junction for enhanced photocatalytic ability under visible light illumination, Journal of Nanoparticle Research, 17 (2015) 1-8.

[129] J. Zhang, Y. Hu, X. Jiang, S. Chen, S. Meng, X. Fu, Design of a direct Z-scheme photocatalyst: Preparation and characterization of Bi_2O_3/g-C_3N_4 with high visible light activity, Journal of hazardous materials, 280 (2014) 713-722.

[130] J.P. Brown, P.S. Dietrich, Mutagenicity of selected sulfonated azo dyes in the Salmonella/microsome assay: use of aerobic and anaerobic activation procedures, Mutation Research/Genetic Toxicology, 116 (1983) 305-315.

[131] J.-X. Sun, Y.-P. Yuan, L.-G. Qiu, X. Jiang, A.-J. Xie, Y.-H. Shen, J.-F. Zhu, Fabrication of composite photocatalyst gC 3 N 4–ZnO and enhancement of photocatalytic activity under visible light, Dalton Transactions, 41 (2012) 6756-6763.

[132] H. Xu, J. Yan, Y. Xu, Y. Song, H. Li, J. Xia, C. Huang, H. Wan, Novel visible-light-driven AgX/graphite-like C 3 N 4 (X= Br, I) hybrid materials with synergistic photocatalytic activity, Applied Catalysis B: Environmental, 129 (2013) 182-193.

[133] Y. Tian, B. Chang, J. Fu, B. Zhou, J. Liu, F. Xi, X. Dong, Graphitic carbon nitride/Cu 2 O heterojunctions: Preparation, characterization, and enhanced photocatalytic activity under visible light, Journal of Solid State Chemistry, 212 (2014) 1-6.

[134] J. Fu, B. Chang, Y. Tian, F. Xi, X. Dong, Novel C_3N_4–CdS composite photocatalysts with organic–inorganic heterojunctions: in situ synthesis, exceptional activity, high stability and photocatalytic mechanism, Journal of Materials Chemistry A, 1 (2013) 3083-3090.

[135] C. Han, L. Ge, C. Chen, Y. Li, X. Xiao, Y. Zhang, L. Guo, Novel visible light induced Co 3O4-g-C3N4 heterojunction photocatalysts for efficient degradation of methyl orange, Applied Catalysis B: Environmental, 147 (2014) 546-553.

[136] S. Wang, D. Li, C. Sun, S. Yang, Y. Guan, H. He, Synthesis and characterization of g-C_3N_4/Ag_3VO_4 composites with significantly enhanced visible-light photocatalytic activity for triphenylmethane dye degradation, Applied Catalysis B: Environmental, 144 (2014) 885-892.

[137] W. Zhao, Y. Guo, S. Wang, H. He, C. Sun, S. Yang, A novel ternary plasmonic photocatalyst: ultrathin gC 3 N 4 nanosheet hybrided by Ag/$AgVO_3$ nanoribbons with enhanced visible-light photocatalytic performance, Applied Catalysis B: Environmental, 165 (2015) 335-343.

[138] B. Peng, S. Zhang, S. Yang, H. Wang, H. Yu, S. Zhang, F. Peng, Synthesis and characterization of g-C_3N_4/Cu_2O composite catalyst with enhanced photocatalytic activity under visible light irradiation, Materials Research Bulletin, 56 (2014) 19-24.

[139] J. Lei, Y. Chen, F. Shen, L. Wang, Y. Liu, J. Zhang, Surface modification of TiO_2 with g-C3N4 for enhanced UV and visible photocatalytic activity, Journal of Alloys and Compounds, 631 (2015) 328-334.

[140] H. Zhang, L. Zhao, F. Geng, L.-H. Guo, B. Wan, Y. Yang, Carbon dots decorated graphitic carbon nitride as an efficient metal-free photocatalyst for phenol degradation, Applied Catalysis B: Environmental, 180 (2016) 656-662.

[141] Y. Ren, Q. Zhao, X. Li, W. Xiong, M. Tade, L. Liu, 2D Porous graphitic C_3N_4 nanosheets/Ag_3PO_4 nanocomposites for enhanced visible-light photocatalytic degradation of 4-chlorophenol, Journal of Nanoparticle Research, 16 (2014) 1-8.

[142] J. Xia, J. Di, S. Yin, H. Li, H. Xu, L. Xu, H. Shu, M. He, Solvothermal synthesis and enhanced visible-light photocatalytic decontamination of bisphenol A (BPA) by g-C_3N_4/BiOBr heterojunctions, Materials Science in Semiconductor Processing, 24 (2014) 96-103.

[143] S.-Z. Wu, C.-H. Chen, W.-D. Zhang, Etching graphitic carbon nitride by acid for enhanced photocatalytic activity toward degradation of 4-nitrophenol, Chinese Chemical Letters, 25 (2014) 1247-1251.

[144] X. Rong, F. Qiu, Z. Jiang, J. Rong, J. Pan, T. Zhang, D. Yang, Preparation of ternary combined ZnO-Ag_2O/porous g-C_3N_4 composite photocatalyst and enhanced visible-light photocatalytic activity for degradation of ciprofloxacin, Chemical Engineering Research and Design, 111 (2016) 253-261.

[145] J. Xue, S. Ma, Y. Zhou, Z. Zhang, M. He, Facile Photochemical Synthesis of Au/Pt/ g-C_3N_4 with Plasmon-Enhanced Photocatalytic Activity for Antibiotic Degradation, ACS Applied Materials & Interfaces, 7 (2015) 9630-9637.

[147] S. Ma, J. Xue, Y. Zhou, Z. Zhang, Enhanced visible-light photocatalytic activity of Ag_2O/ g-C_3N_4 p–n heterojunctions synthesized via a photochemical route for degradation of tetracycline hydrochloride, RSC Advances, 5 (2015) 40000-40006.

[148] L. Basabe-Desmonts, D.N. Reinhoudt, M. Crego-Calama, Design of fluorescent materials for chemical sensing, Chemical Society Reviews, 36 (2007) 993-1017.

[149] E.Z. Lee, Y.-S. Jun, W.H. Hong, A. Thomas, M.M. Jin, Cubic Mesoporous Graphitic Carbon(IV) Nitride: An All-in-One Chemosensor for Selective Optical Sensing of Metal Ions, Angewandte Chemie International Edition, 49 (2010) 9706-9710.

[150] J. Tian, Q. Liu, A.M. Asiri, A.H. Qusti, A.O. Al-Youbi, X. Sun, Ultrathin graphitic carbon nitride nanosheets: a novel peroxidase mimetic, Fe doping-mediated catalytic performance enhancement and application to rapid, highly sensitive optical detection of glucose, Nanoscale, 5 (2013) 11604-11609.

[151] T.Y. Ma, Y. Tang, S. Dai, S.Z. Qiao, Proton-Functionalized Two-Dimensional Graphitic Carbon Nitride Nanosheet: An Excellent Metal-/Label-Free Biosensing Platform, Small, 10 (2014) 2382-2389.

[152] M. Rong, L. Lin, X. Song, Y. Wang, Y. Zhong, J. Yan, Y. Feng, X. Zeng, X. Chen, Fluorescence sensing of chromium (VI) and ascorbic acid using graphitic carbon nitride nanosheets as a fluorescent “switch”, Biosensors and Bioelectronics, 68 (2015) 210-217.

[153] Q. Gao, S. Wang, Y. Ma, Y. Tang, C. Giordano, M. Antonietti, SiO_2-Surface-Assisted Controllable Synthesis of TaON and Ta_3N_5 Nanoparticles for Alkene Epoxidation, Angewandte Chemie International Edition, 51 (2012) 961-965.

[154] X.-H. Li, S. Kurasch, U. Kaiser, M. Antonietti, Synthesis of Monolayer-Patched Graphene from Glucose, Angewandte Chemie International Edition, 51 (2012) 9689-9692.

3

3 Metal-free Melem/g − C_3N_4 Heterojunction Photocatalysts by Hydrothermal synthesis for Water Treatment

This paper has been published in Journal of Colloid and Interface Science in Volume 464, 15 February 2016, Pages 10–17

3.1 Abstract

In this study, a simple method was engineered to synthesise metal-free melem/$g-C_3N_4$ heterojunction photocatalyst through hydrothermal treatment. XRD and SEM investigations revealed that hydrothermal treatment of $g-C_3N_4$ could produce a heterojunctional structure of "thorn ball" liked melem on $g-C_3N_4$ layer at rising temperatures, which leads to modified photoelectric properties of $g-C_3N_4$. The DRS and PL measurements implied that melem/ $g-C_3N_4$ heterojunction has better light absorption but weaken photo electron/hole recombination. The melem/g-C_3N_4 photocatalysts could decompose methylene blue solution under solar radiation with a higher rate.

3.2 Introduction

Global energy crisis and environment deterioration are dramatically threating the ecosystem and human civilization development. New clean energy is urgently considered to tackle this problem once and for all. Latest studies suggest solar energy should be a best candidate to those challenges, because radiation energy is a barely costing, abundant and a sustainable energy resource[1]. In a typical photovoltaic device, photosensitive semiconductor is the core medium to extract and convert radiation into electrical energy, where the electron in semiconductor valence band can be excited into conduction band while an electronic hole remained in the conduction band. This erratic status bestow oxide potentials to photosensitive semiconductor to complete an energy conversion process[2]. In 1967, photocatalysis has been

firstly found to split water into hydrogen gas[3], which presented a bright view of photocatalysis in hydrogen energy production, and now photocatalysis is widely utilized toward environmental treatment due to oxidizing radical generation[4-6].

Generally speaking, crystalline metal oxide compounds with appropriate energy levels have ability to generate hydroxyl (•OH) and superoxide anion radicals ($\bullet O_2^-$) under illumination, which have strong oxidation ability to degrade or decompose pollutants (such as metal leaching and organic compounds) into environmentally friendly compounds [7-10], but classic metal oxide semiconductors have a wide band gap energy requiring high power radiation to excite electronic pairs, at the same time high pair recombination limited photovoltaic quantum yield and photocatalytic efficiency. The wide band gap energy restricts most of photosensitive semiconductors to be excited only by ultra-violet radiation, which only has 5% intensity in solar energy[11, 12]. Recently, a metal-free semiconductor, graphitic carbon nitride ($g-C_3N_4$), was found to split water into hydrogen gas under 430 nm visible radiation[12]. Graphitic carbon nitride has been discerned potentially as a breakthrough in photocatalytic and photovoltaic agents[13]. However, g-C_3N_4 has unsatisfied photocatalytic efficiency contributed to the low surface area and high electronic pair recombination rate [14-16].
Theoretically, polymeric $g-C_3N_4$ is a single layer composite similar to graphene. In spite of nitrogen atom participation, it's skeleton is based on periodic tri-s-triazine aromatic blocks [17]. During the thermal condensation toward $g-C_3N_4$formation, the layer structure unit "Melem" is produced at around 400 - 450 °C [18-20]. It is a three polycyclic aromatic hydrocarbons around by NH_2-bearing groups and the unique electronic state endows melon ability to react with electrophiles to form various Melem derivatives[8]. Meanwhile, melem has special photoelectric properties in band-gap structure and surface properties[21, 22]. Very recently, Melem was reported to show activities to split H_2 from water[18].

Herein, we report a metal-free heterojunction photocatalyst consisted of melem and $g-C_3N_4$, which was prepared by a hydrothermal method at mild temperatures. The Melem/ $g-C_3N_4$heterojunction material exhibited strong photocatalytic activities and high stability toward decomposition of methylene blue solution under artificial solar radiation. The study suggests melem composites can weaken the electronic pair recombination by dislocated photo generated electron from $g-C_3N_4$. The significantly increased surface area enhanced pollutant adsorption thereby leading to high photocatalytic efficiency.

3.3 Experiment

Preparation of graphitic carbon nitride and melem/ $g-C_3N_4$ photocatalysts

All chemicals are in high purity. Melamine powder (99.9%) and methanol (99.8%) were obtained from Sigma-Aldrich Corporation.

Graphitic carbon nitride was prepared by melamine condensation method. Melamine (30 g) was placed in an opened crucible with 50 ml methanol. This suspension was stirred by a glass bar for 5 min and then dried in an oven at 40 ℃. Then the crucible was semi-closed and heated in a muffle furnace at a heating rate of 10 ^{o}C/min to reach 520 ^{o}C and kept for 4 h. A yellow product $g-C_3N_4$was obtained and further grounding into fine powder by an agate mortar[23]. For synthesis of Melem/ $g-C_3N_4$heterojunction photocatalysts, one gram $g-C_3N_4$particle and 50 mL deionized water were put in a 80 mL Teflon autoclave under thermal treatment at 130, 150, 180 and 200 ^{o}C for 12 h, individually. The products were centrifuged at 8000 rpm to

separate liquid phase and then washed by 100 mL ethanol and DI water for three times. The final solids were dried at 80 ^{o}C in air and referred as MGCN-130, MGCN-150, MGCN-180 and MGCN-200, accordingly.

Characterization of materials

The crystalline structure of samples was analyzed by powder X-ray diffraction (XRD) using a Bruker D8-Advance X-Ray diffractometer with Cu Kα radiation (λ = 1.5418 Å) operated at 40 kV and 100 mA. FTIR analysis was performed on a Perkin-Elmer Model FTIR-100 with a MIR detector. UV–vis diffuse reflectance spectra (DRS) were recorded on a JASCO V670 spectrophotometer with an Ø 60 mm integrating sphere, BaSO4 was used as a reference material. Field emission scanning electron microscopy (SEM), performed on Zeiss Neon 40EsB, was used to study morphology, size and texture. Thermogravimetric-differential thermal analysis (TG-DTA) was carried out on a TGA/DSC 1 instrument of Mettler-Toledo under argon flow at a heating rate of 10 ^{o}C/min. Surface area and pore size distribution were evaluated by nitrogen adsorption–desorption isotherms at -196 ^{o}C using a Quantachrome Autosorb AS-1. The degassing operation was processed at 120 ^{o}C for 12 h. X-ray photoelectron spectroscopy (XPS) was on a Thermo Escalab 250 with Al-Kα X-ray, C 1s peak calibration was at 284.6 eV.

Photocatalytic tests

Photodegradation of methylene blue solution (MB) was adopted to evaluate photocatalytic performances and the experiments were conducted under artificial solar light or visible radiation by adding a 430 nm light filter. In a standard process, MB (10 mg/L, 200 mL) solution

and the photocatalysts (100 mg) were put into a 1- L double-jacket cylindrical reactor with stirring and 25 ℃ . The photoreaction vessel was 30 cm away from the radiation source. The intensities of the artificial solar radiation were at 2.31 μW/cm^2 (220-280 nm), 6.94 mW/cm2 (315-400 nm), and 129.3 mW/cm^2 (400-1050 nm). Visible radiation (within a cut-off filter) provides an intensity of 84 mW/cm^2 at 400-1050 nm. All reactions were started by switching on or off the light. In controlled intervals, 3 mL suspension was collected, and centrifuged, MB solution was analyzed by a JASCO UV-vis spectrophotometer at a wavelength of 664 nm.

3.4 Result and discussion

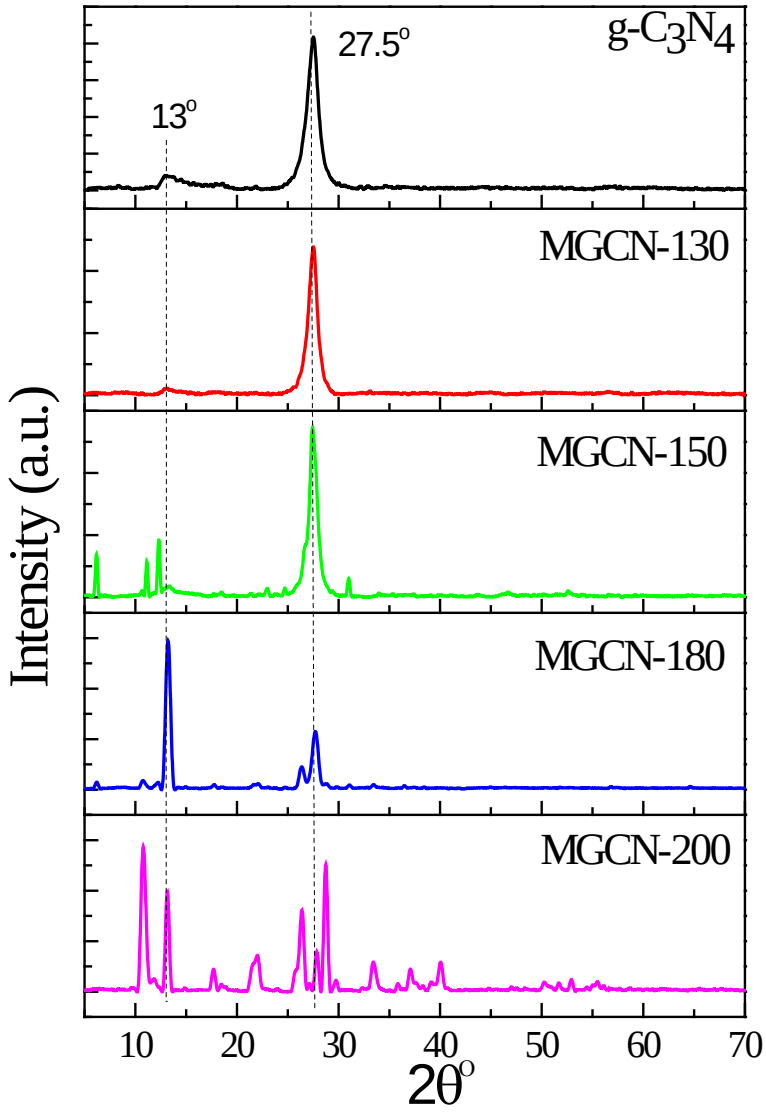

Fig. 5. XRD patterns of g-C3N4, MGCN-130, MGCN-150, MGCN-180 and MGCN-200.

Fig.5 presents XRD patterns of $g-C_3N_4$, MGCN-130, MGCN-150, MGCN-180 and MGCN-200 photocatalysts. Two peaks at 27.5° and 13° in $g-C_3N_4$sample represent (002) and (100) diffraction planes (JCPDS 87-1526)[24]. MGCN-130 is analogous to $g-C_3N_4$. New peaks appear in MGCN-150, the peaks at 6.2, 11.1 and 12.3 ° correspond to trinitrotoluene phenanthrene and the 31 ° is attributed by $C_7H_5NO_4$ which can be implied as structure relocation in high temperature hydrothermal treatment. In MGCN-180 sample, a peak at 26.54^o appeared and the prominent peak at 12.3 ° represents 5,7-dimethyl-2,3-dihydro-1H-1,4-diazepine($C_7H_{12}N_2$), the peak at 11.1° represents 4-(4-dimethylaminophenyl)-1,1-dicyano-1,3-butadiene ($C_{14}H_{13}N_3$). In addition, the symmetry sharp peaks (10.8, 13.16 26.4 and 28.7^o) in MGCN-200 clearly correlates with Melem ($C_3H_6N_6$) units [18, 25]. However the g-C_3N_4 composite also could be detected in the sample. XRD results indicate water has ability to anti-condensation g-C_3N_4 compounds at temperature higher than 150 ℃, this procedure adverse Melem in a genital rate, therefore, MGCN-180 sample is a hybrid with Melem and g-C_3N_4. Until 200 ℃ hot aquaria can hydrolyze $g-C_3N_4$ into melem with an appropriate time.

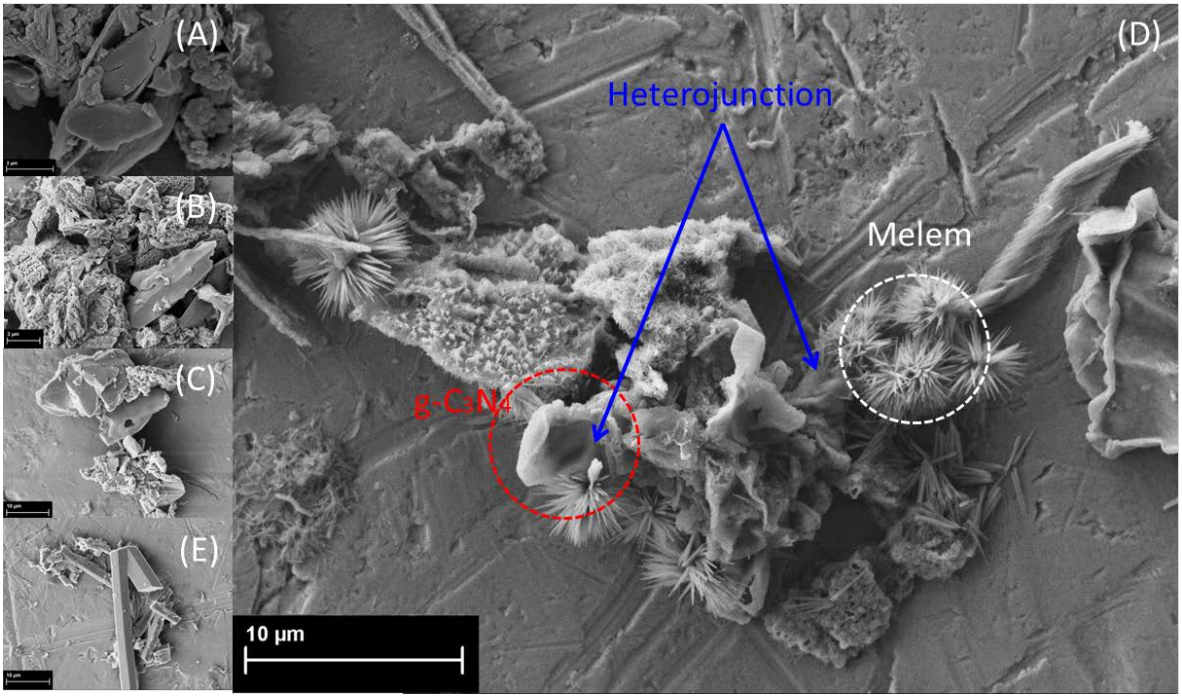

Fig. 6.SEM images of g-C_3N_4 (A), MGCN-130 (B), MGCN-150 (C), MGCN-180 (D) and MGCN-200 (E).

The morphological properties of Melem/ $g-C_3N_4$photocatalysts were studied by SEM. Bulk $g-C_3N_4$ (Fig. 16 A) was clearly seen in stacked layer structure. MGCN-130 and MGCN150 (Fig.16 B, C) present similarly morphological particles as $g-C_3N_4$ indicating thermally stable of $g-C_3N_4$before 150℃ in hydrothermal process. In contrast, MGCN-180 has a dramatically morphologic change. A "thorn ball" liked structure as Melem particles were observed with overlapping $g-C_3N_4$layers. In MGCN-200, a certain amount of hexagonal tubular particle formed, which is contributed to self-assembly construction of melem in the hot solvent [26].

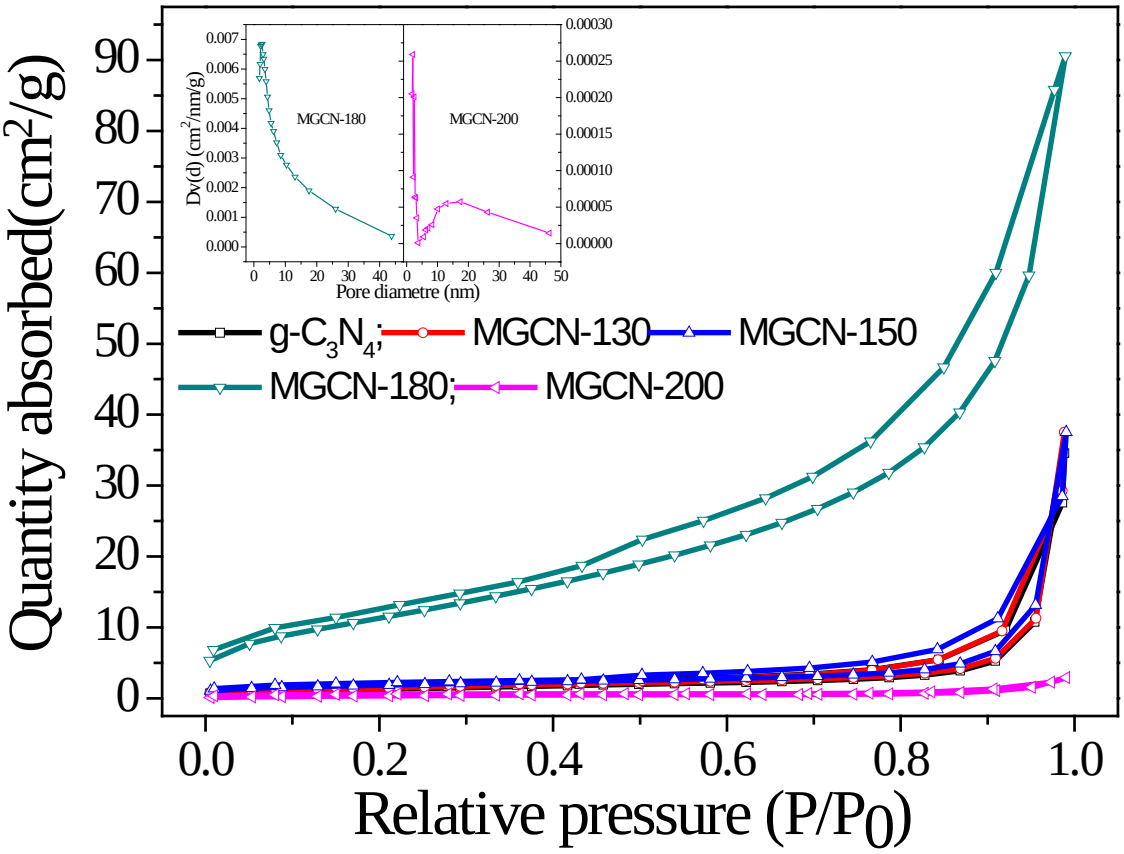

Fig. 7. Nitrogen adsorption–desorption isotherms of g − C_3N_4, MGCN-130, MGCN-150, MGCN-180, MGCN-200; and pore size distribution MGCN-180 and MGCN-200 (Inset graph).

Fig.7 demonstrated N_2 adsorption/desorption isotherms of $g - C_3N_4$, MGCN-130, MGCN-150, MGCN-180 and MGCN-200 samples. All curves show type IV adsorption behavior and H3 type hysteresis loops. The surface areas of $g - C_3N_4$, MGCN-130, MGCN-150, MGCN-180, MGCN-200 are 4.3, 4.9, 6.4, 39.2 and 1.2 m^2/g, respectively. MGCN-180 has the BET surface area about 10 times higher than pristine g-C_3N_4. But the surface area of MGCN-200 is about one quarter of that of carbon nitride. The pore volumes of $g - C_3N_4$and melem/ $g - C_3N_4$ photocatalysts are 0.015 ($g - C_3N_4$), 0.058 (MGCN-130), 0.058 (MGCN-150), 0.140 (MGCN-180) and 0.005 cm^3/g (MGCN-200). The pore size (Fig. 3 inset) of MGCN-180 is in a wide range from 3 to 15 nm Thus, low temperature hydrothermal treatment could not affect

the textural properties of $g-C_3N_4$, but hydrothermal treatment at intermediate temperature could lead to significant enhancements in surface area and pore volume for MGCN-180, which may result in a high activity in photocatalytic performance and unique photoelectric features[27, 28].

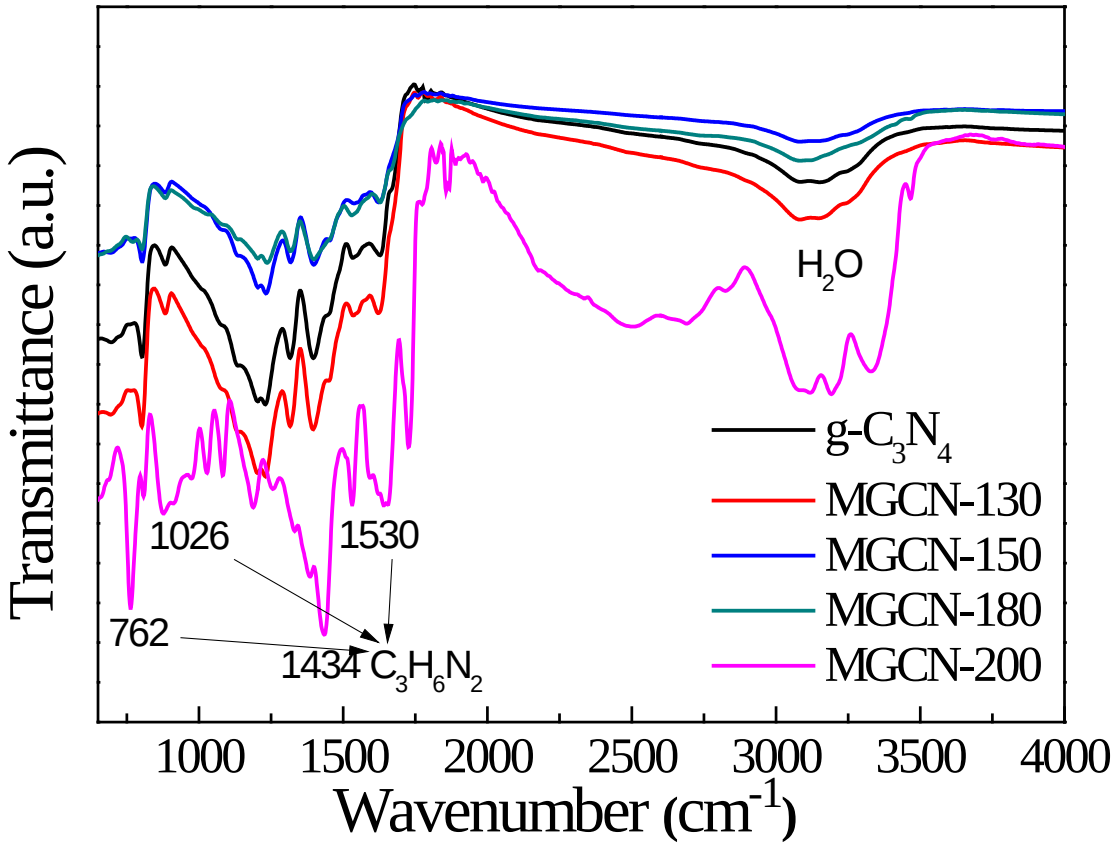

Fig. 8. FTIR spectra of g-C_3N_4, MGCN-130, MGCN-150, MGCN-180 and MGCN- 200.

Surface chemical bonding characteristics of all photocatalysts were studied by FTIR (Fig.8). Pristine $g-C_3N_4$, MGCN-130 and MGCN-150 present similar profiles. The bands in 1200–1650 cm^{-1}correspond to the typical stretching of C-N heterocycles, and the sharp peak at 810 cm^{-1} is attributed to out-of-plane bending vibration of both triazine and heptazine rings [29, 30]. The peak between 3250 and 3070 $cm^{-1}$are referred to the N-H stretching from NH or NH_2 groups. The C-O, C-N and C-C bond are barely distinguished because they have similar force

constants [31]. However, MGCN-180 has similar above bond which is own by exposured g-C_3N_4 substrate. The prominent absorption peaks at 1206, 1235 cm^{-1} and 1316 cm^{-1}have been observed on MGCN-200, attributed to the C-NH-C unit in Melem[32].

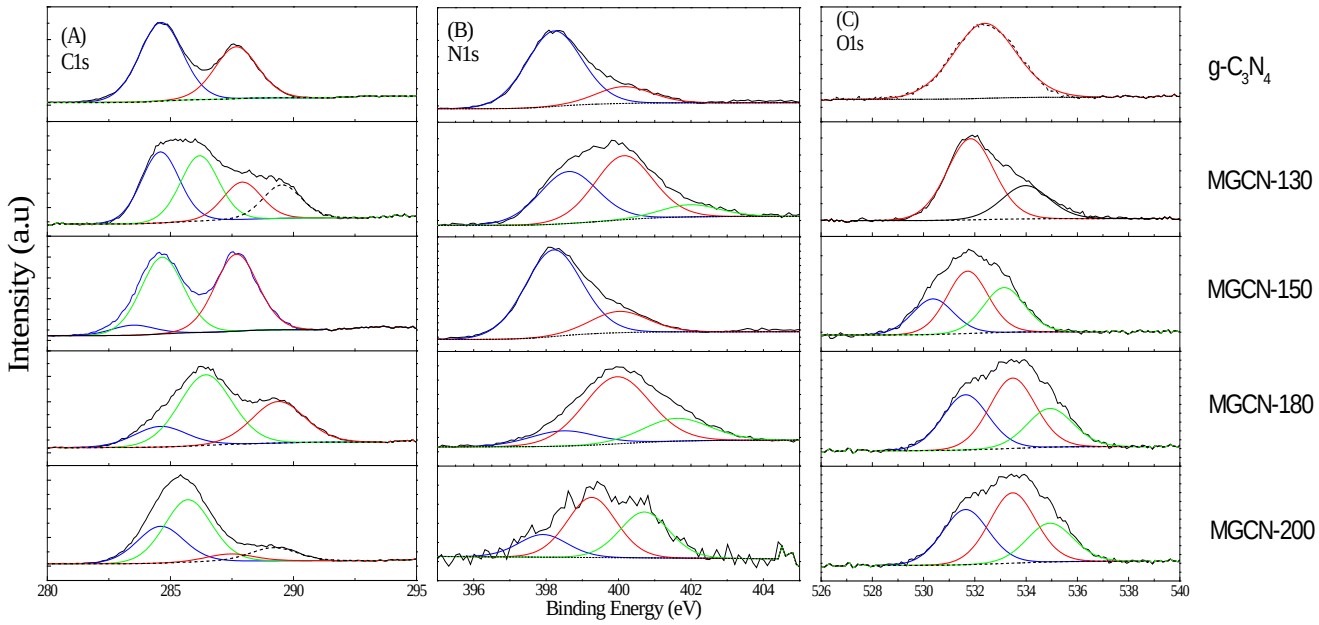

Fig. 9. Carbon 1s, Nitrogen 1s and Oxygen 1s XPS spectra of g-C_3N_4, MGCN-130, MGCN-150, MGCN-180 and MGCN-200 samples.

The surface chemical composites of melem/ $g-C_3N_4$ heterojunction photocatalysts were further determined by XPS. Fig.9 (A) shows the high-resolution C1s XPS spectra of $g-C_3N_4$, MGCN-130, MGCN-150, MGCN-180 and MGCN-200. Two peaks with binding energies at 288.1 and 284.8 eV in g-C_3N_4 are ascribed to the C-N_3 and N_2-C=N coordination in dislocated pi orbits [33, 34]. The binding energy arising at 286.9 eV represents O-bearing bonding (C-OH)[35]. In Fig.20 (A) the binding energy of carbon to nitrogen decreased for the samples at

increasing temperature, while C-OH binding energy apparently enhanced after hydrothermal treatment in H_2O. In N1s XPS spectra (Fig.9 B), three binding energies appeared in all samples, depicting C-N=C (398.6 eV), N-C_3 (399.8 eV) and amino groups C-N-H (401.5 eV)[36]. Fig. 20 C displays oxygen species in melem/ $g-C_3N_4$ particles, and there is a wide binding energy for $g-C_3N_4$at ca. 531.9 eV referred to N-C-O[37]. With hydrothermal treatment, two peaks at 531.6 eV and 534.0 eV appeared in the spectra. These signals could be attributed to the bonds of O–C–N groups and O-O species, respectively [38].

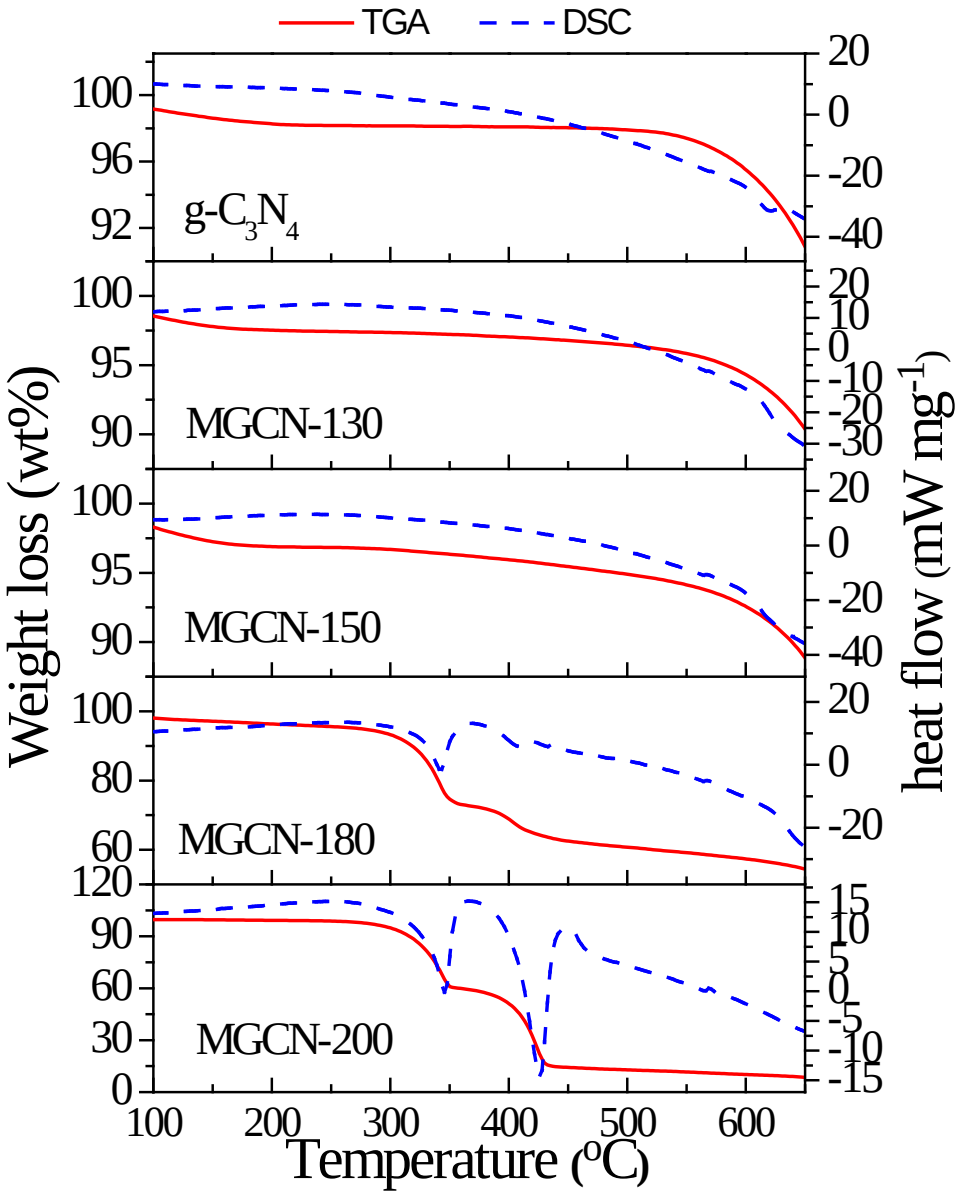

Fig. 10. TG-DSC results of g-C_3N_4, MGCN-130, MGCN-150, MGCN-180 and MGCN- 200.

Thermal gravimetric and differential scanning calorimetric analysis (TG-DSC) of $g-C_3N_4$, MGCN-130, MGCN-150, MGCN-180 and MGCN-200 is demonstrated in Fig.10. The TG-DSC curves of $g-C_3N_4$, MGCN-130, MGCN-150 are roughly the same. The mass losses were mainly happened at 600 ℃ and about 90% weights in sample were remained at the end, whereas MGCN-180 and MGCN-200 have apparently thermal decomposition. Two steps in weight loss at 340 and 420 ℃, were coincided with function groups decomposition and melen recondensation to $g-C_3N_4$[39]. MGCN-180 demonstrated more stabilization than MGCN-

200. After 650 ℃, MGCN-180 remained 60% weight, and MGCN-200 was almost decomposed. It is believed that the regenerated groups of polymeric carbon nitride is unstable at high temperature [26, 40].

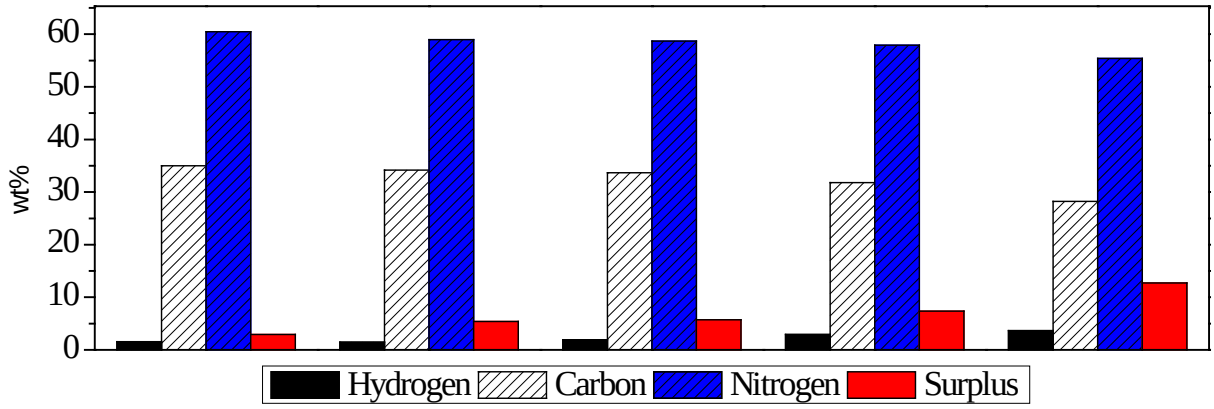

	Carbon (wt%)	*Hydrogen (wt%)*	*Nitrogen (wt%)*	*N:C*
g-C_3N_4	35.0	1.6	60.5	1.7
MGCN-130	34.2	1.5	58.9	1.7
MGCN-150	33.6	1.9	58.7	1.7
MGCN-180	31.8	2.9	57.9	1.8
MGCN-200	28.2	3.7	55.4	1.9

Fig. 11. Carbon, nitrogen and hydrogen element analysis of g-C_3N_4, MGCN-130, MGCN-150, MGCN-180 and MGCN-200,

Carbon, nitrogen and hydrogen contents were analysed for $g - C_3N_4$, MGCN-130, MGCN-150, MGCN-180 and MGCN-200 and are presented in Fig.11. Three elements were contained in all samples; however the hydrothermal treatment led to the decreased carbon and nitrogen contents in samples, especially in MGCN-200. In contrast, the hydrogen and surplus contents have increased because of the amino groups and melem appearance[36]. The surplus is

considered as oxygen-bearing groups [38]. In addition, nitrogen and carbon ratio in $g - C_3N_4$is 1.73 higher than previous report (1.25) [40]. This value was increased with temperature in all samples which indicates that g-C_3N_4 skeleton would be collapsed depriving carbon from the compounds.

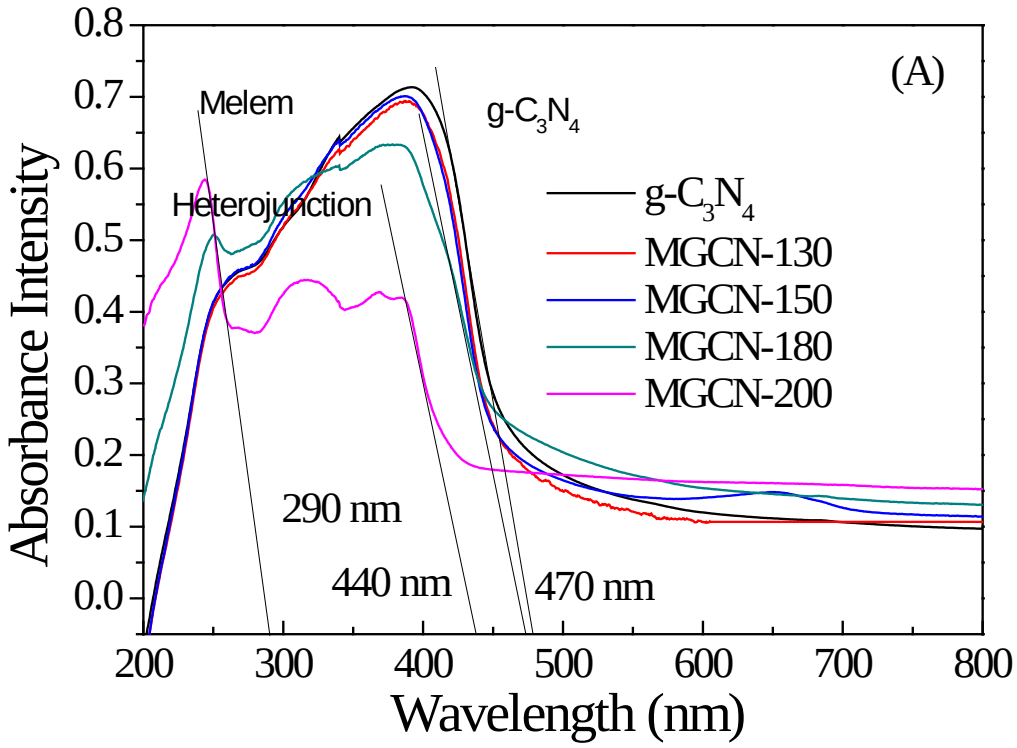

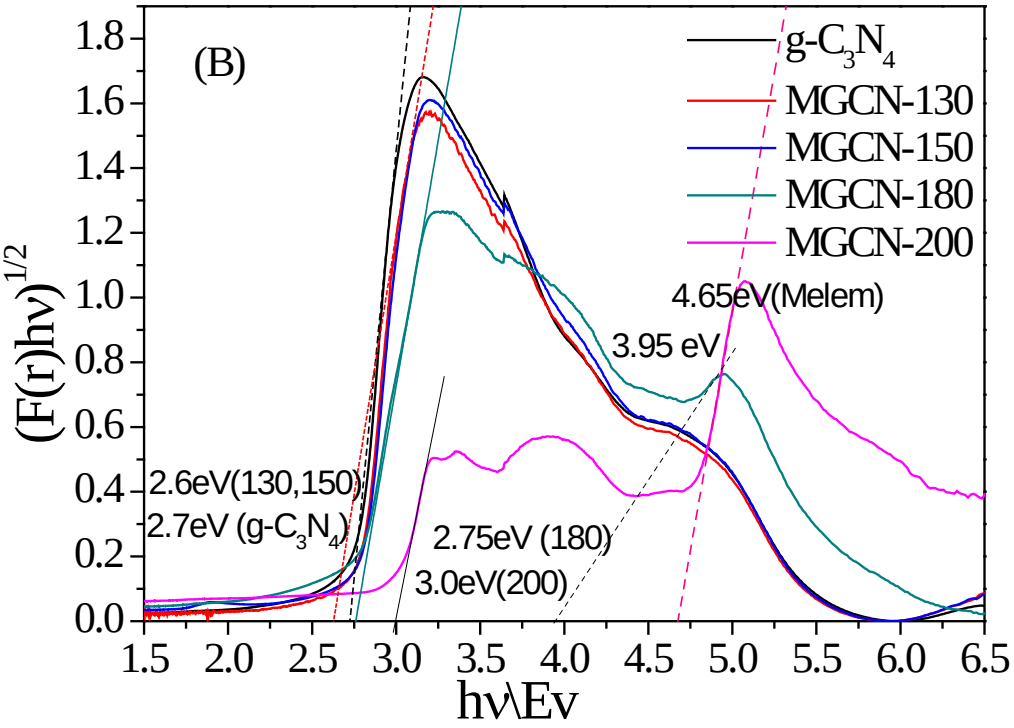

Fig. 12. UV–visible diffuse reflectance absorption spectra (A) of g-C_3N_4, MGCN130, MGCN150, MGCN180 and MGCN 200; Band gap structures (B) of Melem/g-C_3N_4 photocatalysts.

The optical properties of melem/ $g-C_3N_4$heterojunction photocatalysts were studied by UV–vis diffuse reflectance spectra (DRS). In Fig.12, an absorption edge of $g-C_3N_4$was observed at 470 nm giving 2.7 eV band gap[24]. In MGCN-130, MGCN-150 and MGCN-180 a blue shift occurs in the absorption edge, meanwhile this tendency inducted MGCN-200 sample into 400 nm following with light absorption intensity dramatically declined. In MGCN-180 and MGCN-200 composites, a new secondary absorption edge was observed at about 290 nm in ultraviolet area, which is considered as radiation exciting threshold of Melem compounds. The band gap energies of melem/$g-C_3N_4$ photocatalysts were calculated by the Kubelka–Munk equations[41], by transforming the spectra into $(\alpha hv)^{1/2}$ versus hv (Fig.12 B). The band gap energy of pristine $g-C_3N_4$ is 2.7 eV which agreed with previous report[42]. The band gap energies of MGCN-130 and MGCN-150 decreased to 2.6 eV. For MGCN-180, two band gaps

could be detected which corresponded to 2.75 eV and 3.95 eV, respectively. By contrast, MGCN-200 sample had a weak band gap energy at 3.0 eV and a strong one at 4.65 eV, which was ascribed by g-C_3N_4 hydrolysis[37].

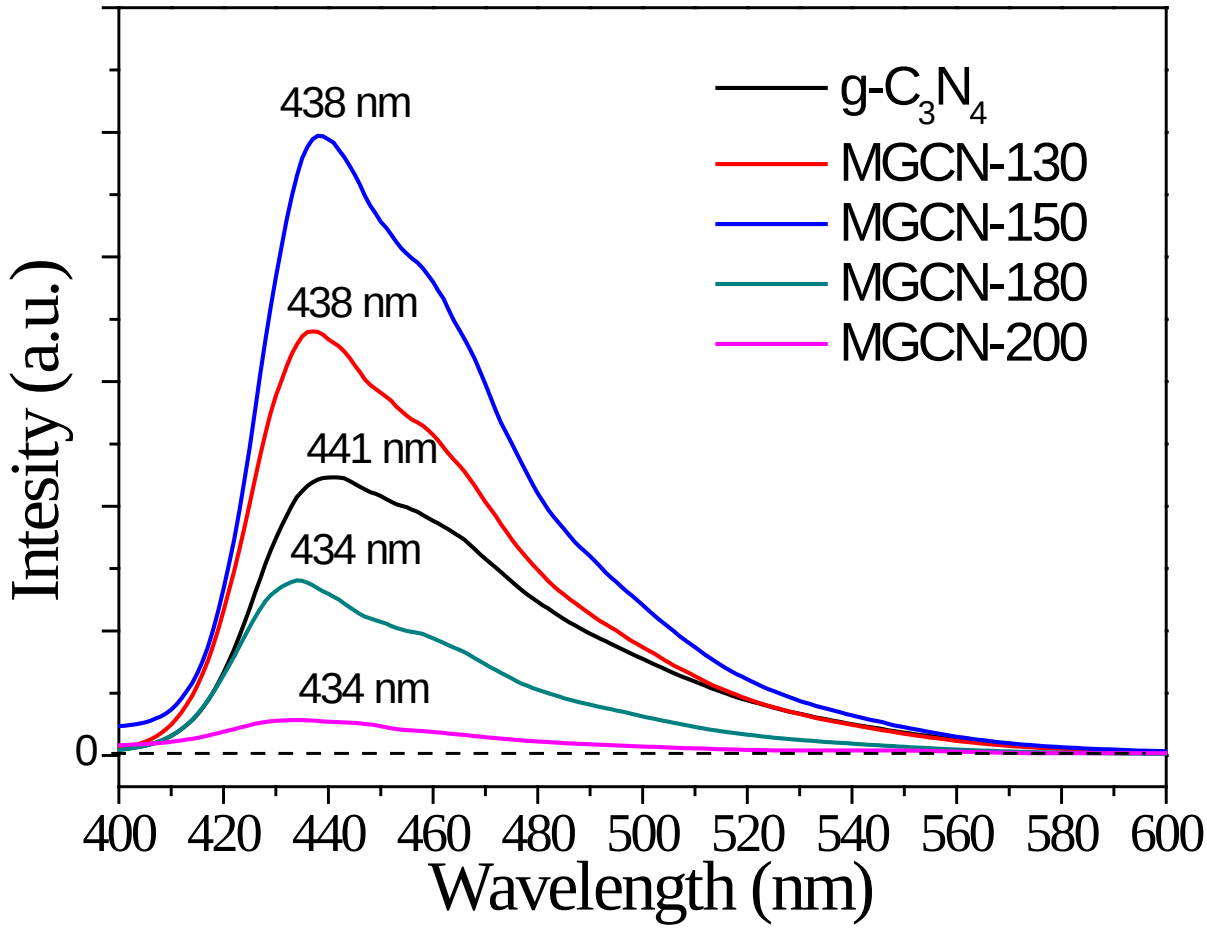

Fig. 13. Photoluminescence spectra of Melem/ $\mathbf{g-C_3N_4}$ heterojunction photocatalysts.

To further study photoelectric features of Melem/ $g-C_3N_4$heterojunction, photoluminescence spectra under 330 nm excitation was applied to investigate electronic pair recombination during photocatalysis [43]. As shown in Fig.13, $g-C_3N_4$has a wide emission peak from 400 to 590 nm representing multiply recombination centres[21]. A main emission peak at 441 nm is attributed to band-gap energy of pristine g-C_3N_4, which is mainly caused by the transitions

between lone pair electrons and anti- π state. Whereas MGCN-130 and MGCN-150 samples give much higher PL intensity comparing with $g - C_3N_4$, and the maximum emission shows a blue shift to 438 nm. This phenomenon can be ascribed to increased visible light absorption. However, the peak intensity of MGCN-180 and MGCN-200 are dramatically declined and emission peaks are blue shifted into 430 nm, which indicates that the band gap of the Melem/g-C_3N_4 heterojunction structure effectively delay the electron/hole pair recombination [14] .

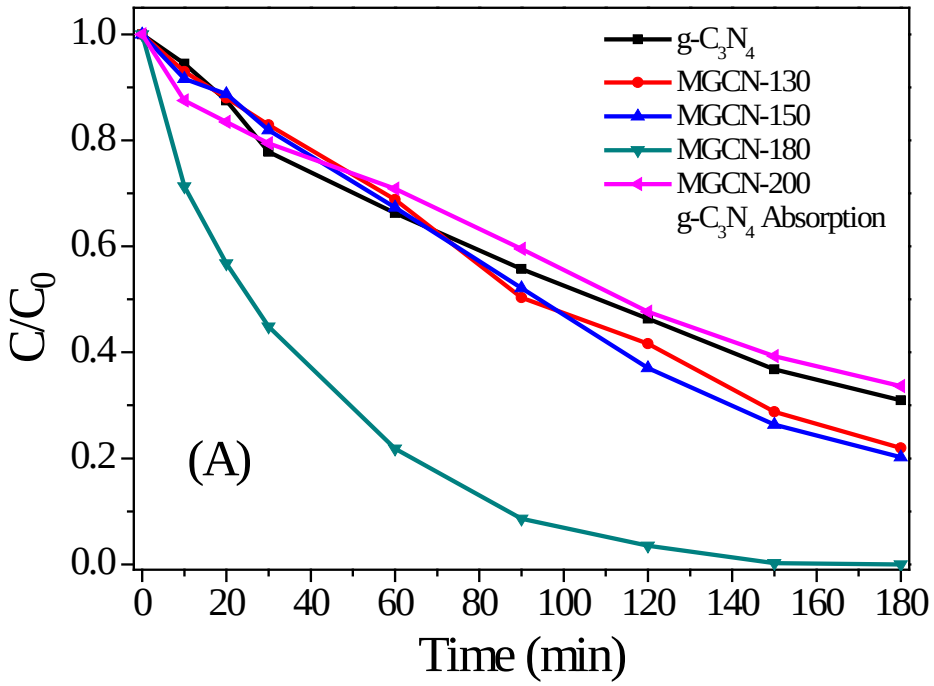

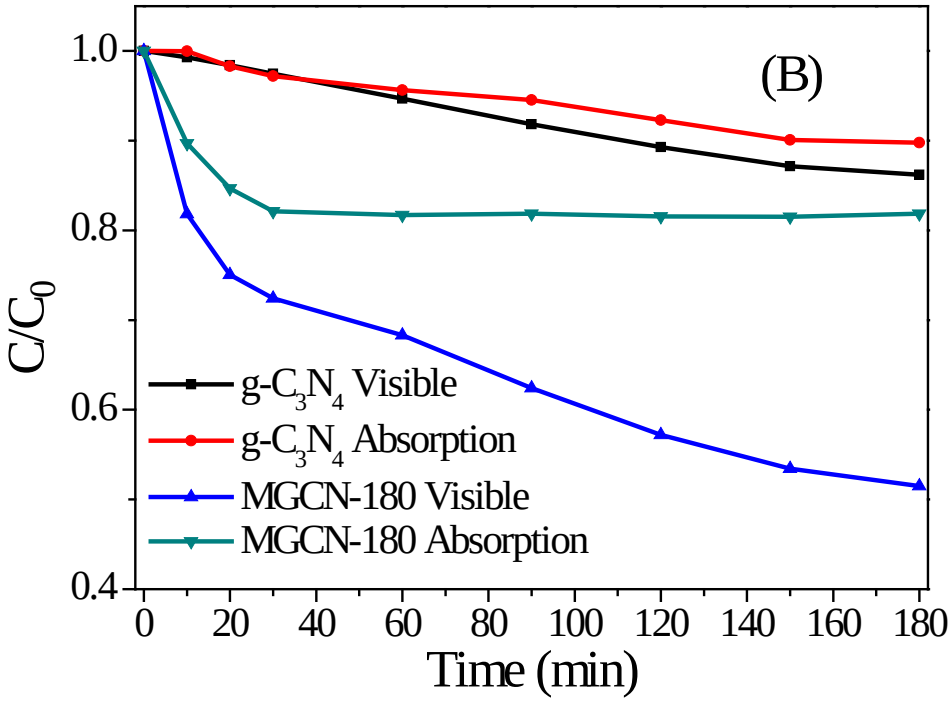

Fig. 14. Photocatalytic performance of Melem/g-C_3N_4 heterojunction catalysts under artificial solar radiation (A); Visible light photocatalytic reaction (B)

For photocatalytic performance, Melem/$g-C_3N_4$photocatalysts were evaluated by methylene blue degradation under artificial solar radiation and visible light. Fig.14 (A) shows the photocatalytic performance of GCN samples under artificial solar radiation. The pristine $g-C_3N_4$ had an activity in MB decomposition, giving 60% MB removal in 3 h. MGCN-130 and MGCN-150 degraded similarly about 80% MB. MGCN-180 had the best activity and all MB was removed in 3 h, whereas MGCN-200 presented similar catalytic behavior as $g-C_3N_4$. For photocatalysis by visible light (Fig. 14B) $g-C_3N_4$ exhibited minor MB adsorption at 8% in 3 h and photocatalytic degradation of MB is slight higher at 12%. In contrast, MGCN-180 presented fast MB adsorption equilibrium in 30 min, showing 18% MB removal. But it produced continuing MB photodegradation, giving 50% MB removal in three hours.

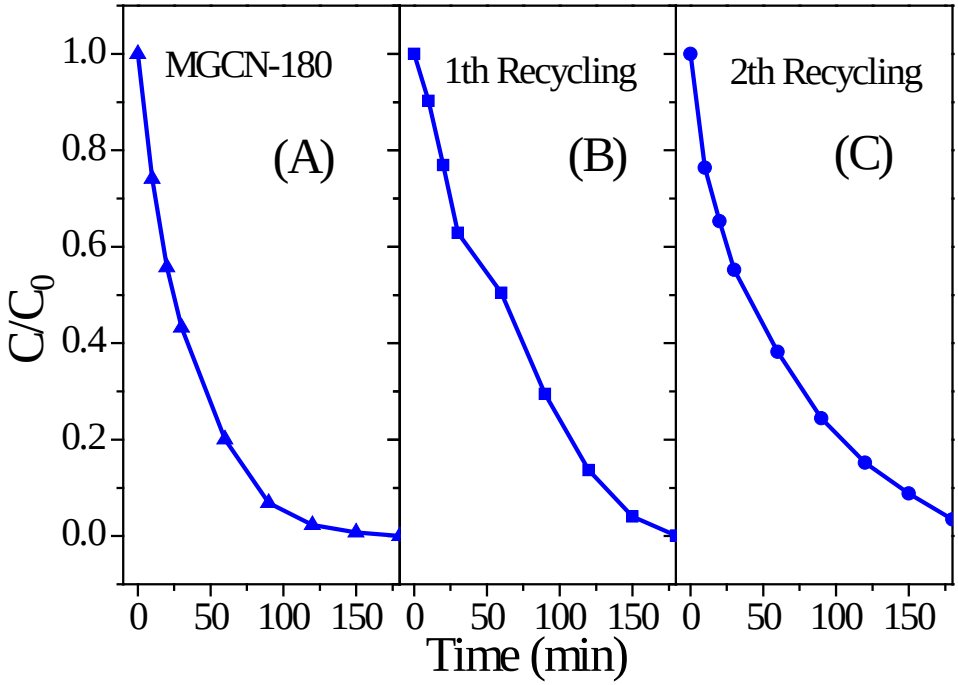

Fig. 15. Cycling degradation efficiency of MB solution by MGCN-180.

The catalytic stability of a photocatalyst is essential to insure its application. MGCN-180 was further tested in cycling photodegradation. Fig.15 shows that MGCN-180 could degrade all MB solution in the second and third runs in three hours, suggesting good photocatalytic stability.

Melem has been reported possessing a band gap and multiple recombination centres owing to defective π states in tri-s-triazine unit[21]. The small size of sp^2 clusters in organic semiconductors typically leads to a large band gap [44], although high nitrogen contained carbonaceous catalyst has optimal catalytic activity[45, 46]. Ammonia groups overlap the π states and lead band gap to decrease and increase the light absorption by Melem/g-C_3N_4 heterojunction. The above factors are well coincided with PL emission intensity, the photo

generated electron from conductive band of $g-C_3N_4$ alternatively devoid by recombination with electronic hole in valence band, it will redirect in to the empty energy orbit in Melem co-catalyst, this dislocation can make electron injection to photocatalytic reaction rather than fluorescence recombination. At the same time a high surface area also afforded the better catalysis, which increased the contact potential between photo generated electronic pair and pollutants. Totally speaking, the Melem/g-C_3N_4 heterojunction photocatalyst affords a synergistic function toward MB degradation.

3.5 Conclusions

In this report, melem/ $g-C_3N_4$ heterojunction photocatalysts had been generated by hydrothermal treatment of $g-C_3N_4$ in DI water between 130-200 ℃. Photocatalytic methylene blue degradation on the samples indicated MGCN-180 presented much better photocatalytic performance comparing with other $g-C_3N_4$ catalysts under artificial solar radiation. Melom fibre was identified by XRD and SEM, and optical properties of Melem/ $g-C_3N_4$ hybrid show a synergistic effect of heterojunction. Melem in $g-C_3N_4$ catalyst support provides a new energy level to $g-C_3N_4$ for effectively weaken inset recombination by electron dislocation from $g-C_3N_4$ in to melem cocatalyst therefor increase photo generated electron to reaction.

3.6 References

[1] D. Bahnemann, Photocatalytic water treatment: solar energy applications, Solar energy, 77 (2004) 445-459.

[2] I.K. Konstantinou, T.A. Albanis, TiO_2-assisted photocatalytic degradation of azo dyes in aqueous solution: kinetic and mechanistic investigations: a review, Applied Catalysis B: Environmental, 49 (2004) 1-14.

[3] A. Fujishima, Electrochemical photolysis of water at a semiconductor electrode, Nature, 238 (1972) 37-38.

[4] S. Liu, H. Sun, S. Liu, S. Wang, Graphene facilitated visible light photodegradation of methylene blue over titanium dioxide photocatalysts, Chemical Engineering Journal, 214 (2013) 298-303.

[5] H. Sun, S. Liu, S. Liu, S. Wang, A comparative study of reduced graphene oxide modified TiO_2, ZnO and Ta_2O_5 in visible light photocatalytic/photochemical oxidation of methylene blue, Applied Catalysis B: Environmental, 146 (2014) 162-168.

[6] S. Liu, H. Sun, A. Suvorova, S. Wang, One-pot hydrothermal synthesis of ZnO-reduced graphene oxide composites using Zn powders for enhanced photocatalysis, Chemical Engineering Journal, 229 (2013) 533-539.

[7] R. Thiruvenkatachari, S. Vigneswaran, I.S. Moon, A review on UV/TiO_2 photocatalytic oxidation process (Journal Review), Korean Journal of Chemical Engineering, 25 (2008) 64-72.

[8] A. Schwarzer, U. Böhme, E. Kroke, Use of Melem as a Nucleophilic Reagent to Form the Triphthalimide $C_6N_7(phthal)_3$—New Targets and Prospects, Chemistry – A European Journal, 18 (2012) 12052-12058.

[9] H.S. Jung, Y.J. Hong, Y. Li, J. Cho, Y.-J. Kim, G.-C. Yi, Photocatalysis using GaN nanowires, Acs Nano, 2 (2008) 637-642.

[10] T. Murase, H. Irie, K. Hashimoto, Visible light sensitive photocatalysts, nitrogen-doped Ta_2O_5 powders, The Journal of Physical Chemistry B, 108 (2004) 15803-15807.

[11] K. Hashimoto, H. Irie, A. Fujishima, TiO_2 Photocatalysis: A Historical Overview and Future Prospects, Japenese Journal Of Applied Physics Part 1 Regular Papers Short Notes And Review Papers, 44 (2005) 8269.

[12] X. Wang, K. Maeda, A. Thomas, K. Takanabe, G. Xin, J.M. Carlsson, K. Domen, M. Antonietti, A metal-free polymeric photocatalyst for hydrogen production from water under visible light, Nature materials, 8 (2008) 76-80.

[13] D.J. Martin, K. Qiu, S.A. Shevlin, A.D. Handoko, X. Chen, Z. Guo, J. Tang, Highly Efficient Photocatalytic H_2 Evolution from Water using Visible Light and Structure-Controlled Graphitic Carbon Nitride, Angewandte Chemie International Edition, 53 (2014) 9240-9245.

[14] Q. Xiang, J. Yu, M. Jaroniec, Preparation and Enhanced Visible-Light Photocatalytic H_2-Production Activity of Graphene/C_3N_4 Composites, The Journal of Physical Chemistry C, 115 (2011) 7355-7363.

[15] Z. Zhao, Y. Sun, F. Dong, Graphitic carbon nitride based nanocomposites: a review, Nanoscale, 7 (2015) 15-37.

[16] G. Dong, Y. Zhang, Q. Pan, J. Qiu, A fantastic graphitic carbon nitride (g-C_3N_4) material: Electronic structure, photocatalytic and photoelectronic properties, Journal of Photochemistry and Photobiology C: Photochemistry Reviews, 20 (2014) 33-50.

[17] A. Thomas, A. Fischer, F. Goettmann, M. Antonietti, J.-O. Müller, R. Schlögl, J.M. Carlsson, Graphitic carbon nitride materials: variation of structure and morphology and their use as metal-free catalysts, Journal of Materials Chemistry, 18 (2008) 4893-4908.

[18] S. Chu, C. Wang, J. Feng, Y. Wang, Z. Zou, Melem: A metal-free unit for photocatalytic hydrogen evolution, International Journal of Hydrogen Energy, 39 (2014) 13519-13526.

[19] B.V. Lotsch, W. Schnick, New Light on an Old Story: Formation of Melam during Thermal Condensation of Melamine, Chemistry – A European Journal, 13 (2007) 4956-4968.

[20] A. Sattler, S. Pagano, M. Zeuner, A. Zurawski, D. Gunzelmann, J. Senker, K. Müller-Buschbaum, W. Schnick, Melamine–Melem Adduct Phases: Investigating the Thermal Condensation of Melamine, Chemistry – A European Journal, 15 (2009) 13161-13170.

[21] Y. Zhang, Q. Pan, G. Chai, M. Liang, G. Dong, Q. Zhang, J. Qiu, Synthesis and luminescence mechanism of multicolor-emitting g-C_3N_4 nanopowders by low temperature thermal condensation of melamine, Scientific reports, 3 (2013).

[22] S. Wang, C. Li, T. Wang, P. Zhang, A. Li, J. Gong, Controllable synthesis of nanotube-type graphitic C_3N_4 and their visible-light photocatalytic and fluorescent properties, Journal of Materials Chemistry A, 2 (2014) 2885-2890.

[23] X. Li, J. Zhang, L. Shen, Y. Ma, W. Lei, Q. Cui, G. Zou, Preparation and characterization of graphitic carbon nitride through pyrolysis of melamine, Applied Physics A, 94 (2009) 387-392.

[24] X. Wang, K. Maeda, A. Thomas, K. Takanabe, G. Xin, J.M. Carlsson, K. Domen, M. Antonietti, A metal-free polymeric photocatalyst for hydrogen production from water under visible light, Nat Mater, 8 (2009) 76-80.

[25] B. Jürgens, E. Irran, J. Senker, P. Kroll, H. Müller, W. Schnick, Melem (2,5,8-Triamino-tri-s-triazine), an Important Intermediate during Condensation of Melamine Rings to Graphitic Carbon Nitride: Synthesis, Structure Determination by X-ray Powder Diffractometry, Solid-State NMR, and Theoretical Studies, Journal of the American Chemical Society, 125 (2003) 10288-10300.

[26] M. Tahir, C. Cao, F.K. Butt, F. Idrees, N. Mahmood, Z. Ali, I. Aslam, M. Tanveer, M. Rizwan, T. Mahmood, Tubular graphitic-C_3N_4: a prospective material for energy storage and green photocatalysis, Journal of Materials Chemistry A, 1 (2013) 13949-13955.

[27] G. Dong, L. Zhang, Porous structure dependent photoreactivity of graphitic carbon nitride under visible light, Journal of Materials Chemistry, 22 (2012) 1160-1166.

[28] Y. Zhang, J. Liu, G. Wu, W. Chen, Porous graphitic carbon nitride synthesized via direct polymerization of urea for efficient sunlight-driven photocatalytic hydrogen production, Nanoscale, 4 (2012) 5300-5303.

[29] P. Larkin, Infrared and Raman spectroscopy; principles and spectral interpretation, Elsevier, 2011.

[30] G. Liao, S. Chen, X. Quan, H. Yu, H. Zhao, Graphene oxide modified g-C_3N_4 hybrid with enhanced photocatalytic capability under visible light irradiation, Journal of Materials Chemistry, 22 (2012) 2721-2726.

[31] P. Niu, G. Liu, H.-M. Cheng, Nitrogen Vacancy-Promoted Photocatalytic Activity of Graphitic Carbon Nitride, The Journal of Physical Chemistry C, 116 (2012) 11013-11018.

[32] B.V. Lotsch, M. Döblinger, J. Sehnert, L. Seyfarth, J. Senker, O. Oeckler, W. Schnick, Unmasking Melon by a Complementary Approach Employing Electron Diffraction, Solid-State NMR Spectroscopy, and Theoretical Calculations—Structural Characterization of a Carbon Nitride Polymer, Chemistry-a European Journal, 13 (2007) 4969-4980.

[33] J. Du, X. Lai, N. Yang, J. Zhai, D. Kisailus, F. Su, D. Wang, L. Jiang, Hierarchically ordered macro− mesoporous TiO_2− graphene composite films: Improved mass transfer, reduced charge recombination, and their enhanced photocatalytic activities, Acs Nano, 5 (2010) 590-596.

[34] S.C. Yan, S.B. Lv, Z.S. Li, Z.G. Zou, Organic-inorganic composite photocatalyst of g-C_3N_4 and TaON with improved visible light photocatalytic activities, Dalton Transactions, 39 (2010) 1488-1491.

[35] Y. Sun, C. Li, Y. Xu, H. Bai, Z. Yao, G. Shi, Chemically converted graphene as substrate for immobilizing and enhancing the activity of a polymeric catalyst, Chemical Communications, 46 (2010) 4740-4742.

[36] S.C. Yan, Z.S. Li, Z.G. Zou, Photodegradation Performance of g-C_3N_4 Fabricated by Directly Heating Melamine, Langmuir, 25 (2009) 10397-10401.

[37] L. Ming, H. Yue, L. Xu, F. Chen, Hydrothermal synthesis of oxidized g-C_3N_4 and its regulation of photocatalytic activity, Journal of Materials Chemistry A, 2 (2014) 19145-19149.

[38] J. Li, B. Shen, Z. Hong, B. Lin, B. Gao, Y. Chen, A facile approach to synthesize novel oxygen-doped g-C_3N_4 with superior visible-light photoreactivity, Chemical Communications, 48 (2012) 12017-12019.

[39] S. Yan, Z. Li, Z. Zou, Photodegradation performance of g-C3N4 fabricated by directly heating melamine, Langmuir, 25 (2009) 10397-10401.

[40] Q. Guo, Y. Xie, X. Wang, S. Zhang, T. Hou, S. Lv, Synthesis of carbon nitride nanotubes with the C_3N_4 stoichiometry via a benzene-thermal process at low temperatures, Chemical Communications, (2004) 26-27.

[41] G. Zhou, H. Sun, S. Wang, H. Ming Ang, M.O. Tadé, Titanate supported cobalt catalysts for photochemical oxidation of phenol under visible light irradiations, Separation and Purification Technology, 80 (2011) 626-634.

[42] H. Yan, Y. Chen, S. Xu, Synthesis of graphitic carbon nitride by directly heating sulfuric acid treated melamine for enhanced photocatalytic H_2 production from water under visible light, International Journal of Hydrogen Energy, 37 (2012) 125-133.

[43] M. Hiramoto, K. Hashimoto, T. Sakata, Electron transfer and photoluminescence dynamics of CdS particles deposited on porous vycor glass, Chemical physics letters, 133 (1987) 440-444.

[44] Y. Iwano, T. Kittaka, H. Tabuchi, M. Soukawa, S. Kunitsugu, K. Takarabe, K. Itoh, Study of Amorphous Carbon Nitride Films Aiming at White Light Emitting Devices, Japanese Journal of Applied Physics, 47 (2008) 7842.

[45] L. Jia, D.-H. Wang, Y.-X. Huang, A.-W. Xu, H.-Q. Yu, Highly durable N-doped graphene/CdS nanocomposites with enhanced photocatalytic hydrogen evolution from water under visible light irradiation, The Journal of Physical Chemistry C, 115 (2011) 11466-11473.

[46] P. Chen, T.-Y. Xiao, H.-H. Li, J.-J. Yang, Z. Wang, H.-B. Yao, S.-H. Yu, Nitrogen-doped graphene/ZnSe nanocomposites: Hydrothermal synthesis and their enhanced electrochemical and photocatalytic activities, Acs Nano, 6 (2011) 712-719.

4 Oxygen functional groups in graphitic carbon nitride for enhanced photocatalysis

This paper has been published in Journal of Colloid and Interface,

Volume 468, 15 April 2016, Pages 176–182

4.1 ABSTRACT

Metal-free semiconductors offer a new opportunity for environmental photocatalysis in a potential breakthrough on high photo efficiency with complete prevention of metal leaching. In this study, graphitic carbon nitride (GCN) modified by oxygen functional groups was synthesized by a hydrothermal treatment of pristine GCN at different temperatures with H_2O_2. Insights into the emerging characteristics of the modified GCN in photocatalysis were obtained by determining the optical property, band structure, electrochemical activity and pollutant degradation efficiency. It was found that the introduction of GCN with oxygen functional groups can enhance light absorption and accelerate electron transfer so as to improve the photocatalytic reaction efficiency. The photoinduced reactive radicals and the associated photodegradation were investigated by in situ electron paramagnetic resonance (EPR).

4.2 Introduction

A modern society heavily depends on massive energy consumption, which inevitably results in energy crisis and environmental deterioration. Solar energy is a cheap, abundant and sustainable energy resource, and has been widely acknowledged as a fascinating alternative to fossil fuels. Solar cells [1], solar fuels [2], and environmental photocatalysis [3] have been extensively investigated for efficient solar energy utilization. Heterogeneous photocatalysis has attracted particular attention because of its great potential for environmental remediation using solar energy, simultaneously addressing both critical issues of energy shortage and environmental pollution [4-9]. The photocatalysis in practical applications is critically dependent on the photocatalytic performances of the catalyst materials. Over the past four decades, numerous materials have been employed as photocatalysts, for example, metal oxides [4, 8], metal sulphides [10], metal nitrides[11] and metal complexes [12, 13]. Among those

semiconductor materials, TiO_2 is the most popular photocatalyst. However, the wide band gap energy (3.2 eV for anatase) and high recombination rate of the photoinduced carries have limited its practical applications [3, 14, 15]. Heteroatoms doping and other modification approaches have been used to manipulate the properties of TiO_2 photocatalysts [4, 5, 7, 16, 17], however, expected photocatalytic performance has not yet been achieved.

Recently, graphitic carbon nitride (GCN), a metal-free polymeric semiconductor, and its based composites are discerned to be promising photocatalysts for producing hydrogen by water splitting under visible light irradiations [18-20]. GCN molecular skeleton is based on tri-s-triazine (C_6N_7, also referred as melem) building blocks, which presents a layered structure as polycyclic aromatic hydrocarbons [21], and the electrons can transport between the dislocated π-π^* and n-π^* orbitals [22, 23]. GCN also has an intrinsic band gap energy at 2.7 eV, which can be activated by visible light to produce electron/hole pairs[24]. Due to the high reduction ability originated from the high conduction band, GCN has demonstrated effective photoreduction for H_2 production and CO_2 reduction [18, 19, 25-30]. Recently, we applied different nanocarbons or polyoxometalate to modify GCN and enhanced photooxidation was obtained [31-33]. For a higher efficiency and wide applications, heteroatom doping using carbon, phosphorus, sulphur was also applied by other researchers to manipulate the properties of GCN [14, 34-36].

In general, the doping technologies are able to manipulate multiple defects and distortion into a semiconductor system, leading to changes in electronic properties. The dopant heteroatom is required to have a diameter similar to or smaller than original atom, and the electronegativity of the dopant can be lower or higher than the target atom. As a result, the dopant could become a positive or negative centre in original electron cloud, then would restrain the electronic motivation [37]. The electronegativity of oxygen atom is 3.44 eV (in Pauling scale) and the atomic radius is 48 pm. The high electronegativity of oxygen could limit electronic mobility

and protect photo-generated holes without lattice distortions. Therefore, oxygen was regarded as a good candidate for modification of GCN semiconductor. Li et al. [38] suggested that oxygen modification can enlarge surface area, improve physisorption and chemisorption, extend light absorption edge and then increase the photocatalytic activity [39-41]. Theoretical studies indicated that lower band gap energy can be obtained after oxygen modification of g-C_3N_4. The high concentration of oxygen alerts the direct semiconductor into an indirect semiconductor, meanwhile the negative oxygen atom becomes the active centre for enhanced light harvesting [41].

In this work, oxygen modification was achieved via a hydrothermal treatment of GCN with H_2O_2 solutions. Compared to the reported study [38], the effects of hydrothermal temperature on the characteristics such as crystalline structure, surface area, chemical states, optical property, band structure, recombination rate of carriers and photoelectrochemical properties were comprehensively investigated. The enhanced photocatalysis was confirmed by photodegradation of methylene blue and the related mechanism was studied by electrochemical analysis and electron paramagnetic resonance (EPR).

4.3 Experimental section

Chemicals and materials

Melamine, tert-butyl alcohol, 5,5-dimethyl-1-pyrroline N-oxide (DMPO) and p-benzoquinone (pBQ) in analytical grade were provided by Sigma-Aldrich. Hydrogen peroxide at 30 wt%, methylene blue, sulphuric acid, $K_3[Fe(CN)_6]$, KCl, Nafion, Na_2SO_4, NaOH, KH_4PO_4 were obtained from Biolab, Australia

2.1.1. Synthesis of graphitic carbon nitride

Graphitic carbon nitride was prepared by calcination of melamine powder [42]. Typically, 10 g melamine was dissolved in 10 mL methanol in a 20 mL alumina crucible. Then the crucible was put into an oven for drying at 60 ^{o}C for 24 h and then heated in a muffle furnace with a semi-closed cover. The sample was firstly heated at 400 ^{o}C for 2 h and then heated at 520 ^{o}C with a heating rate of 1 ^{o}C/min for another 2 h. The produced yellow particles were named as GCN.

Preparation of oxygen modified GCN

Typically, one gram GCN was placed in a 120 mL Teflon-lined stainless steel autoclave. Then 50 mL hydrogen peroxide solution was added and the mixed solution was kept stirring for 10 min. After that the autoclave was put into an oven for a hydrothermal treatment at four different temperatures (110, 130, 150, and 180 ^{o}C, respectively) for 12 h. The orange precipitate was collected by filtration and washed by 200 mL deionization water for three times. The final products, GCN-O-x (x is the hydrothermal temperature), were dried in a vacuum oven at 40 ^{o}C for 24 h.

Characterization of materials

X-ray diffraction (XRD) was used to observe the chemical phases of samples on a Bruker D8-Advance X-ray diffractometer. The chemical composition was determined using both the energy dispersive X-ray spectroscopy (EDS) and X-ray photoelectron spectroscopy (XPS) on a Thermo Escalab 250 with Al-Kα X-ray, calibrated with the C 1s peak at 284.6 eV. Fourier transform infrared spectroscopy (FTIR) was performed on a Perkin–Elmer FTIR-100 with a MIR detector. Field emission scanning electron microscopy (FE-SEM) was used to analyze the morphology, size and textural information of the samples on Zeiss Neon 40EsB. UV–vis diffuse reflectance spectra (DRS) of samples were recorded on a JASCO V670 spectrophotometer with an Ø60 mm integrating sphere, and $BaSO_4$ as a reference material.

Photoluminescence spectra were acquired on a spectrometer from Agilent technologies. Thermogravimetric-differential thermal analysis (TG-DTA) was carried out on a Mettler-Toledo instrument under an air flow at a heating rate of 10 °C/min. The Brunauer–Emmett–Teller (BET) surface area and the pore size distribution of the samples were evaluated by N_2 adsorption-desorption isotherm using a Micromeritics Tristar 3000. Prior to measurement, samples were degassed at 100 ^oC overnight under vacuum condition. Electron paramagnetic resonance (EPR) experiments were carried out on a Bruker EMX-E spectrometer (Germany). DMPO was applied as the radical capturing agent. EPR settings were centerfield at 3514.5 G; data collected within 100 G range; microwave frequency was 9.87 GHz; modulation frequency was 100 GHz; wattage is 18.11 mW.

Evaluation of photocatalytic performance

Photocatalytic performances of various catalysts were evaluated by the photodegradation of methylene blue (MB) under both artificial solar light and visible light irradiations. In a typical process, MB solutions (10 mg/L, 200 mL) and the photocatalysts (100 mg) were mixed in a 1 L double-jacket cylindrical reactor with cooling water (25 °C) under constant stirring at 350 rpm. The photocatalytic reactor was positioned 30 cm below the light source. Two light sources were employed. One was UV–vis light with intensities at 2.31×10^{-3} mW/cm^2 (220–280 nm), 6.94 mW/cm^2 (315–400 nm), and 129.3 mW/cm^2 (400–1050 nm), respectively. The other one was visible light irradiation with intensity of 84 mW/cm^2 at 400–1050 nm using a cut-off filter. Before the photodegradation, the suspension was stirred in dark for 30 min to reach adsorption/desorption equilibrium. The photocatalytic reaction was initiated by switching on the lamp. In certain time intervals, the reaction solution was withdrawn and centrifuged and then the concentration of MB solution was analyzed by a JASCO UV–vis spectrophotometer at a wavelength of 664 nm.

Electrochemical analysis

Electrochemical measurements were performed on a Zennium electrochemical workstation, in a conventional three-electrode cell. The working electrode was prepared on a glassy carbon electrode (CHI104). Before coating samples, the glassy carbon electrode was cleaned and activated by sulphuric acid solution (0.5 M) and $K_3[Fe(CN)_6]$/KCl solution (5 mM/100 mM in deionized (DI) water). Then the working electrode was washed with DI water and methanol and dried at room temperature. GCN particles were then dispersed in 0.5 M Nafion solution to produce slurry suspension (2.0 mg/mL). After that, 5 µL suspension was finally dropped on the working electrode and dried in air. $Hg/HgCl_2$ was applied as the reference electrode and a platinum wire was used as the auxiliary electrode.

The Mott-Schottky analysis was carried out in a 0.2 M Na_2SO_4 aqueous solution with prior nitrogen purging for 1 h. The potential ranged from -0.1 to 0.8 V, and the perturbation signal was 20 mV with a frequency at 1 KHz. Cyclic voltammetry (CV) was measured in a 2×10^{-4} M MB solution (pH = 6.5 adjusted by NaOH and KH_4PO_4). Five-cycle scans were recorded with sweep rates of 30, 50, 70, 90 and 110 V/s, respectively.

4.4 Results and discussion

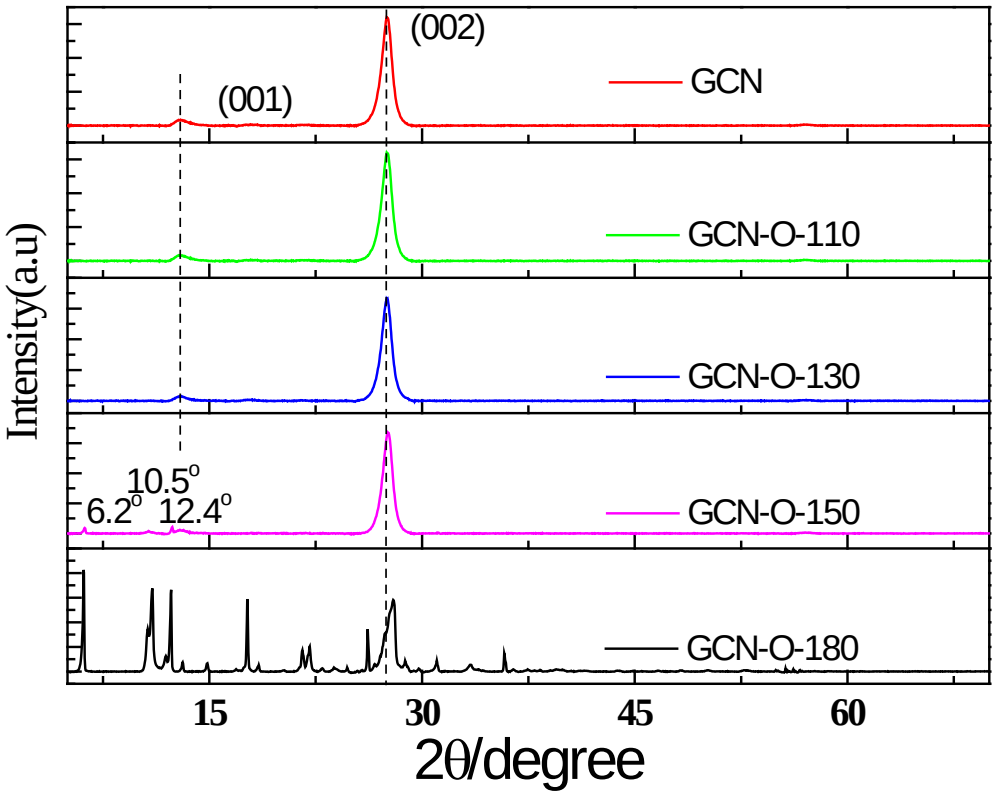

Fig. 16. XRD patterns of GCN and modified forms obtained at different hydrothermal temperatures.

Fig. 16 shows XRD patterns of GCN, GCN-O-110, GCN-O-130, GCN-O-150 and GCN-O-180. The peaks at 27.4 and 13.1° in XRD profile indicate the (002) and (100) diffraction planes of GCN (JCPDS 87-1526), respectively. The peak at 27.4° arises from the long-range interplanar stacking of the conjugated aromatic system and the weak peak at 13.1° is due to the parallel inter-layer structure [43, 44]. GCN, GCN-O-110 and GCN-O-130 have similar patterns indicating similar crystal structures. However, three new small peaks appear at 6.2, 10.5 and 12.4º in XRD profile of GCN-O-150, implying the occurrence of new structures. The XRD pattern of GCN-O-180 displays significantly different pattern with many new peaks and the dominated (002) peak is dislocating to a higher 2θ. Those emerging planes indicate the generation of melamine compound or melon compound from degradation/oxidation of graphitic structure at a higher hydrothermal temperature [25]. Moreover, the FWHM value of

GCN-O-180 is 0.20°, which is smaller than that of GCN-O-110 sample (0.51°), indicating a smaller particle size. XRD results suggested that GCN presented a hydrothermal stability up to 130 ℃ in H_2O_2 solutions. When the hydrothermal temperature was higher than 150 ℃, the graphitic structure became degradation and would almost collapse at 180 ℃. The results confirmed that H_2O_2 can oxidize GCN at a high temperature, which has not been reported.

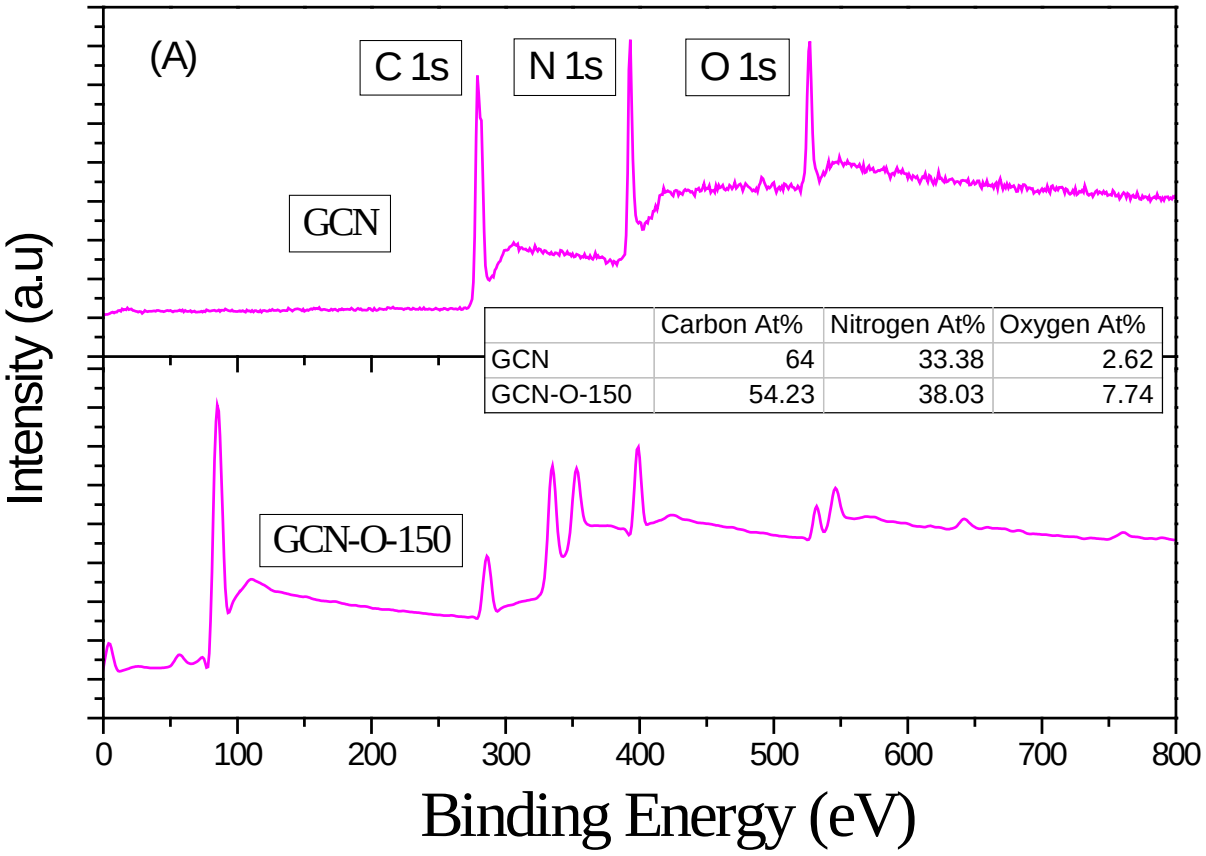

	Carbon At%	Nitrogen At%	Oxygen At%
GCN	64	33.38	2.62
GCN-O-150	54.23	38.03	7.74

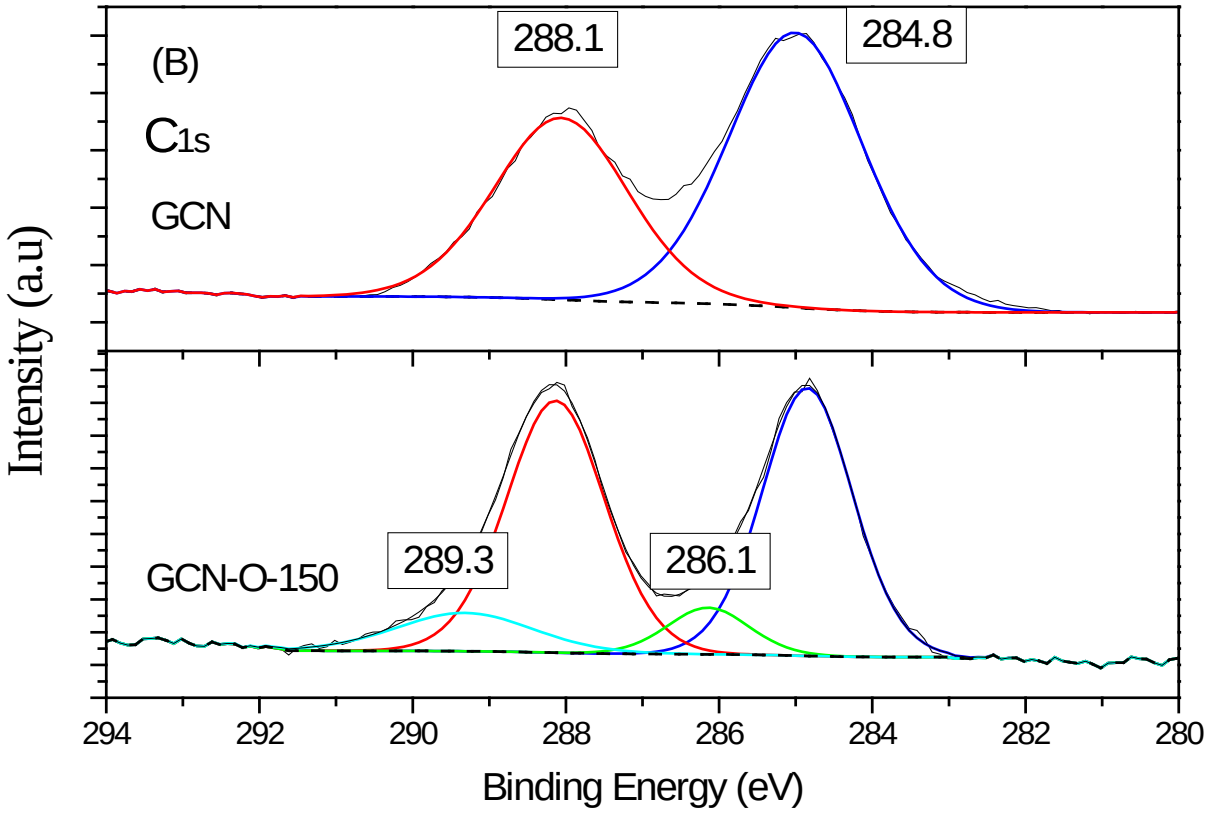
(B)
C1s
GCN
288.1
284.8
GCN-O-150
289.3
286.1
Intensity (a.u)
294
292
290
288
286
284
282
280
Binding Energy (eV)

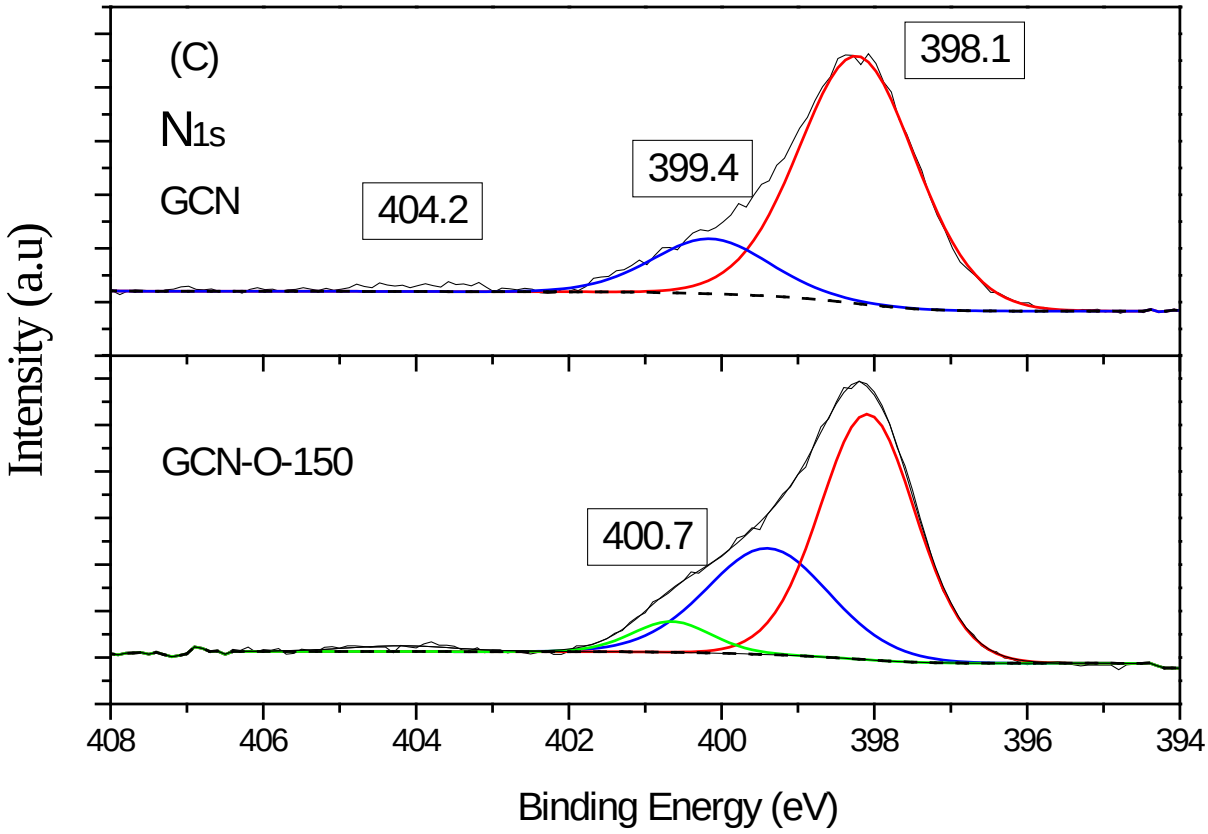
(C)
N1s
GCN
404.2
399.4
398.1
GCN-O-150
400.7
Intensity (a.u)
408
406
404
402
400
398
396
394
Binding Energy (eV)

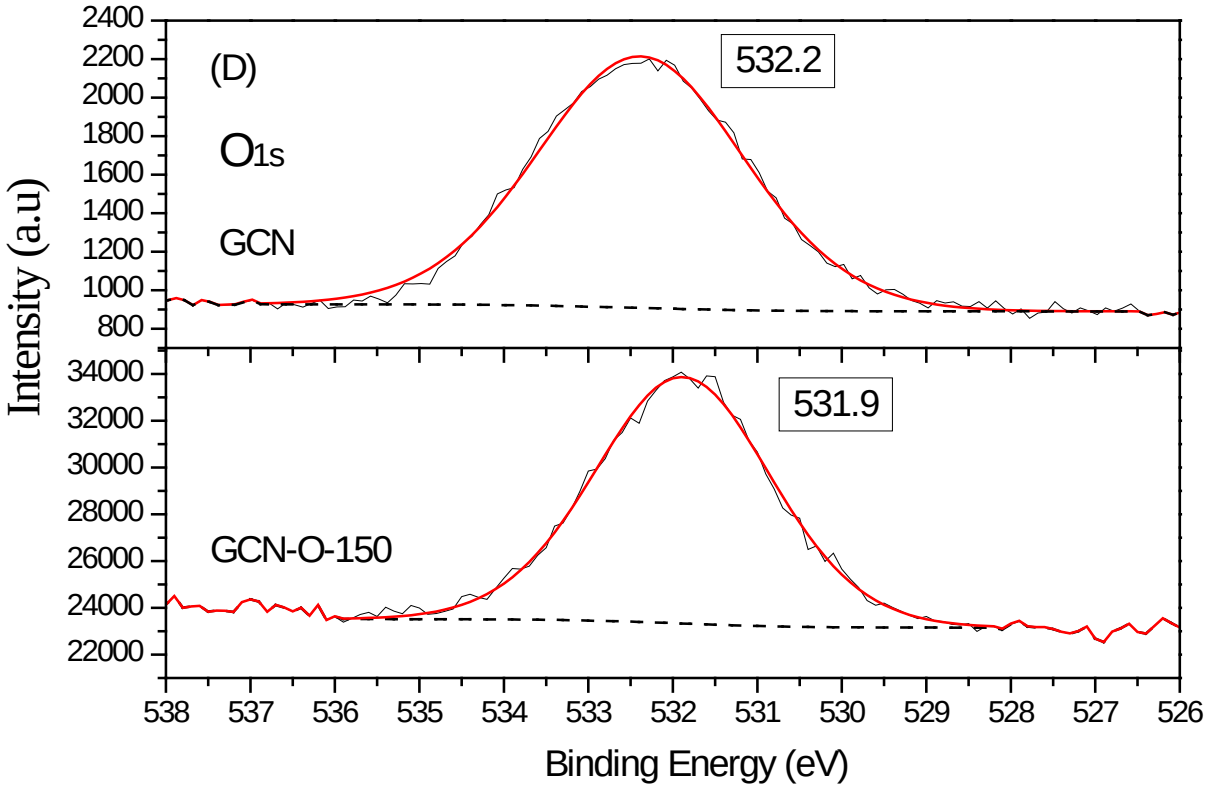

Fig. 17. XPS survey (A), C 1s (B), N 1s (C) and O 1s (D) spectra of GCN and GCN-O-150 samples.

In this study XPS analysis was applied to investigative the surface chemical states of both GCN and modified GCN-O-150 samples. Three elements (carbon, nitrogen and oxygen) can be identified in two composites in the survey scan, the chemical compositions of GCN are 2.62, 64 and 33.38 at% for O, C and N, respectively, in contrast the proportion in GCN-O-150 are 7.74, 54.23 and 38.03% for O, C and N. In Fig.17 (B) for C1s, two peaks in GCN and GCN-O-150 samples with binding energies at 288.1 and 284.8 eV are ascribed to the sp^2 (N-C=N) bonds in adventitious carbon. The peak at 289.3 eV in GCN-O-150 is attributed to the C bonding with O in O=CO or C-O in the skeleton. The deconvolution in XPS N 1s in Fig. 28 (C), in both GCN and GCN-O-150 samples, the peaks at 398.1, 399.4 and 404.2 eV can be attributed to the pyridines-like nitrogen (N−C sp^2), graphitic nitrogen ($N-(C)_3$) and the charging effects[45, 46]. The binding energy at 400.7 eV in GCN-O-150 represents the formation of N-O species. O 1s spectrum in Fig. 17 (D) shows a broad peak at binding energy

of 532.2 eV, corresponding to N-C-O bond in GCN composite, however, this binding energy intensity in GCN-O-150 is ca. 10 times higher than original value, as well as a tiny shift relocates this peak into 531.9 eV, which may be caused by chemical skeleton distortion. Both XPS and FTIR (Fig. 25s) could suggest the formation of surface oxygen-containing functional groups [47]. Energy-dispersive X-ray spectroscopy (EDS) mapping technology was employed to analyze the element distribution in the oxygen-modified GCN. Three elements of carbon (Fig.26s C), oxygen (Fig.26sD) and nitrogen (Fig.26sE) could be identified in GCN-O-150. Carbon and nitrogen could homogeneously disperse according to the shapes of the GCN particles while oxygen showed an intensive distribution around particle edges, indicating more oxygen atoms at the surface and/or edges. Furthermore, TGA indicates that GCN-O-150 has the similar thermal property with pristine GCN (Fig. 27s). In contrast, GCN-O-180 has three stages of weight loss, which correspond to the decomposition of O-bearing groups, particle recondensation, and GCN decomposing, respectively [48].

.

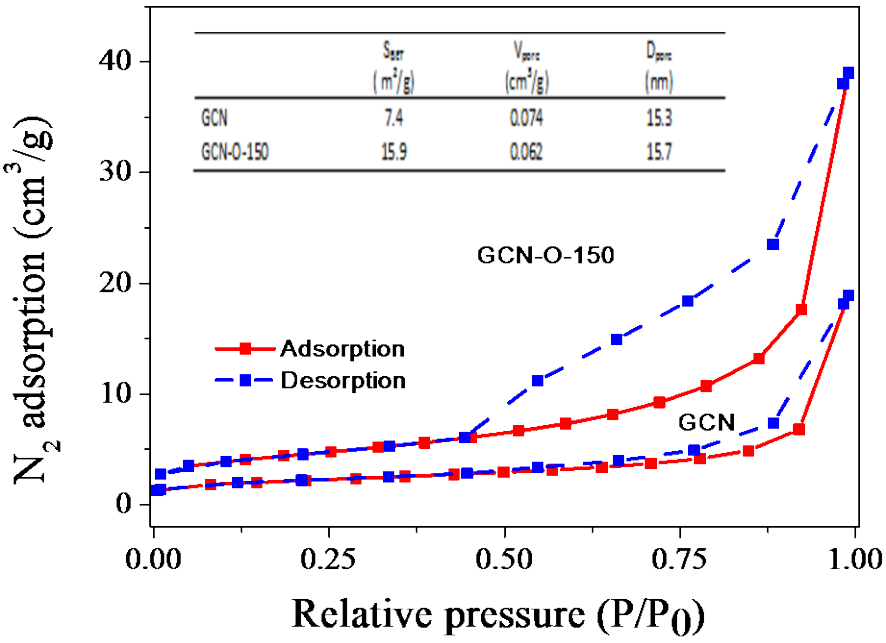

Fig. 18. $\mathbf{N_2}$ adsorption−desorption isotherms of GCN and GCN-O-150 samples. Inset: the textural properties.

N_2 adsorption-desorption isotherms of GCN and GCN-O-150 are shown in Fig.18. The isotherms show type IV adsorption behavior. The hysteresis loops are H3 type and indicate a mesoporous structure. The specific surface area and pore volume are shown in inset table. GCN-O-150 has a higher surface area than pristine GCN.

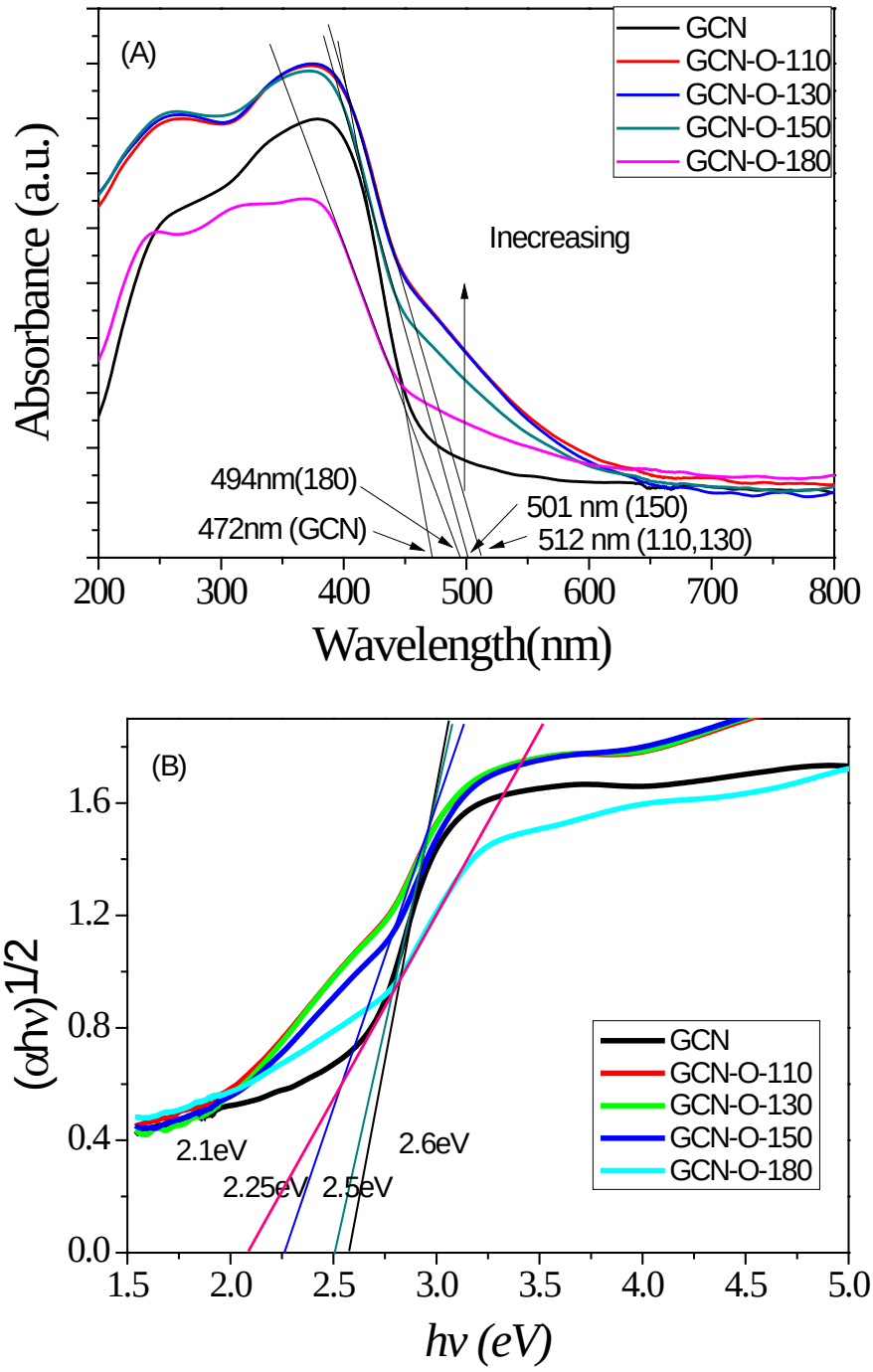

Fig. 19. UV−vis DRS spectra (A) and estimation of band gap energies (B) of different GCN samples.

The optical properties of oxygen-modified GCN photocatalysts were studied by UV-vis DRS. Fig.19 (A) displays the UV−vis DRS spectra of GCN and GCN-O samples. It was seen that oxygen modification could extend the absorption edge of GCN from 450 to 600 nm [49]. Hydrothermal treatments at 110 and 130 ºC significantly increase the absorption of GCN in visible light region. Once the hydrothermal temperature increases to 150 ºC, the absorption intensity in visible light region and the absorption threshold start declining. The band gap energies of the materials were also estimated by the Kubelka–Munk equation by transforming the spectra into (αhv)1/2 versus hv [50], as shown in Fig. 19 (B). The band gap energies are 2.7 eV for GCN, 2.5 eV for GCN-O-110 and GCN-O-130, 2.65 eV for GCN-O-150, and 2.3 eV for GCN-O-180, respectively. It was suggested that the hydrothermal treatment with H_2O_2 at a proper temperature can enhance light absorption due to new energy levels appearing between instinct valence and conduction bands of pristine GCN.

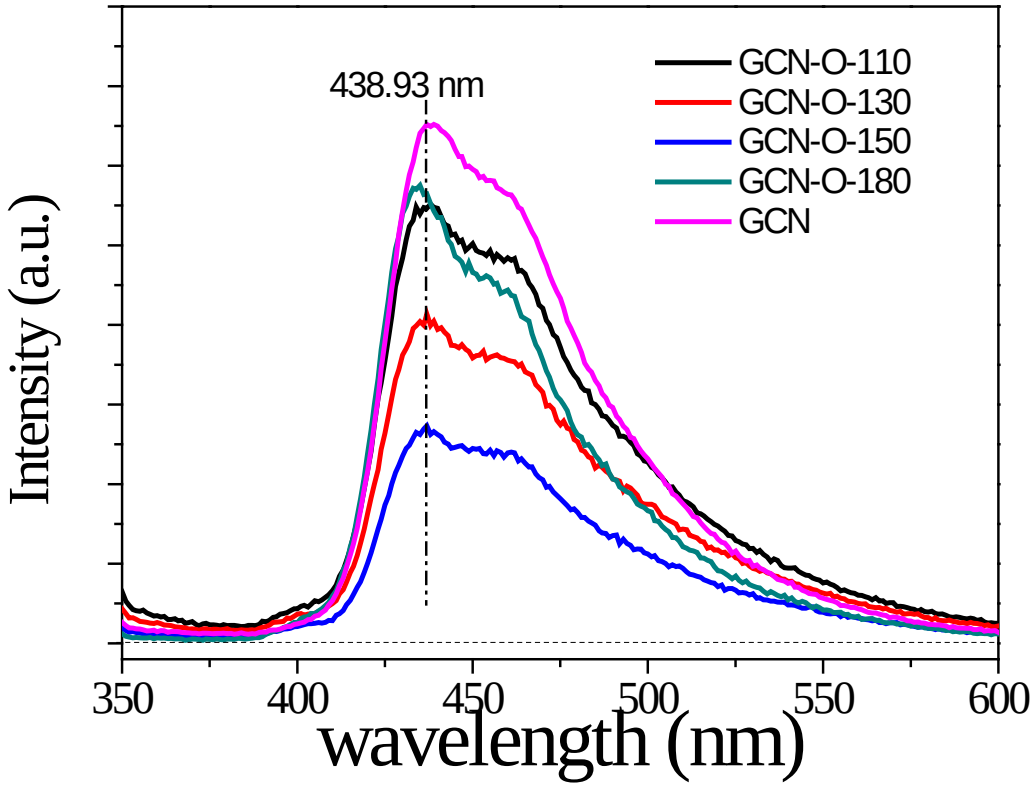

Fig. 20. Photoluminescence spectra of a series of GCN-O photocatalysts.

The recombination of photogenerated carriers of a photocatalyst can be analyzed by the photoluminescence spectra (PL) [51, 52]. Fig.20 shows the PL emission peaks between 400 to 600 nm of GCN samples. The spectra possess the similar shapes with a wide PL range and multiple intensive PL peaks, which indicate a steady PL properties and multiple recombination centres. But the intensities of the oxygen modified GCN at exciting wavelength of 340 nm were lower than that of GCN. Meanwhile the O-bearing GCN photocatalysts show a decreasing tendency of emission light with the rising hydrothermal temperature except GCN-O-180. When electron/hole pairs recombine, the potential energy of photogenerated carriers will be converted into electromagnetic wave or crystalline vibration as thermal energy, thus the reduced emission intensity indicates a weaken recombination. Moreover, the emission peaks did not show a shift, indicating the stable GCN crystals after hydrothermal treatment up to 150 ^{o}C. However, GCN-O-180 had a slight red shift of emission peak, suggesting a very high recombination rate.

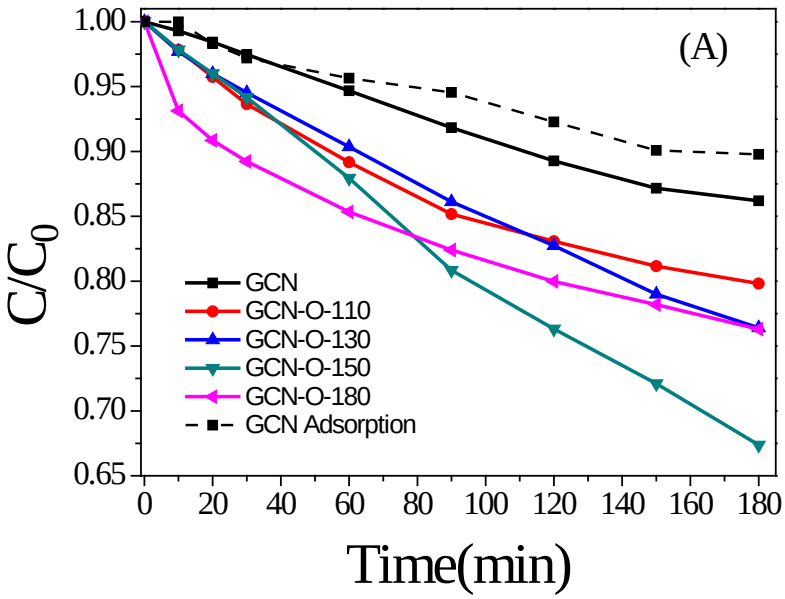

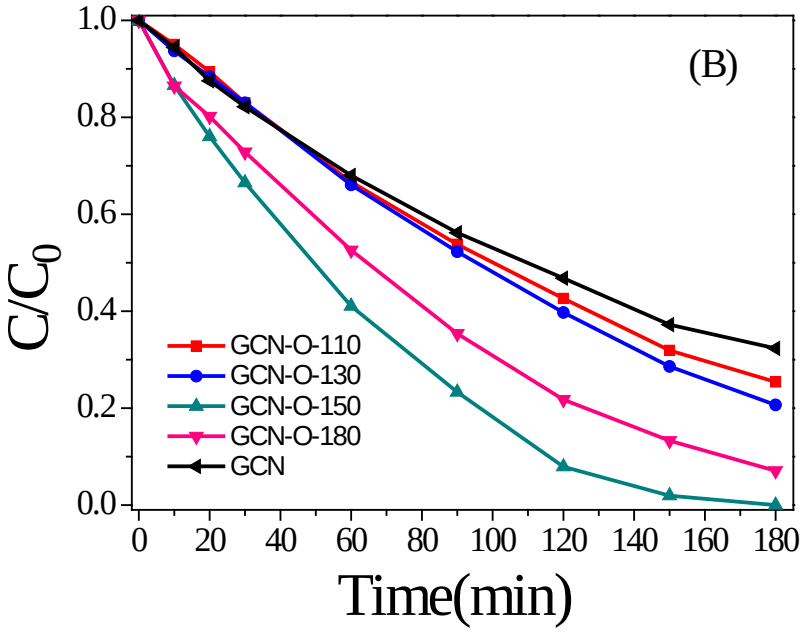

Fig. 21. MB photodegradation on GCN-O photocatalysts under (A) visible light irradiations and (B) artificial solar light irradiations.

Photocatalytic performances of the oxygen modified GCN photocatalysts were evaluated by MB degradation under both artificial sunlight and visible light irradiations. Fig.21 (A) shows the MB photodegradation on GCN samples under visible light irradiations. The bulk GCN had a weak activity in MB decomposition and about 10% MB was degraded in 3 h. GCN-O-110 and GCN-O-130 degraded 20% and 25% MB, respectively. GCN-O-150 showed the best activity and provided 35% MB degradation in 3 h, while GCN-O-180 sample had good initial MB degradation but only decomposed 25% MB. Similar experiments were carried out under artificial solar light irradiations (Fig.21 (B)), and the degradation efficiency showed a similar tendency as that in visible light photocatalysis. All oxygen modified GCN samples possessed better performances than bulk GCN. GCN-O-150 sample was able to decompose all MB in the solution in 2.5 h due to the contribution from UV activation. It was deduced that oxygen modification extended the absorbance of the GCN-O in visible light region, resulting in a

higher activity than pristine GCN under visible light. Moreover, the UV activity remained well, so their performances under sunlight would be still better than unmodified GCN. Fig. 28s shows that after three runs, the GCN-O-150 sample sustained 80% MB degradation. This stability is promising especially when the metal-free nature of GCN is taken into account.

Typically, in a graphitic carbon nitride participated photocatalytic reaction, two reactive radicals (hydroxyl radicals •OH and superoxide anion radical $\bullet O_2^-$) play essential roles in an aquatic system. The photogenerated electron appearing in conductive band is able to reduce oxygen (O_2) into $\bullet O_2^-$ (-0.286 V vs. NHE) [53], on the other hand, •OH radicals can be further generated via chemical transformation of $\bullet O_2^-$ radical but with a minor role in reaction [54]. Two radicals are easy pervasion and easily participate in chemical reactions which is the key factor for photocatalytic effectiveness

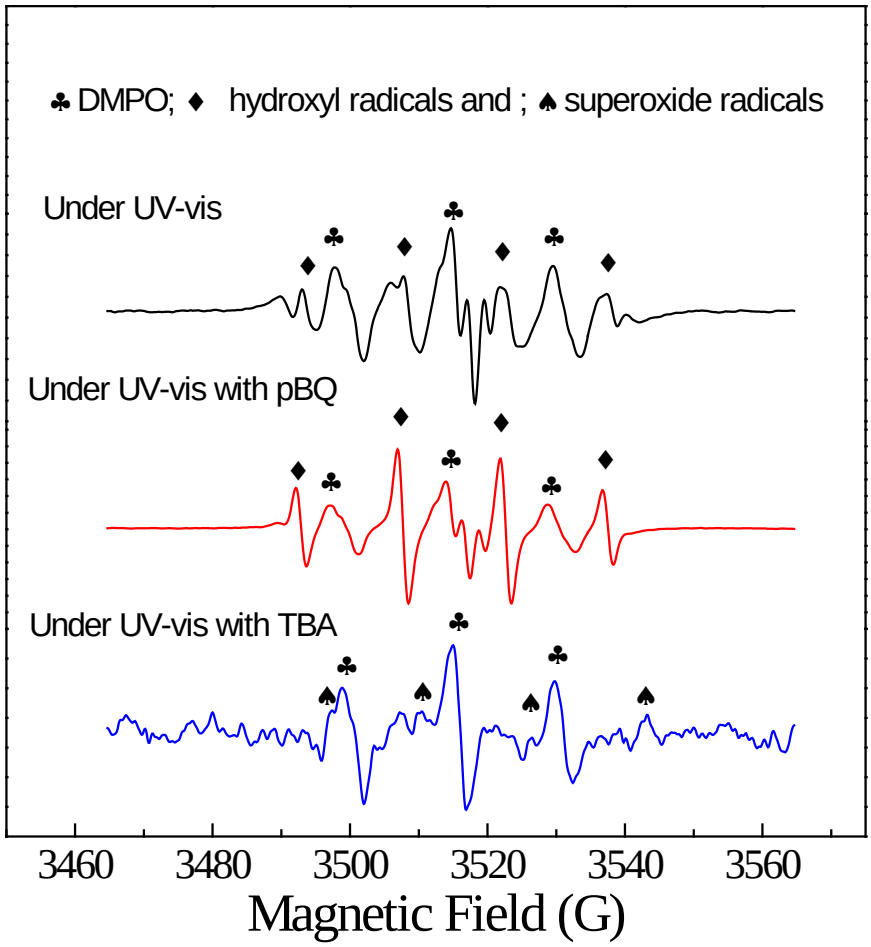

Fig. 22. EPR spectra of GCN-O-150 under irradiations with TBA or pBQ.

In this study, two reactive radicals were detected by EPR spectra for photocatalysis on GCN-O-150. In Fig. 22, besides the signals from oxidized DMPO [55], other two types of reactive radicals were observed. Two radical scavengers of TBA (tert-butanol) and pBQ (p-benzoquinone) were used to differentiate hydroxyl radicals and superoxide anions, respectively [56]. Spin-trapped signals of DMPO−•OH adducts were very strong, while weak superoxide radicals ($\bullet O_2^-$) were also identified.

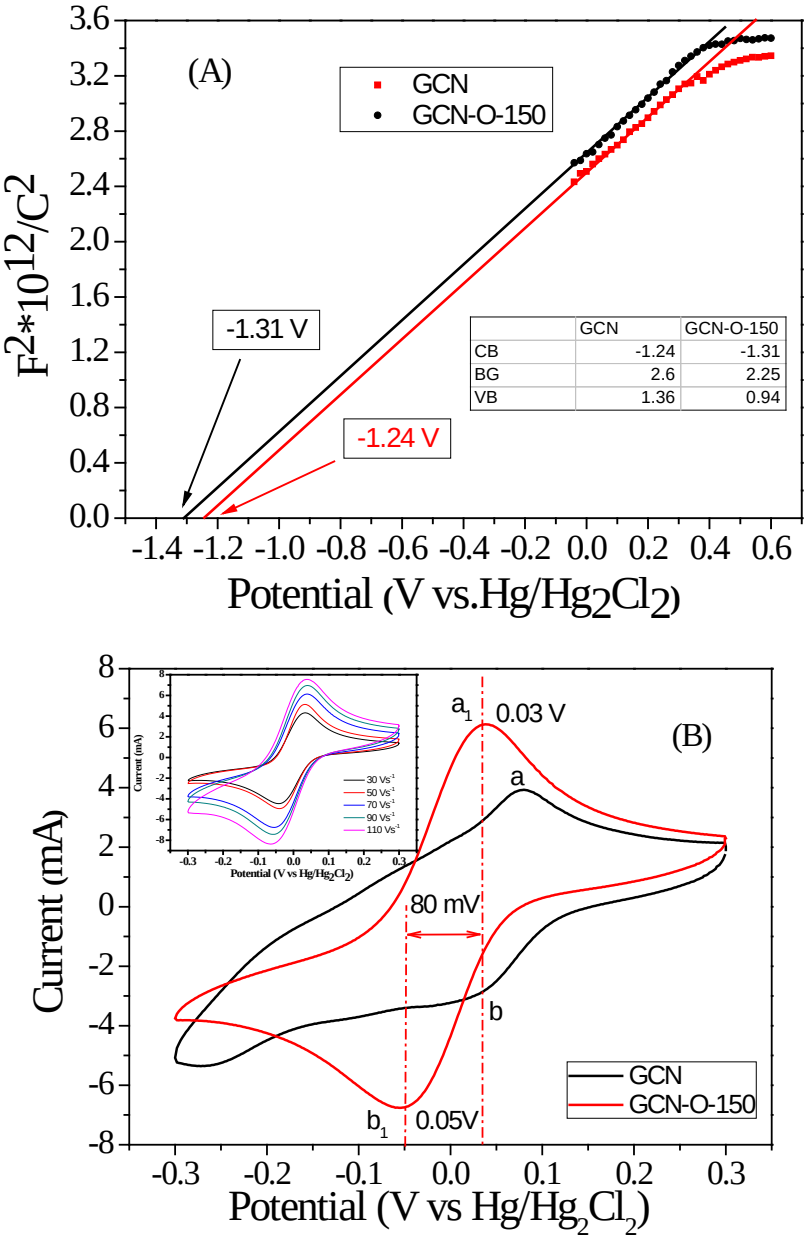

Fig. 23. Mott–Schottky plots and band structure (inset table; CB: conduction band, VB: valence band) of GCN and GCN-O-150(A); Cyclic voltammetry performed for GCN and GCN-O-150 (B).

For determining the energy levels of GCN and O-modified GCN samples, the Mott–Schottky plots and cyclic voltammetry (CV) were acquired. Fig.23 shows typical Mott–Schottky plots of bulk GCN and GCN-O-150 without light exciting. The n-type semiconductor feature can be

determined due to the positive slope in the linear plot section. The flat-band potential can be estimated by the tangent point potential with zero capacitance, because an electron has an ability to inject into conduction band at this potential [57]. The conduction band energies were then estimated to be -1.24 and -1.31 V vs. Hg/Hg_2Cl_2 (-1.48 and -1.55V vs NHE) for GCN and GCN-O-150, respectively. According to the band gap energies from UV-vis DRS analysis, the valence band was determined to be 1.36 and 0.94 V (1.12 and 0.7 V vs NHE) for GCN and GCN-O-150, which are feasible for superoxide anion radical generation. Fig. 23B shows cyclic voltammetry curves for analysis of the electrocatalytic activity in 2×10^{-4} mol/L MB solution at pH = 6.5. GCN-O-150 has a typical redox voltammogram loop, and the third cycle suggests that the electron can be easily injected into MB. Also two peaks had a discrimination of 80 mV, which can secure an outstanding reversible reaction performance with a reliable stabilization [58].

Fig. 24 schematically shows the band structure and associated photocatalysis. For GCN-O-150, a narrow band gap can absorb sufficient visible light to produce excited photoelectrons from VB to CB. With a potential of -1.55 V potential, the electron has an ability to oxidize water-soluble oxygen into $\bullet O_2^-$. It has been found that the potential energy of valence band (VB) holes (0.7 eV) from g-C_3N_4 is lower that of $OH^-/^{\bullet}OH$ (1.99 eV) and $H_2O/^{\bullet}OH$ (2.37 eV), the holes cannot directly oxidize OH^- or H_2O into $^{\bullet}OH$ [54]. The $^{\bullet}OH$ was generated by the further reaction of photogenerated electron with $\bullet O_2^-$. The reactive radicals ($\bullet O_2^-$ and $^{\bullet}OH$) can then decompose MB into CO_2 and H_2O.

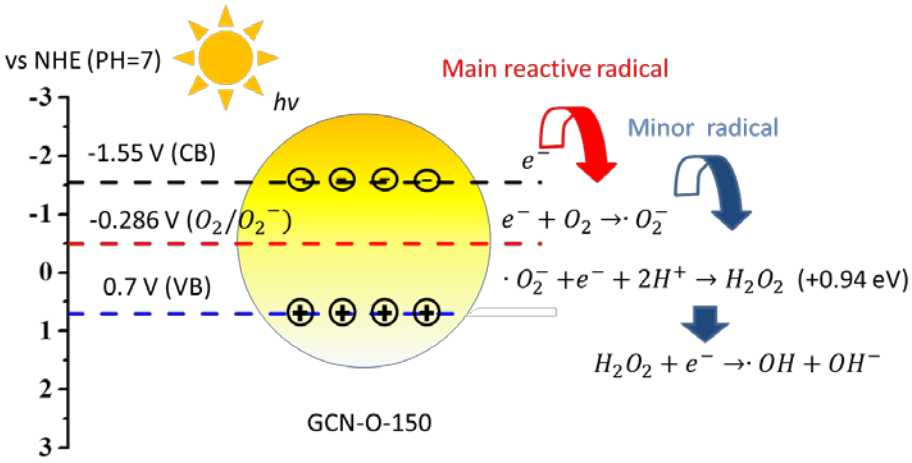

Fig. 24. Band structure and the photocatalysis on GCN-O-150.

4.5 Conclusions

In this study，oxygen modified graphitic carbon nitride photocatalysts were prepared by hydrothermal treatment of GCN and hydrogen peroxide at controlled temperatures. The oxygen functional groups incorporated into GCN structure have induced a positive photoelectronic effect in dye degradation procedure. UV-vis DRS and Mott–Schottky plots suggested the band gap energies and band gap positions were manipulated by the oxygen functional groups. All modified GCN performed better degradation of methylene blue under visible light (wavelength more than 420 nm) and sunlight irradiations than pristine GCN. The electrochemical study reveals the multiple roles of oxygen functional groups on GCN in electrocatalysis for increased electron and hole activities. It has been believed that the oxygen-bearing groups suppress the recombination of electron-hole pairs, increase the light radiation absorption and pollutant adsorption on GCN. Therefore, oxygen modification of GCN provides a feasible synthesis for highly efficient metal-free photocatalysts for economic and environmentally friendly solar energy applications.

4.6 Acknowledgments

This project was partially supported by Australian Research Council (ARC) under Project No.: DP150103026. The authors thank Dr Keyu Liu, Earth Science and Resource Engineering Department, CSIRO for his valuable discussion. Characterizations were partially obtained from Curtin University Electron Microscope Facility and Centre for Microscopy Characterization. H. S. thanks Curtin Research Fellowship and Opening Project (KL13-02) of State Key Laboratory of Materials-Oriented Chemical Engineering, China.

4.7 Supporting Information

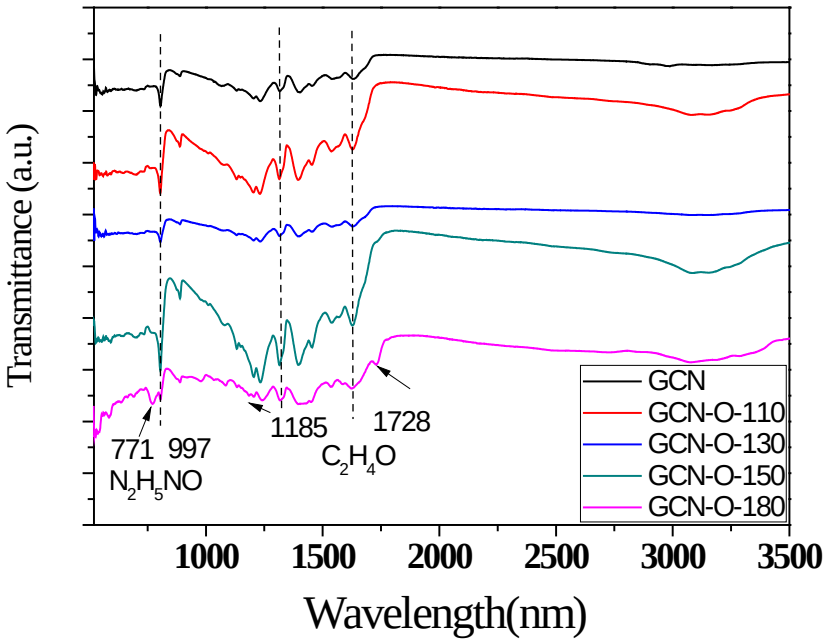

Fig. 25s. FTIR spectra of GCN and modified GCN photocatalysts.

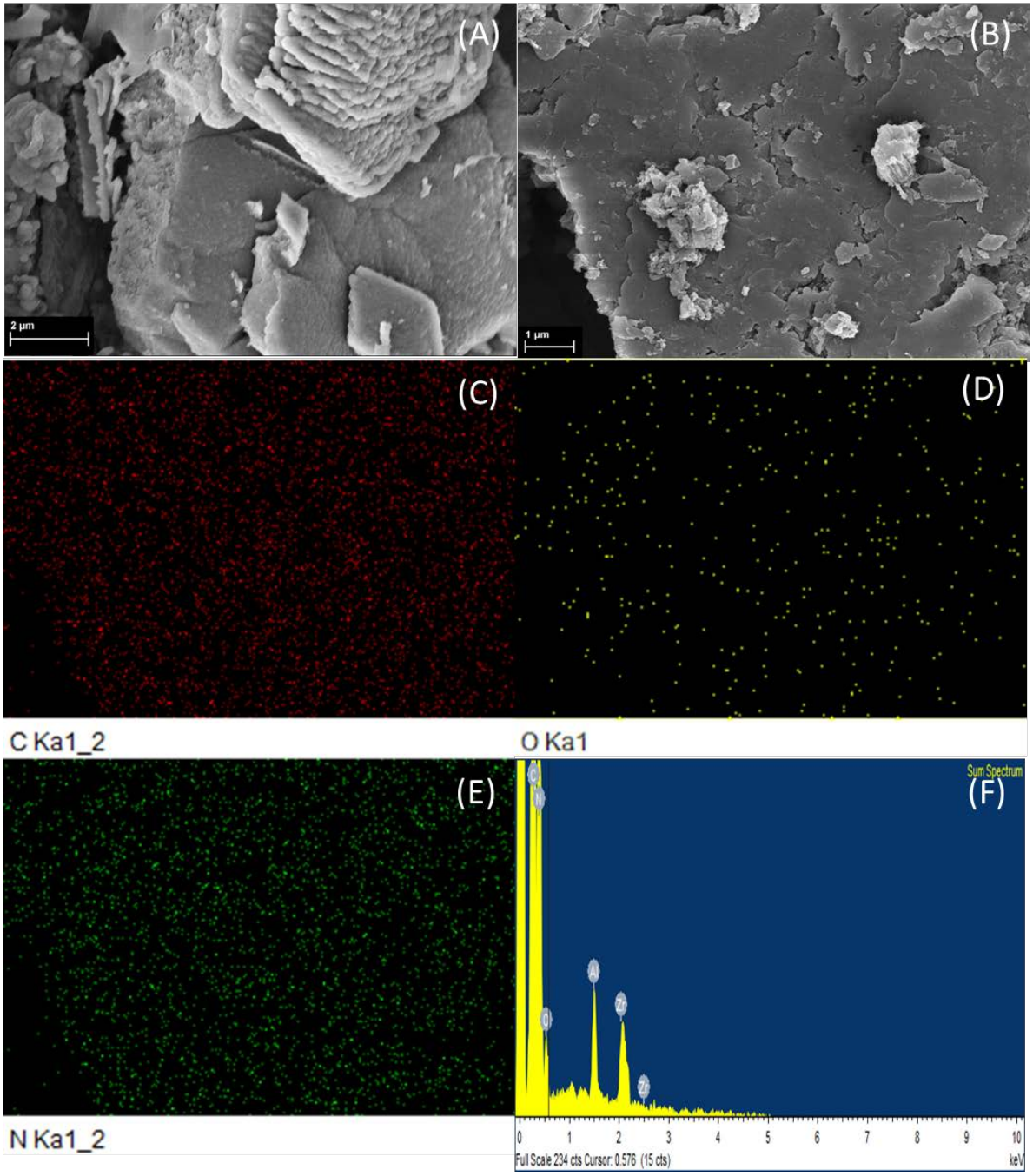

Fig. 26s. SEM images of GCN (A) and GCN-O-150 (B); Elemental mapping of carbon (C), oxygen (D) and nitrogen (E) of GCN-O-150 sample; EDS of GCN-O-150 (F).

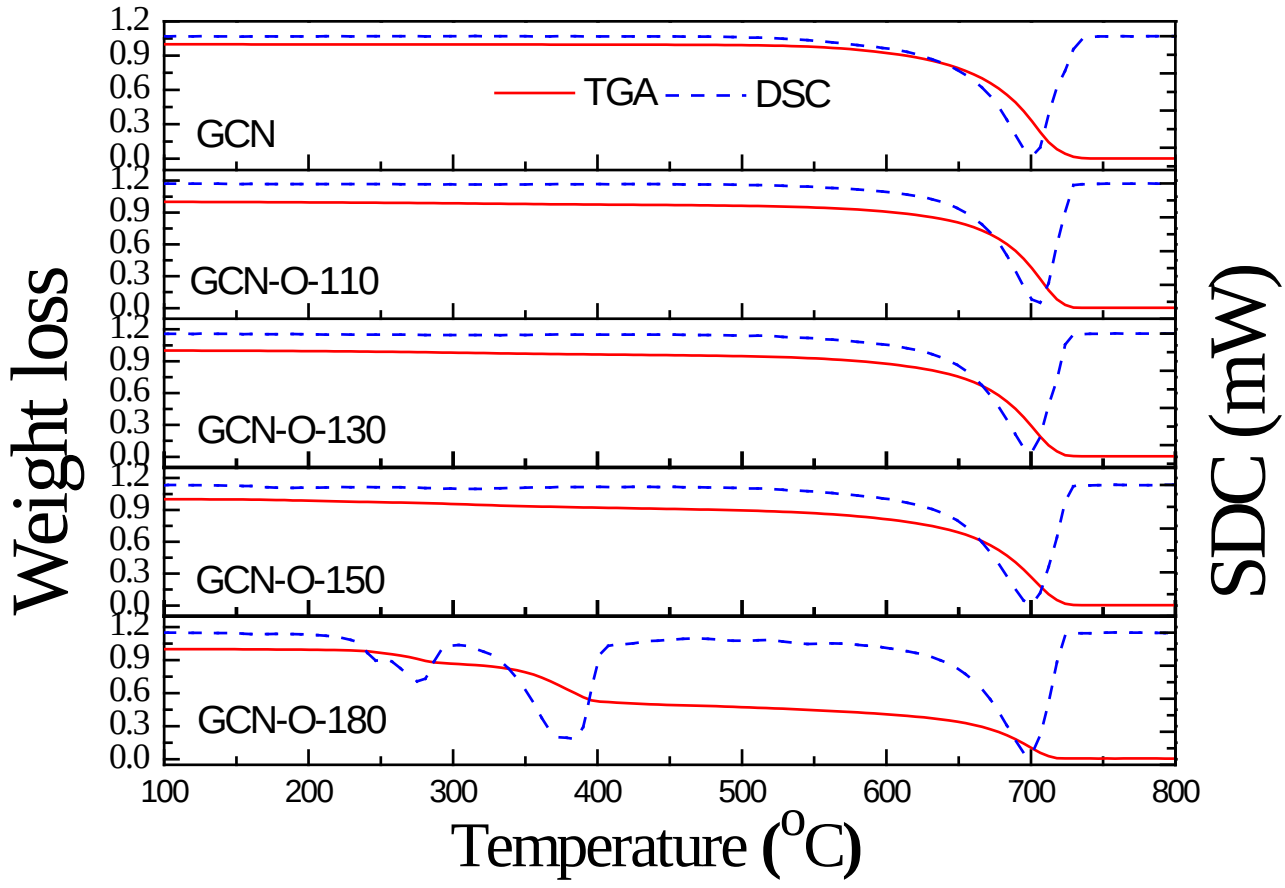

Fig. 27s. TGA and DSC analysis of O-doping GCN photocatalysts.

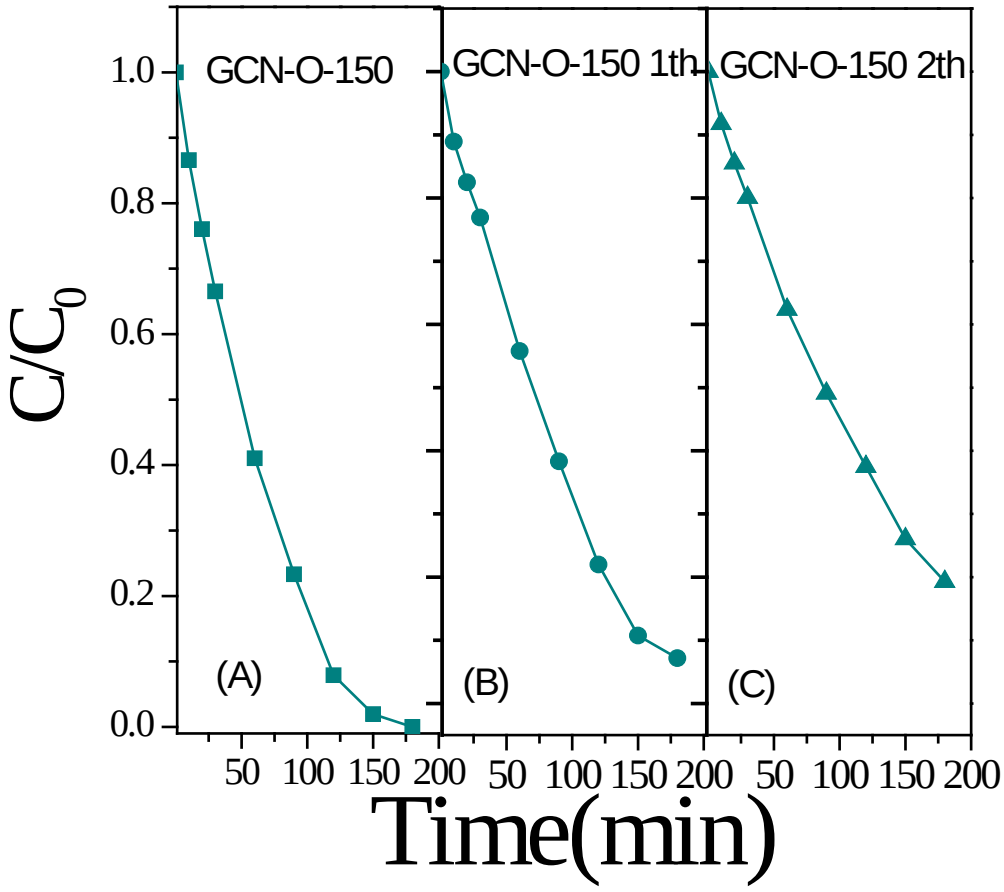

Fig. 28s. Recycling tests of degradation efficiency of MB solution by GCN-O-150.

4.8 References

[1] S. Chu, A. Majumdar, Opportunities and challenges for a sustainable energy future, Nature, 488 (2012) 294-303.

[2] J.K. Hurst, In pursuit of water oxidation catalysts for solar fuel production, Science, 328 (2010) 315-316.

[3] A.L. Linsebigler, G. Lu, J.T. Yates Jr, Photocatalysis on TiO_2 surfaces: principles, mechanisms, and selected results, Chemical Reviews, 95 (1995) 735-758.

[4] H.Q. Sun, S.Z. Liu, S.M. Liu, S.B. Wang, A comparative study of reduced graphene oxide modified TiO_2, ZnO and Ta_2O_5 in visible light photocatalytic/photochemical oxidation of methylene blue, Applied Catalysis B-Environmental, 146 (2014) 162-168.

[5] H.Q. Sun, G.L. Zhou, S.Z. Liu, H.M. Ang, M.O. Tade, S.B. Wang, Visible light responsive titania photocatalysts codoped by nitrogen and metal (Fe, Ni, Ag, or Pt) for remediation of aqueous pollutants, Chemical Engineering Journal, 231 (2013) 18-25.

[6] H.Q. Sun, R. Ullah, S.H. Chong, H.M. Ang, M.O. Tade, S.B. Wang, Room-light-induced indoor air purification using an efficient Pt/N-TiO_2 photocatalyst, Applied Catalysis B-Environmental, 108 (2011) 127-133.

[7] Y. Sun, C. Li, Y. Xu, H. Bai, Z. Yao, G. Shi, Chemically converted graphene as substrate for immobilizing and enhancing the activity of a polymeric catalyst, Chemical Communications, 46 (2010) 4740-4742.

[8] S.Z. Liu, H.Q. Sun, A. Suvorova, S.B. Wang, One-pot hydrothermal synthesis of ZnO-reduced graphene oxide composites using Zn powders for enhanced photocatalysis, Chemical Engineering Journal, 229 (2013) 533-539.

[9] D. Bahnemann, Photocatalytic water treatment: solar energy applications, Solar energy, 77 (2004) 445-459.

[10] H. Yan, J. Yang, G. Ma, G. Wu, X. Zong, Z. Lei, J. Shi, C. Li, Visible-light-driven hydrogen production with extremely high quantum efficiency on Pt–PdS/CdS photocatalyst, Journal of Catalysis, 266 (2009) 165-168.

[11] M.G. Kibria, F.A. Chowdhury, S. Zhao, B. AlOtaibi, M.L. Trudeau, H. Guo, Z. Mi, Visible light-driven efficient overall water splitting using p-type metal-nitride nanowire arrays, Nat Commun, 6 (2015).

[12] R. Ullah, H. Sun, H.M. Ang, M.O. Tade, S. Wang, Visible light photocatalytic degradation of organics on nanoparticles of bi-metallic oxides, Separation and Purification Technology, 89 (2012) 98-106.

[13] R. Ullah, H. Sun, H.M. Ang, M.O. Tade, S. Wang, Photocatalytic oxidation of water and air contaminants with metal doped $BiTaO_4$ irradiated with visible light, Catalysis Today, 192 (2012) 203-212.

[14] J. Liu, H. Bai, Y. Wang, Z. Liu, X. Zhang, D.D. Sun, Self-Assembling TiO_2 Nanorods on Large Graphene Oxide Sheets at a Two-Phase Interface and Their Anti-Recombination in Photocatalytic Applications, Advanced Functional Materials, 20 (2010) 4175-4181.

[15] H. Kato, K. Asakura, A. Kudo, Highly efficient water splitting into H_2 and O_2 over lanthanum-doped $NaTaO_3$ photocatalysts with high crystallinity and surface nanostructure, Journal of the American Chemical Society, 125 (2003) 3082-3089.

[16] H.Q. Sun, S.B. Wang, Research Advances in the Synthesis of Nanocarbon-Based Photocatalysts and Their Applications for Photocatalytic Conversion of Carbon Dioxide to Hydrocarbon Fuels, Energy & Fuels, 28 (2014) 22-36.

[17] S.Z. Liu, H.Q. Sun, S.M. Liu, S.B. Wang, Graphene facilitated visible light photodegradation of methylene blue over titanium dioxide photocatalysts, Chemical Engineering Journal, 214 (2013) 298-303.

[18] X. Wang, K. Maeda, A. Thomas, K. Takanabe, G. Xin, J.M. Carlsson, K. Domen, M. Antonietti, A metal-free polymeric photocatalyst for hydrogen production from water under visible light, Nature materials, 8 (2009) 76-80.

[19] D.J. Martin, K. Qiu, S.A. Shevlin, A.D. Handoko, X. Chen, Z. Guo, J. Tang, Highly Efficient Photocatalytic H_2 Evolution from Water using Visible Light and Structure-Controlled Graphitic Carbon Nitride, Angewandte Chemie International Edition, 53 (2014) 9240-9245.

[20] Z. Zhao, Y. Sun, F. Dong, Graphitic carbon nitride based nanocomposites: a review, Nanoscale, 7 (2015) 15-37.

[21] A. Thomas, A. Fischer, F. Goettmann, M. Antonietti, J.-O. Müller, R. Schlögl, J.M. Carlsson, Graphitic carbon nitride materials: variation of structure and morphology and their use as metal-free catalysts, Journal of Materials Chemistry, 18 (2008) 4893-4908.

[22] X.-H. Li, J.-S. Chen, X. Wang, J. Sun, M. Antonietti, Metal-free activation of dioxygen by graphene/g-C_3N_4 nanocomposites: functional dyads for selective oxidation of saturated hydrocarbons, Journal of the American Chemical Society, 133 (2011) 8074-8077.

[23] J. Gracia, P. Kroll, First principles study of C_3N_4 carbon nitride nanotubes, Journal of Materials Chemistry, 19 (2009) 3020-3026.

[24] A.Y. Liu, M.L. Cohen, Structural properties and electronic structure of low-compressibility materials: β-Si_3N_4 and hypothetical β-C_3N_4, Physical Review B, 41 (1990) 10727-10734.

[25] H. Yan, Y. Chen, S. Xu, Synthesis of graphitic carbon nitride by directly heating sulfuric acid treated melamine for enhanced photocatalytic H_2 production from water under visible light, International Journal of Hydrogen Energy, 37 (2012) 125-133.

[26] Q. Xiang, J. Yu, M. Jaroniec, Preparation and Enhanced Visible-Light Photocatalytic H_2-Production Activity of Graphene/C_3N_4 Composites, The Journal of Physical Chemistry C, 115 (2011) 7355-7363.

[27] R. Kuriki, K. Sekizawa, O. Ishitani, K. Maeda, Visible-Light-Driven CO_2 Reduction with Carbon Nitride: Enhancing the Activity of Ruthenium Catalysts, Angewandte Chemie-International Edition, 54 (2015) 2406-2409.

[28] Y. Zheng, L.H. Lin, X.J. Ye, F.S. Guo, X.C. Wang, Helical Graphitic Carbon Nitrides with Photocatalytic and Optical Activities, Angewandte Chemie-International Edition, 53 (2014) 11926-11930.

[29] P. Niu, Y.Q. Yang, J.C. Yu, G. Liu, H.M. Cheng, Switching the selectivity of the photoreduction reaction of carbon dioxide by controlling the band structure of a g-C_3N_4 photocatalyst, Chemical Communications, 50 (2014) 10837-10840.

[30] K. Maeda, R. Kuriki, M.W. Zhang, X.C. Wang, O. Ishitani, The effect of the pore-wall structure of carbon nitride on photocatalytic CO_2 reduction under visible light, Journal of Materials Chemistry A, 2 (2014) 15146-15151.

[31] J. He, H. Sun, S. Indrawirawan, X. Duan, M.O. Tade, S. Wang, Novel polyoxometalate@g-C_3N_4 hybrid photocatalysts for degradation of dyes and phenolics, Journal of Colloid and Interface Science, 456 (2015) 15-21.

[32] H.Q. Sun, G.L. Zhou, Y.X. Wang, A. Suvorova, S.B. Wang, A New Metal-Free Carbon Hybrid for Enhanced Photocatalysis, ACS Applied Materials & Interfaces, 6 (2014) 16745-16754.

[33] B. Ai, X. Duan, H. Sun, X. Qiu, S. Wang, Metal-free graphene-carbon nitride hybrids for photodegradation of organic pollutants in water, Catalysis Today, 258, Part 2 (2015) 668-675.

[34] W. Wang, J.C. Yu, D. Xia, P.K. Wong, Y. Li, Graphene and g-C_3N_4 Nanosheets Cowrapped Elemental α-Sulfur As a Novel Metal-Free Heterojunction Photocatalyst for Bacterial Inactivation under Visible-Light, Environmental science & technology, 47 (2013) 8724-8732.

[35] Y. Wang, Y. Di, M. Antonietti, H. Li, X. Chen, X. Wang, Excellent Visible-Light Photocatalysis of Fluorinated Polymeric Carbon Nitride Solids, Chemistry of materials, 22 (2010) 5119-5121.

[36] J.-C. Tan, B. Civalleri, A. Erba, E. Albanese, Quantum mechanical predictions to elucidate the anisotropic elastic properties of zeolitic imidazolate frameworks: ZIF-4 vs. ZIF-zni, CrystEngComm, (2015).

[37] G. Liu, L. Wang, H.G. Yang, H.-M. Cheng, G.Q.M. Lu, Titania-based photocatalysts—crystal growth, doping and heterostructuring, Journal of Materials Chemistry, 20 (2010) 831-843.

[38] J. Li, B. Shen, Z. Hong, B. Lin, B. Gao, Y. Chen, A facile approach to synthesize novel oxygen-doped g-C_3N_4 with superior visible-light photoreactivity, Chemical Communications, 48 (2012) 12017-12019.

[39] G. Dong, Z. Ai, L. Zhang, Efficient anoxic pollutant removal with oxygen functionalized graphitic carbon nitride under visible light, RSC Advances, 4 (2014) 5553-5560.

[40] L. Ming, H. Yue, L. Xu, F. Chen, Hydrothermal Synthesis of Oxidized g-C_3N_4 and Its Photocatalytic Activity Regulation, Journal of Materials Chemistry A, (2014).

[41] Z.-F. Huang, J. Song, L. Pan, Z. Wang, X. Zhang, J.-J. Zou, W. Mi, X. Zhang, L. Wang, Carbon nitride with simultaneous porous network and O-doping for efficient solar-energy-driven hydrogen evolution, Nano Energy, 12 (2015) 646-656.

[42] S. Yan, Z. Li, Z. Zou, Photodegradation performance of g-C3N4 fabricated by directly heating melamine, Langmuir, 25 (2009) 10397-10401.

[43] X. Wang, X. Chen, A. Thomas, X. Fu, M. Antonietti, Metal-Containing Carbon Nitride Compounds: A New Functional Organic–Metal Hybrid Material, Advanced Materials, 21 (2009) 1609-1612.

[44] H. Xu, J. Yan, Y. Xu, Y. Song, H. Li, J. Xia, C. Huang, H. Wan, Novel visible-light-driven AgX/graphite-like C_3N_4 (X = Br, I) hybrid materials with synergistic photocatalytic activity, Applied Catalysis B: Environmental, 129 (2013) 182-193.

[45] M. Xu, L. Han, S. Dong, Facile Fabrication of Highly Efficient g-C_3N_4/Ag_2O Heterostructured Photocatalysts with Enhanced Visible-Light Photocatalytic Activity, ACS Applied Materials & Interfaces, 5 (2013) 12533-12540.

[46] M. Tahir, C. Cao, F.K. Butt, F. Idrees, N. Mahmood, Z. Ali, I. Aslam, M. Tanveer, M. Rizwan, T. Mahmood, Tubular graphitic-C_3N_4: a prospective material for energy storage and green photocatalysis, Journal of Materials Chemistry A, 1 (2013) 13949-13955.

[47] X. Wang, K. Maeda, A. Thomas, K. Takanabe, G. Xin, J.M. Carlsson, K. Domen, M. Antonietti, A metal-free polymeric photocatalyst for hydrogen production from water under visible light, Nature materials, 8 (2008) 76-80.

[48] X. Wang, K. Maeda, A. Thomas, K. Takanabe, G. Xin, J.M. Carlsson, K. Domen, M. Antonietti, A metal-free polymeric photocatalyst for hydrogen production from water under visible light, Nat Mater, 8 (2009) 76-80.

[49] J. Du, X. Lai, N. Yang, J. Zhai, D. Kisailus, F. Su, D. Wang, L. Jiang, Hierarchically ordered macro− mesoporous TiO_2− graphene composite films: Improved mass transfer, reduced charge recombination, and their enhanced photocatalytic activities, Acs Nano, 5 (2010) 590-596.

[50] J. Tauc, Absorption edge and internal electric fields in amorphous semiconductors, Materials Research Bulletin, 5 (1970) 721-729.

[51] G. Liao, S. Chen, X. Quan, H. Yu, H. Zhao, Graphene oxide modified g-C_3N_4 hybrid with enhanced photocatalytic capability under visible light irradiation, Journal of Materials Chemistry, 22 (2012) 2721-2726.

[52] F. He, G. Chen, Y. Yu, S. Hao, Y. Zhou, Y. Zheng, Facile Approach to Synthesize g-PAN/g-C_3N_4 Composites with Enhanced Photocatalytic H_2 Evolution Activity, ACS Applied Materials & Interfaces, 6 (2014) 7171-7179.

[53] M. Pelaez, N.T. Nolan, S.C. Pillai, M.K. Seery, P. Falaras, A.G. Kontos, P.S.M. Dunlop, J.W.J. Hamilton, J.A. Byrne, K. O'Shea, M.H. Entezari, D.D. Dionysiou, A review on the visible light active titanium dioxide photocatalysts for environmental applications, Applied Catalysis B: Environmental, 125 (2012) 331-349.

[54] F. Dong, Z. Wang, Y. Li, W.-K. Ho, S.C. Lee, Immobilization of Polymeric g-C_3N_4 on Structured Ceramic Foam for Efficient Visible Light Photocatalytic Air Purification with Real Indoor Illumination, Environmental science & technology, 48 (2014) 10345-10353.

[55] L.-Y. Zang, K. Stone, W.A. Pryor, Detection of free radicals in aqueous extracts of cigarette tar by electron spin resonance, Free Radical Biology and Medicine, 19 (1995) 161-167.

[56] G.V. Buxton, C.L. Greenstock, W.P. Helman, A.B. Ross, Critical Review of rate constants for reactions of hydrated electrons, hydrogen atoms and hydroxyl radicals ($^{\cdot}OH/^{\cdot}O^{-}$ in Aqueous Solution, Journal of Physical and Chemical Reference Data, 17 (1988) 513-886.

[57] D.-S. Kong, The Influence of Fluoride on the Physicochemical Properties of Anodic Oxide Films Formed on Titanium Surfaces, Langmuir, 24 (2008) 5324-5331.

[58] S.M. Lyth, Y. Nabae, S. Moriya, S. Kuroki, M.-a. Kakimoto, J.-i. Ozaki, S. Miyata, Carbon Nitride as a Nonprecious Catalyst for Electrochemical Oxygen Reduction, The Journal of Physical Chemistry C, 113 (2009) 20148-20151.

Ever reasonable effort has been made to acknowledge the owner of copyright material. I would be pleased to hear from any copyright owner who has been omitted or incorrectly acknowledged.

5 Integrated oxygen-doping and dye sensitization of graphitic carbon nitride for enhanced visible light photodegradation

This paper has been published in Journal of Colloid and Interface Science in Volume 476, 15 August 2016, Pages 193–199

5.1 ABSTRACT

Graphitic carbon nitride (GCN) is a promising metal-free photocatalyst while suffering from low charge mobility induced inefficient photocatalysis. In this work, oxygen doping was employed to enhance the photodegradation of organic pollutants in water on graphitic carbon nitride (GCNO) under visible light. For further absorption extension, four organic dyes (Eosin-Y, Perylene, Nile-red and Coumarin) were adopted to dye-sensitize the GCNO photocatalyst. It was found that O-doping can promote dye sensitization, which was dependent on the type of dyes and influenced the photodegradation efficiencies of methylene blue (MB) and phenol. Nile-red sensitized GCNO presented the best activity in MB degradation under $\lambda > 480$ nm irradiations while Eosin-Y showed the best sensitization performance for phenol degradation under $\lambda > 420$ nm light source. However, dye sensitization was not effective for enhanced pollutant degradation on GCN without O-doping. UV-vis diffuse reflectance spectra (UV-vis DRS), photoluminescence (PL) spectra, and photocurrent analyses were applied to investigate the mechanism of carriers' transfer, which indicated that dye molecules could inject extra electrons into GCNO energy band and the energy dislocation could supress electron/hole recombination, enhancing photocatalytic performances.

5.2 Introduction

In the 21th century, it has been a big challenge to explore renewable energy to replace traditional fossil fuels because of the over-depletion and numerous environmental issues associated with fuel combustion. Since the discovery of hydrogen production by photoelectrochemical water splitting in 1972[1], semiconductor-based photocatalysis has been widely devoted to the new energy innovation. However, until now there is no such a semiconductor ideally balancing the

low cost, high activity, high sunlight harvest and satisfactory chemical stability[2, 3]. Recently, graphitic carbon nitride (g-C_3N_4, GCN) has been considered as a metal-free, photosensitive semiconductor, which can be adopted in photoelectrochemical applications, because it is chemically stable, environmentally compatible, and has suitable band gap energy toward visible light absorption[4]. GCN-based materials have demonstrated great potential in hydrogen production from water splitting[5, 6], photodegradation of gaseous or liquid pollutants [7, 8], electrochemical fluorescence sensors[9, 10], and electrode materials for fuel cells or batteries[11, 12]. But GCN has a limited light absorption and low photocatalytic efficiency due to the high recombination rate of photo-excited electron/hole pairs, which become the main barricade to practical photocatalytic application [5, 13]. Many methods have been developed for modification of GCN to overcome the limitation, such as improved textural porosity[14, 15], heteroatom doping[16-18], semiconductor coupling[19, 20], and activating[5, 7], etc. Among the modifications, oxygen doping is able to enlarge the porosity, increase light absorption, and reduce the carrier recombination. Moreover, O-doped GCN could be easily prepared from mild hydrothermal treatment with H_2O_2, making the O-doped GCN a promising future in fabrication of solar energy devices [21-24]. But it still suffers from a high disparity of quantum yield compared to classical metal-based photocatalysts (such as TiO_2 and ZnO).

Today, dye sensitization technology is widely utilized in fabrication of photovoltaic devices, namely low-cost but commercially feasible solar cells. Dye photosensitization can extend the light absorption range, enhance photon harvesting efficiency, provide extra excited electronic pairs from a dye and accelerate charge transfer, leading to a high efficiency of photoelectric conversion [25]. TiO_2 semiconductor film was successfully grafted with a dye, $RuL_2(\mu-(CN)Ru(CN)L'_2$ (where L represented 2,2' bipyridine-4,4'-dicarboxylic and L' is 2,2'-bipyridine) and the derived photovoltaic system showed a higher proration solar energy harvesting (46%), and a high photo-generated electrical current (80% higher than TiO_2)[26].

Recent studies revealed that organic dye molecules with a porphyrin core and alternative π-system have a good ability in photosensitization [27-30]. In GCN studies, Eosin-Y sensitized, Pt doped mesoporous $g-C_3N_4$ showed a good activity in H_2 generation. Eosin-Y assistance not only extended the light absorption but also improved the apparent quantum efficiency at 19.4%[28]. Erythrosin B sensitized, Pt doped $g-C_3N_4$ nanosheets were reported to present 7.1 times higher activity in photocatalytic H_2 generation[31]. However, the photocatalytic activity highly depends on $g-C_3N_4$ textural properties and metal co-catalyst [32-34], and there are no reports on dye sensitized only with a high activity.

In this study, we present an investigation on the synergistic effect of oxygen doping and dye sensitization on GCN for photocatalysis. Oxygen doped GCN (GCNO) catalysts sensitized by several cooperative asymmetric organophotoredox organic dyes, Eosin-Y, Perylene, Nile Red and Coumarin were prepared and found to exhibit high activities in methylene blue (MB) and phenol photodegradation under visible light irradiations. Nile-Red effectively enhanced the light harvesting of GCNO with the highest activity in MB degradation while Eosin-Y grafted GCNO demonstrated the best activity in phenol degradation. The photosensitization mechanism was studied by UV-vis diffuse reflectance spectra (DRS), photoluminescence (PL) spectra analysis, and photocurrent analysis.

5.3 Experimental section

Materials

All chemicals utilized in this study are of analytical grade. Melamine, Nafion, Eosin-Y, Perylene, Nile Red and Coumarin were supplied by Sigma-Aldrich. Hydrogen peroxide (30

wt%), methylene blue, acetone, sodium sulfate and phenol were obtained from Biolab, Australia.

Preparation of GCNO and dye sensitized GCNO.

Oxygen doped graphitic carbon nitride (GCNO) was synthesized by a hydrothermal treatment of GCN with hydrogen peroxide (30 wt%). Firstly, 10 g melamine was put in a 20 mL alumina crucible, with semi-covering. Then the precursor in the crucible was heated in a muffle furnace at 400 ℃ for 2 h and then heated at 520 ℃ for another 2 h with a heating rate of 1 ℃/min. The well grinded yellow product was referred as GCN. Secondly, 1 g GCN was mixed with 50 mL hydrogen peroxide solution in a 120 mL Teflon-lined stainless steel autoclave with vigorously stirring for 30 min. After that the autoclave was sealed and put into an oven for a hydrothermal treatment at 130 ℃ for 12 h. The product was named as GCNO. For dye sensitization, 0.5 g GCNO was mixed with 30 mL acetone and 2 mg dye (Eosin-Y, Perylene, Nile Red and Coumarin), the suspensions were vigorously stirred for 3 h and dried at 100 ℃ for 12 h. The Eosin-Y, Perylene, Nile Red and Coumarin grafted products were labelled as GCNO-E, GCNO-P, GCNO-N and GCNO-C, respectively. The structures of the dyes are presented in Fig. 36s (SD).

Preparation of working electrodes

An ITO conductive glass (Sigma-Aldrich) with 8 ohm resistance was cut into $2 \times 1\ cm^2$ dimension as a working electrode substrate. Before coating samples, the ITO surface was cleaned by ethanol, acetone and isopropanol, successively, and then dried by argon flush. One side of ITO slice ($1 \times 1\ cm^2$) was covered with copper wire and heat conductive and electrical insulated adhesive, and the other side was coated with catalyst particle suspensions. The suspension was obtained from 40 mg particle sample, 5 mL Nafion, and 200 mL ethanol with

2 h sonication treatment. The slurry suspension gradually dropped on the 1 cm^2 substrate and dried at 110 ℃ for 3 h.

Evaluation of photocatalytic performance

Photocatalytic performances of dye sensitized GCNO catalysts were evaluated by the photodegradation of MB and phenol solutions under λ > 480 and λ > 420 nm visible light irradiations, respectively. In a typical process, 10 mg/L, 200 mL MB solutions (or 10 mg/L, 200 mL phenol) and the photocatalysts (100 mg) were mixed in a 1 L double-jacket cylindrical reactor with water cycling at 25 °C, under a constant stirring of 350 rpm. Two light sources were applied in this study: λ > 420 nm (the photon intensity were 0.01, 9.24, 84.1×10^3 $\mu W/cm^2$ in 220~280, 315~400, 400~1050 nm) and λ > 480 nm (the photon intensity were 0, 0.24, 60.5×10^3 $\mu W/cm^2$ in 220~280, 315~400, 400~1050 nm), by light cut-off filters from a MSR 575/2 metal halide lamp (575 W, Philips). The light was positioned 30 cm away from the reactor. The reaction was initiated by switching on the lamp. At certain time intervals, the reaction solution was withdrawn by a 5 mL syringe. MB would be analyzed by a JASCO UV–vis spectrophotometer at a wavelength of 664 nm. Phenol solution was analyzed by an ultra-high performance liquid chromatography (UHPLC) system (Thermo-Fisher Scientific 3000) with a UV detector at the wavelength of 270 nm.

Characterization methods

X-ray diffraction (XRD) was used to observe the crystal phases of GCN and GCNO samples on a Bruker D8-Advance X-ray diffractometer. Field emission scanning electron microscopy (SEM) was used to analyze the morphology, size, and pattern information on Zeiss Neon 40EsB. Textural properties from N_2 adsorption-desorption isotherms were evaluated on a Micromeritics Tristar 3000, and all samples were prepared via a degassing procedure at 110 ℃ in vaccum. UV–vis diffuse reflectance spectra (DRS) were recorded on a JASCO V670

spectrophotometer with an Ø60 mm integrating sphere, and $BaSO_4$ was used as a reference material. Photoluminescence spectra (PL) were investigated by a PerkinElmer LS 55 Fluorescence Spectrometer. Photocurrent analysis was determined on a Zennium electrochemical workstation in a conventional three-electrode cell, Hg/Hg_2Cl_2 was applied as the reference electrode, a platinum wire was used as the auxiliary electrode, and Na_2SO_4 solution (0.2 M) was as electrolyte. Five cycles were applied and the intermission for turning on/off light was 30 s.

5.4 Results and discussion

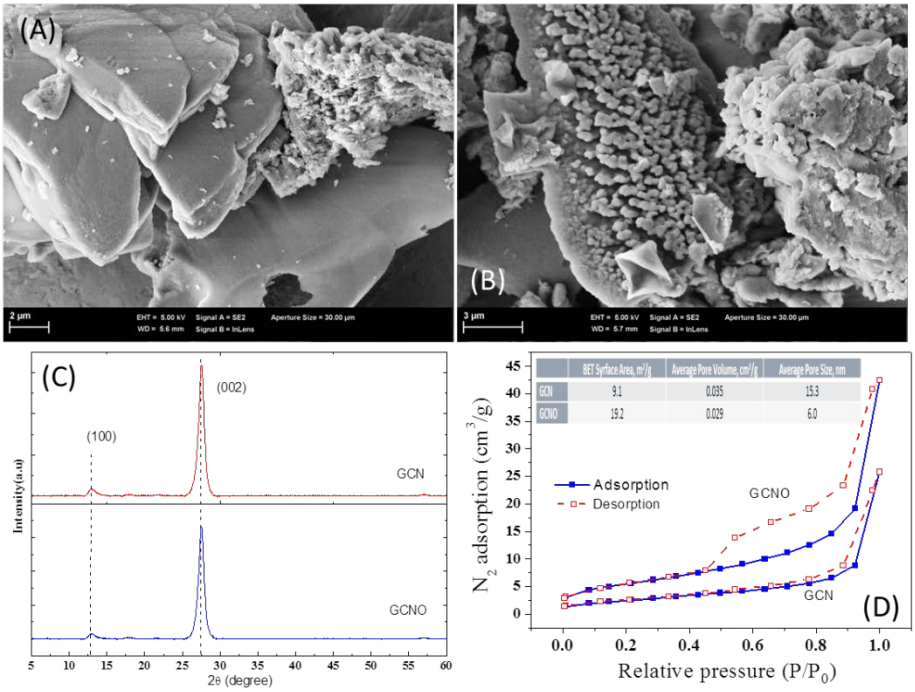

Fig. 29. SEM images of GCN (A) and GCNO (B); XRD patterns (C) of GCN and GCNO; N_2 adsorption−desorption isotherms and the textural properties (D) of GCN and GCNO.

Fig. 29 shows SEM images, XRD patterns and nitrogen adsorption-desorption isotherms of GCN and oxygen doped GCN. A multiple layer-stacked, nearly bulk structure appears in Fig.40 (A) due to the synthesis route of melamine condensation and crystallization during calcination. The inhomogeneity morphology was caused by uneven thermal distribution[35]. Oxygen

doped GCN sample showed rough surface with improved layered structure (Fig.40B). GCN and GCNO presented negligible difference in XRD profiles (Fig.40C). Two peaks located at 27.4 and 13.1°, respectively, indicate the (002) and (100) diffraction planes of GCN layer-stacked structure (JCPDS 87-1526). Fig.40(D) demonstrates nitrogen adsorption-desorption isotherms of GCN and GCNO. The curves show a type IV adsorption behavior with a H3 type hysteresis loop. The loop of GCNO is much wider under mild and high relative pressure range, implying more mesopores of GCNO and higher BET surface area (19.2 m^2/g) than GCN (9.1 m^2/g). The pore volumes were 0.035 and 0.029 cm^2/g and average pore sizes were 15.3 and 6.0 nm for GCNO and GCN, respectively, suggesting that the hydrothermal treatment caused a more porous structure for GCN [14].

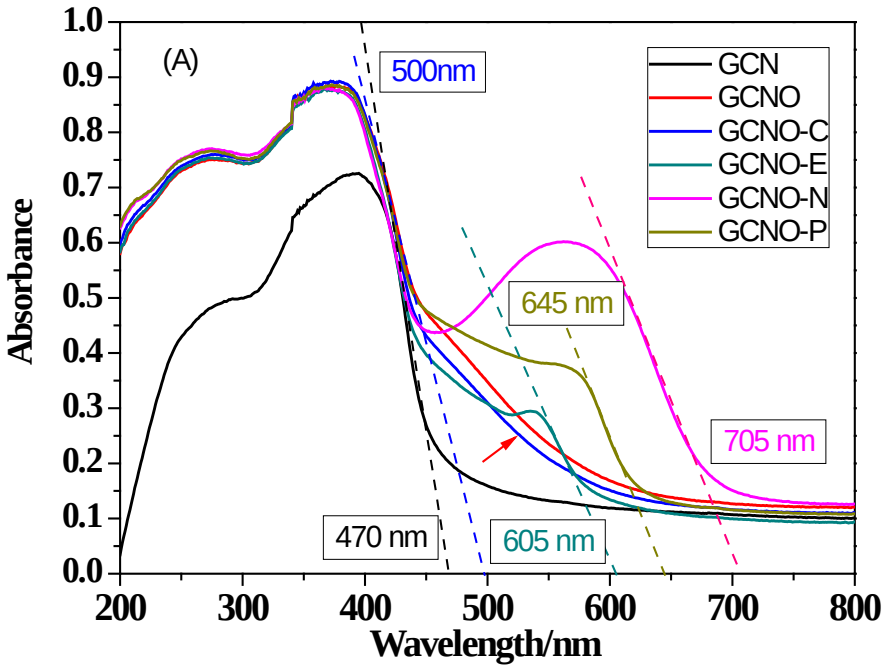

Fig. 30. UV–vis DRS of (A) of GCN, GCNO, GCNO-C, GCNO-E, GCNO-N, GCNO-P and GCN-N; Band gap (B) of GCN and dye photosensitized GCNO particles.

In this work, UV–vis diffuse reflectance spectra (DRS) were used to characterize the optical properties of dye photosensitized GCNO catalysts. In Fig.30, oxygen doping and dye photosensitizing treatments can extend the absorption threshold. GCN has an absorption edge

at 470 nm, which is corresponding to 2.7 eV band gap energy[36]. The oxygen doped GCN has an improved absorption up to 500 nm, and an additional absorption extended to 600 nm, which may be caused by oxygen functional groups. In contrast, this function is weakened on GCNO-C, which might be attributed to the interaction between Coumarin and O-bearing functional groups[37]. GCNO-E has an absorption edge at 605 nm, while GCNO-P has an absorption edge at 645 nm, and GCNO-N shows 705 nm absorption edge in a near infrared region. The band gap energies of the dye sensitized photocatalysts were calculated and it was found that oxygen doping led to a decreasing band gap energy to 2.6 eV for GCNO sample and GCNO-C has the same value (see information in Fig. 37s)[38].

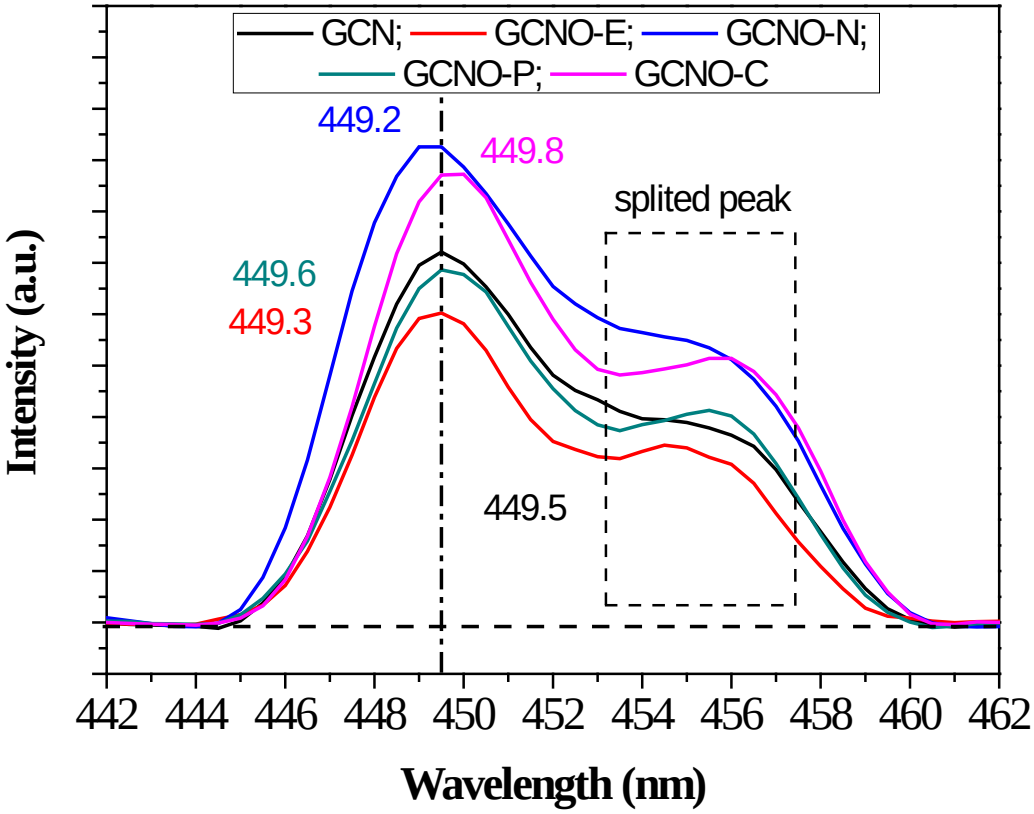

Fig. 31. Photoluminescence spectra of GCN, GCNO-E, GCNO-P, GCNO-N, and GCNO-C.

Photoluminescence spectroscopy is able to show fluorescence quenching by electron/hole pair recombination[39]. All the samples were measured by photoluminescence under 325 nm exciting radiation (Fig. 31). GCN could emit a strong PL peak at 449.5 nm, which is contributed

by the lone pairs of electrons in nitrogen atom jumping and being injected into anti-π orbit with 2.7 eV band gap energy[40]. GCNO-N resulted in the strongest PL emission at 449.2 nm. Coumarin also enhanced the PL intensity of GCNO, with the emission peak shifted into 449.8 nm. Perylene sensitized GCNO (GCNO-P) has weaker PL with the emission peak shifted into 449.6 nm. GCNO-E has the weakest PL intensity located at 449.3 nm. In photoluminescence, the shift in the emission peak is from the interaction of photo-electron relocation between GCNO and dye molecules[28]. The higher PL emission peak on GCNO-N may be caused by high light absorption as shown in DRS. Coumarin molecules instinctively possess strong PL emitting properties which are widely adopted in sensitive fluorescence probes [41]. Eosin-Y and Perylene could reduce the PL intensity because the excited dye can accept the photo-electron from the lowest unoccupied molecular orbital (LUMO) in GCNO and decrease the recombination potential from the semiconductor. It is notable that five PL spectra present split peaks with 6~8 nm red shift away from their main PL peaks. Such phenomenon indicates the interaction between diluted luminescence molecules[42].

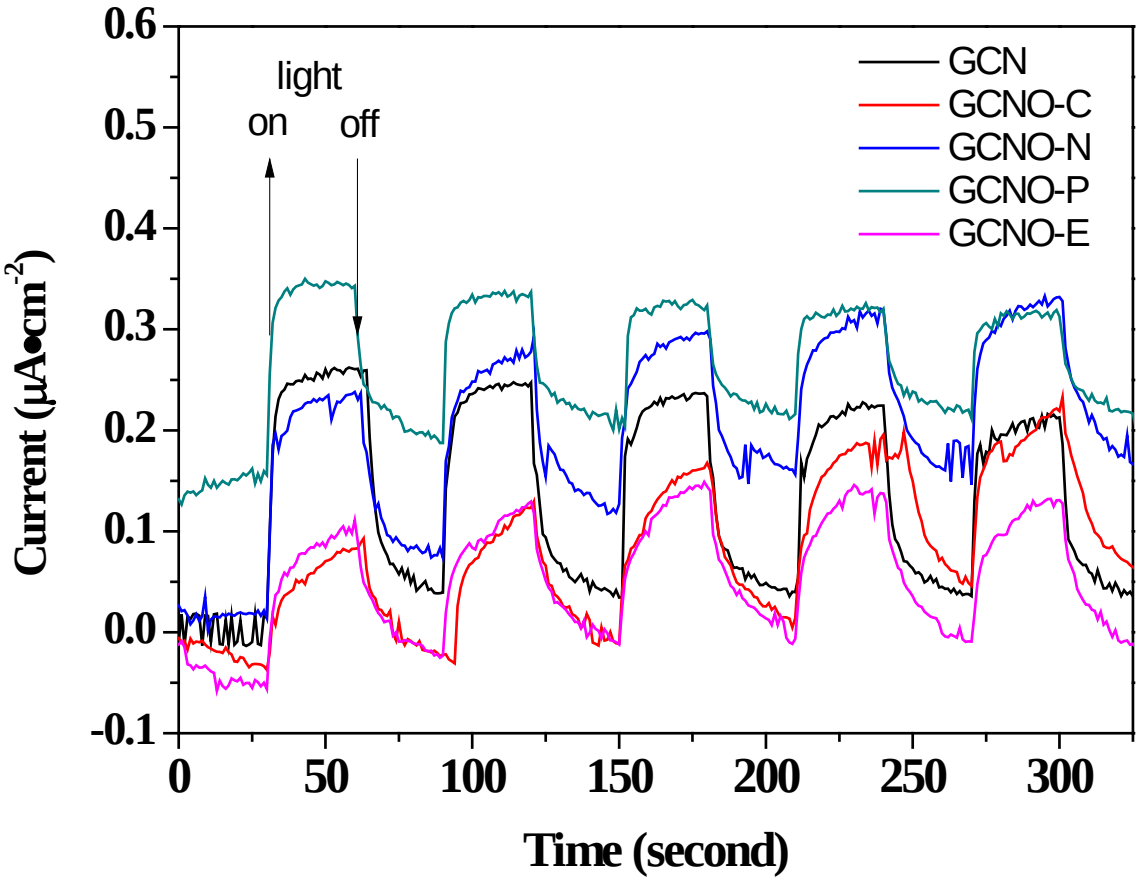

Fig. 32. Transient photocurrent curves of GCN, GCNO-E, GCNO-P, GCNO-N and GCNO-C in 0.1 M $\mathbf{Na_2SO_4}$ solution.

The generation of photocurrents of the samples was studied by photoelectrochemical experiments. All samples produced a clear transient photocurrent during on–off cycles of irradiation and the unbiased photocurrent lags were observed on all the samples. In Fig. 32, GCN was able to produce a density of ca. 0.25 μA photocurrent; however the current intensity decreased gradually after five photo-exciting cycles. GCNO-P generated the highest current, which is due to the strong electron transfer from Perylene into GCNO[43]. But the photocurrent was unstable during the 300 s duration. GCNO-N has a stronger photocurrent than GCN with an increasing tendency, but its initial cycle was weaker than GCN, which indicated an activity between GCNO and Nile-Red. The photocurrent-lags and the significant dark-current appeared in GCNO-N, suggesting an electric drifting hinder between the GCNO and Nile-Red in an

insensitive photocatalytic system[44]. GCNO-E and GCNO-C samples could not generate stronger photocurrent than GCN which may be due to the newly formed recombination centres in Eosin-Y and Coumarin molecules[32]. GCNO-C presented a higher current intensity and a stronger dark current at the same time. GCNO-E presented the most stable photocurrent cycles implying its stable chemical properties.

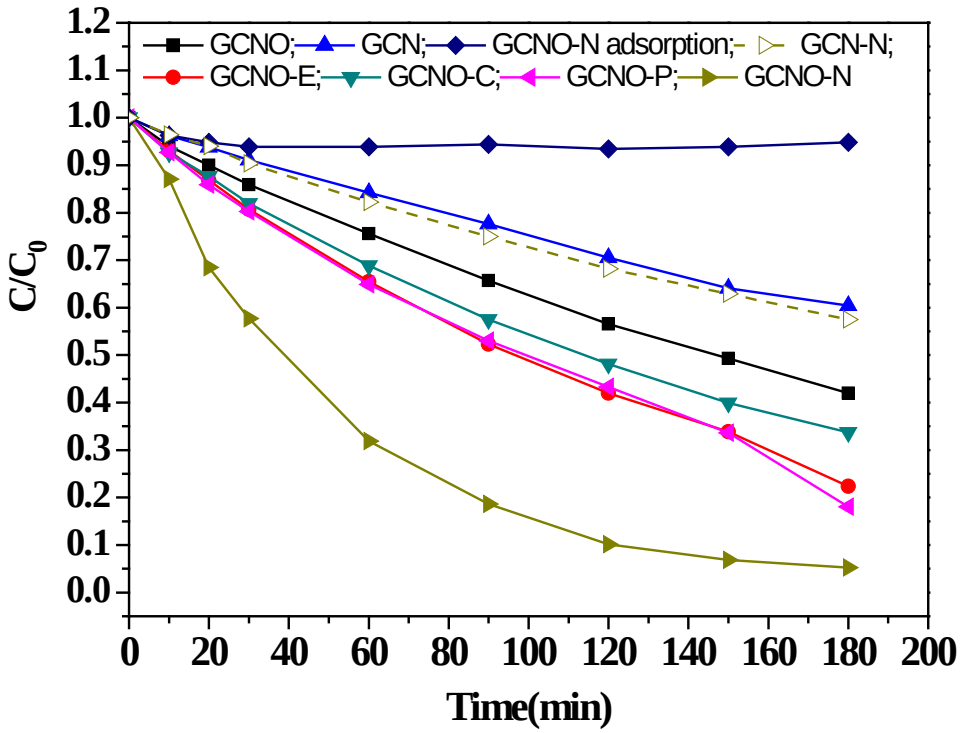

Fig. 33. Photocatalytic activity evaluation in MB degradation under (or without) λ > 480 nm lights.

In Fig. 33, photocatalytic performances of GCN, GCNO, GCNO-E, GCNO-P, GCNO-N, and GCNO-C are displayed for methylene blue removal under irradiations with wavelength larger than 480 nm. The adsorption of MB on GCNO-N was shown as a reference. GCNO-N unlikely adsorbs MB, and after 3 h adsorption in dark less than 5% MB was removed. GCN presented a very weak activity in photodegradation, and about 20% MB was degraded after 3 h. Oxygen doping can enhance the activity, and more than 50% MB could be degraded at the same time.

It was further found that dye sensitization can influence the photocatalytic activity and GCNO-C was able to decompose more than 60% MB. GCNO-E and GCNO-P degraded ca. 80% MB in 3 h. GCNO-N possessed the best activity for eliminating all MB from water in 3 h. Interestingly, Nile Red sensitized GCN (referred as GCN-N in above graph) was not effective for MB degradation under $\lambda > 480$ nm light. In addition, Fig. 38s (SD) confirmed that other dye sensitized GCN samples produced from another synthesis procedure, i.e. decomposition of dicyandiamide precursor, were ineffective either.

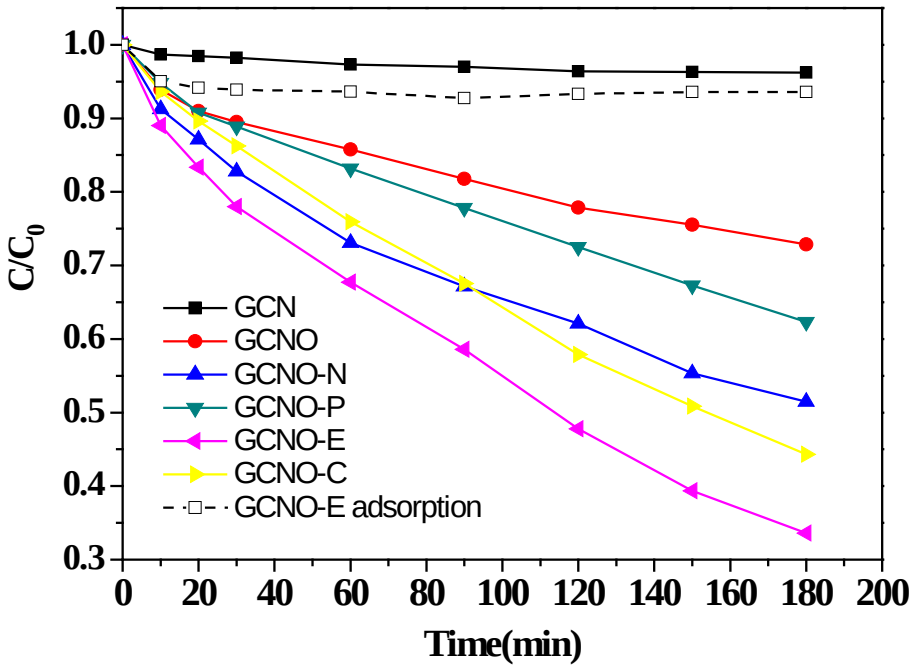

Fig. 34. Photodegradation of phenol solutions on GCN, GCNO, GCNO-E, GCNO-P, GCNO-N, and GCNO-C under (or without) $\lambda > 420$ nm radiation.

GCN, GCNO, and dye photosensitized GCNO catalysts (GCNO-E, GCNO-P, GCNO-N, GCNO-C) were further evaluated in phenol degradation. GCNO-E was also tested for adsorption in dark. Herein the photocatalytic performances are obviously different in the two systems. In Fig. 34, GCNO-E could adsorb 5% phenol in 3 h. GCN has nearly no removal of phenol from water. But O-doped GCN was able to degrade around 25% of phenol in 3 h. All

dye sensitized GCNO samples produced better phenol photo-degradation than GCNO. GCNO-E exhibited the highest activity with about 65% phenol elimination from water in 3 h. GCNO-C showed a better activity (60%) than GCNO-N with about 45% phenol decomposition. Perylene sensitized GCNO slightly enhanced the activity and more than 30% phenol was removed.

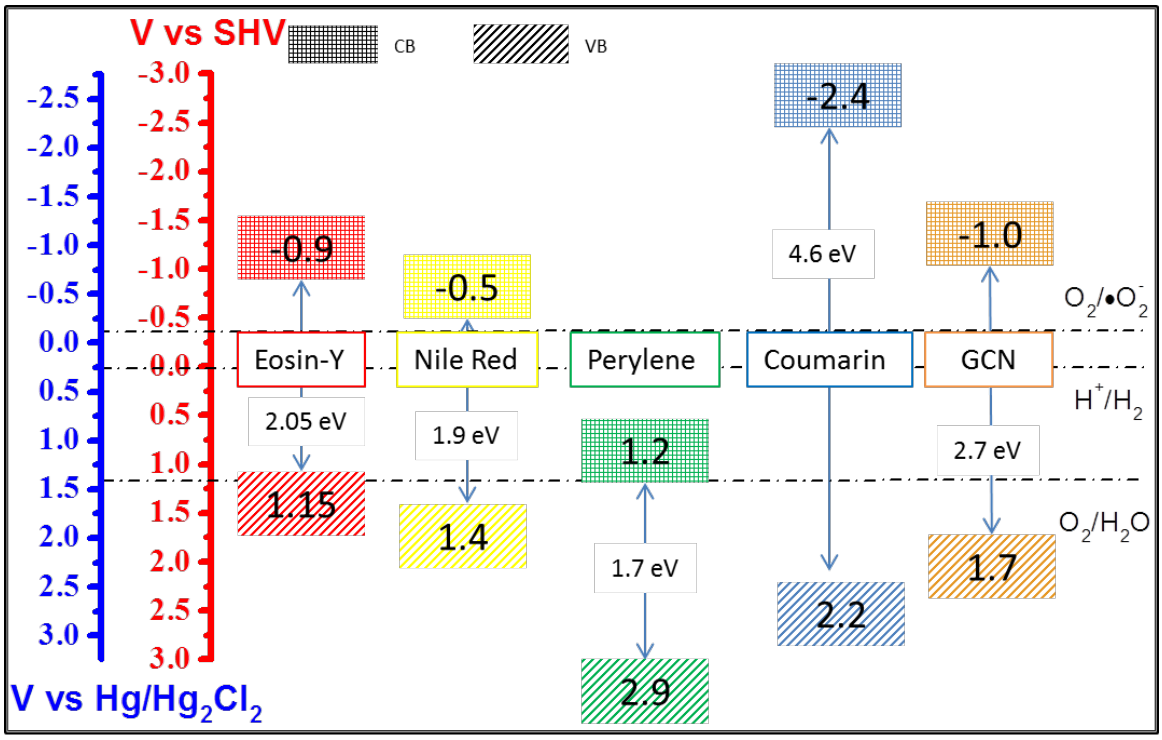

Fig. 35. The VB/CB energy structures of GCN, Eosin-Y, Nile-Red, Perylene and Coumarin.

Fig. 35 demonstrates the valence band (VB) and conduction band (CB) levels and the band gap energy of Eosin-Y, Nile-Red, Perylene, Coumarin and GCN vs SHV and Hg/Hg_2Cl_2 reference electrodes. The energy bands of Eosin-Y, Nile-Red, Perylene and Coumarin are 2.05[45], 1.9[46, 47], 1.7 [48] and 4.6 eV [49, 50], respectively. The band gap energy of GCN is 2.7 eV[51] while GCNO has a lower band energy of 2.6 eV. The band gap energies of Eosin-Y, Nile red and Perylene are narrow enough to absorb visible light and extend the light absorption range of GCNO, while Coumarin with 4.6 eV band gap energy can only respond UV. It was

shown that photosensitization by the four organic dyes is able to enhance photocatalytic activities under visible light irradiations. Eosin-Y sensitized GCNO (GCNO-E) has produced the best performance, because Eosin-Y can extend the absorption of GCNO up to 605 nm. The PL spectra also indicated that Eosin-Y can suppress the recombination of electron/hole pairs. Additionally, energy structures show that Eosin-Y's VB (1.4 V) could accept the electrons generated in VB of GCN (2.7 V) [52] accelerating the electron/hole pairs separation, resulting in the highest phenol photodegradation efficiency.

Nile-Red is also a good photo sensitizer toward GCNO photocatalysis. It can enlarge the strongest absorption spectrum at 500 - 705 nm leading to the greatest harvesting of visible light and thus the best activity in MB degradation. For photocurrent generation, Nile Red produced increasing electronic current in GCNO-N, due to the gradually increased dark current, suggesting electron accumulation in GCNO-N composite, which will also favor photocatalysis.

Perylene sensitization could induce high light absorption up to 645 nm and declined PL intensity. GCNO-P also has demonstrated the highest electronic current under dark or light, suggesting the strong electron transfer. Thus, GCNO-P also exhibited better activities of MB and phenol degradation than GCNO.

Coumarin could neither extend light absorption nor suppress carriers' recombination. But the photocurrent of GCNO-C continually increased after periodic irradiation, which implied an activation between GCNO and Coumarin for electron generation and accumulation at more intense light radiation. Previous studies reported that Coumaring can accelerate electron/hole separation [52, 56]. The energy levels of GCNO and Coumarin also suggest that Coumarin could accept more electrons from GCNO, which will make GCNO-C exhibit better photodegradation of phenol and MB than GCNO.

The poor photodegradation of MB on dye sensitized GCN samples suggested that direct sensitization without oxygen doping on GCN could not produce an incentive to enhance photoactivity. Oxygen-bearing function groups on GCN are beneficial for decreasing molecular spatial effect and increasing electronic cloud overlapping[53], thus the photoelectrons are easily transferring between GCNO and dye molecules for dye sensitization [14, 28]. Therefore, a synergistic effect will be only created on GCNO.

5.5 Conclusions

A photocatalyst, GCNO, was synthesized by hydrothermal treatment of graphitic carbon nitride with hydrogen peroxide at 130 ℃ for effective dye sentisization. Meanwhile four cooperative asymmetric organophotoredox organic dyes, Eosin-Y, Perylene, Nile Red and Coumarin, were adopted to sensitize the GNCO. O-doping can promote dye sensitization on GCN and the dyes presented different effects on photocatalytic activity. Eosin-Y and Nile Red produced a better synergistic effects on photocatalysis. Nile-red effectively extends the light absorption and hence giving a good activity in methylene blue degradation. Eosin-Y could balance the absorption and the electron/hole pair recombination, leading to the best activity in phenol decomposition. The photocurrent studies reveal the different effects of the dyes, which are able to inject extra photoelectron into GCNO orbits and reduce the recombination. Therefore, integration of oxygen doping and dye sensitizing has potential to create highly efficient metal-free photocatalysts for efficient solar energy applications.

5.6 Acknowledgements

This project was partially supported by Australian Research Council (ARC) under Project No.: DP150103026. Characterizations were partially obtained from Curtin University Electron Microscope Facility and Centre for Microscopy Characterization. H. S. thanks Curtin Research

Fellowship and Opening Project (KL13-02) of State Key Laboratory of Materials-Oriented Chemical Engineering, China.

5.7 Support information

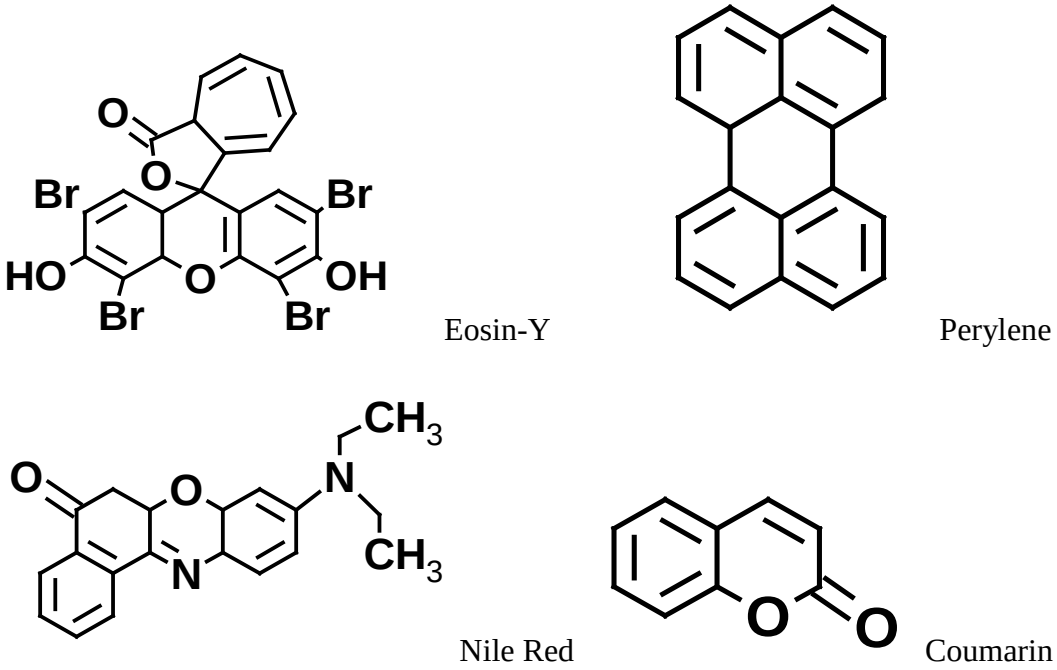

Fig. 36s. Chemical structure of the four dyes.

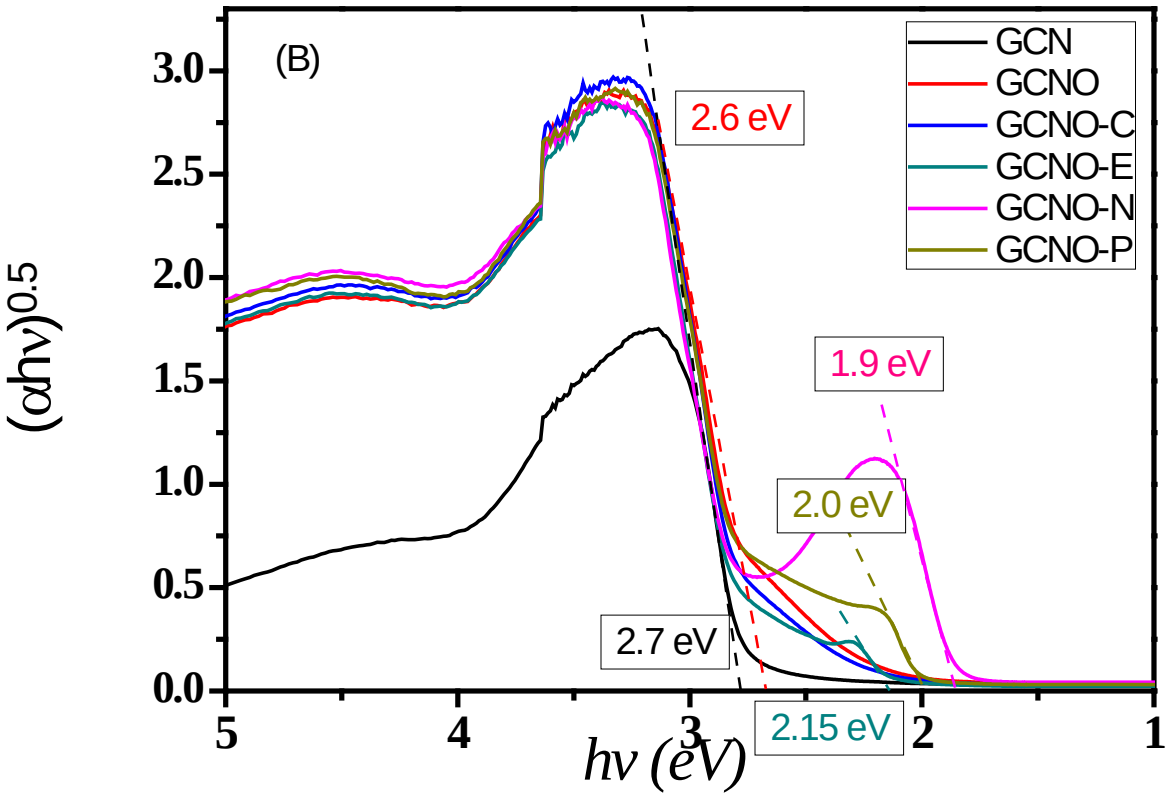

Fig. 37s. Band gap energies of GCN-P, GCN-N, GCN-E, GCN-C, GCNO and GCN estimated by the Kubelka–Munk equation by transforming the UV−vis DRS into (αhv)1/2 versus hv.

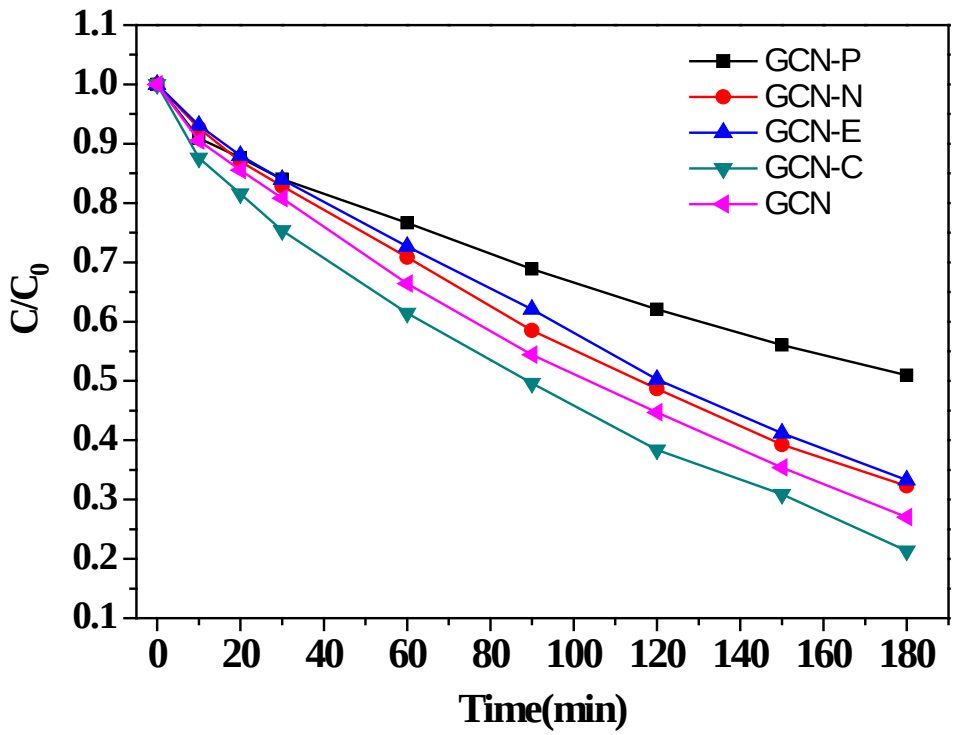

Fig. 38s. Photocatalytic activity evaluation for MB degradation by GCN-P, GCN-N, GCN-E, GCN-C and GCN prepared from dicyandiamide.

In our study, GCN was also prepared from a dicyandiamide precursor at 520 ℃. The produced GCN was sensitized by Perylene, Nile-Red, Eosin-Y and Coumarin, which were represented by GCN-P, GCN-N, GCN-E, and GCN-C, respectively. All the photocatalysts were employed in photo-degradation of MB (10 ppm, 200 mL) under $\lambda > 480$ nm irradiations. The results are shown in Fig. 38s. As demonstrated, dye photosensitized effects on GCN for photocatalysis are not effective.

5.8 References

[1] A. Fujishima, K. Honda, Electrochemical Photolysis of Water at a Semiconductor Electrode, Nature, 238 (1972) 37-38.

[2] A.J. Bard, M.A. Fox, Artificial Photosynthesis: Solar Splitting of Water to Hydrogen and Oxygen, Accounts of Chemical Research, 28 (1995) 141-145.

[3] A.J. Bard, Inner-Sphere Heterogeneous Electrode Reactions. Electrocatalysis and Photocatalysis: The Challenge, Journal of the American Chemical Society, 132 (2010) 7559-7567.

[4] S.C. Yan, Z.S. Li, Z.G. Zou, Photodegradation Performance of g-C_3N_4 Fabricated by Directly Heating Melamine, Langmuir, 25 (2009) 10397-10401.

[5] Q. Xiang, J. Yu, M. Jaroniec, Preparation and Enhanced Visible-Light Photocatalytic H_2-Production Activity of Graphene/C_3N_4 Composites, The Journal of Physical Chemistry C, 115 (2011) 7355-7363.

[6] S. Cao, J. Yu, g-C_3N_4-Based Photocatalysts for Hydrogen Generation, The Journal of Physical Chemistry Letters, 5 (2014) 2101-2107.

[7] T. Sano, S. Tsutsui, K. Koike, T. Hirakawa, Y. Teramoto, N. Negishi, K. Takeuchi, Activation of graphitic carbon nitride (g-C_3N_4) by alkaline hydrothermal treatment for photocatalytic NO oxidation in gas phase, Journal of Materials Chemistry A, 1 (2013) 6489-6496.

[8] Z. Zhao, Y. Sun, F. Dong, Graphitic carbon nitride based nanocomposites: a review, Nanoscale, 7 (2015) 15-37.

[9] E.Z. Lee, S.U. Lee, N.-S. Heo, G.D. Stucky, Y.-S. Jun, W.H. Hong, A fluorescent sensor for selective detection of cyanide using mesoporous graphitic carbon(iv) nitride, Chemical Communications, 48 (2012) 3942-3944.

[10] S. Liu, J. Tian, L. Wang, Y. Luo, X. Sun, A general strategy for the production of photoluminescent carbon nitride dots from organic amines and their application as novel peroxidase-like catalysts for colorimetric detection of H_2O_2 and glucose, RSC Advances, 2 (2012) 411-413.

[11] S.M. Aspera, H. Kasai, H. Kawai, Density functional theory-based analysis on O_2 molecular interaction with the tri-s-triazine-based graphitic carbon nitride, Surface Science, 606 (2012) 892-901.

[12] Y. Zheng, Y. Jiao, M. Jaroniec, Y. Jin, S.Z. Qiao, Nanostructured Metal-Free Electrochemical Catalysts for Highly Efficient Oxygen Reduction, Small, 8 (2012) 3550-3566.

[13] L. Shi, L. Liang, F. Wang, M. Liu, J. Sun, Enhanced visible-light photocatalytic activity and stability over g-C_3N_4/Ag_2CO_3 composites, Journal of Materials Science, 50 (2014) 1718-1727.

[14] Y. Zheng, Y. Jiao, J. Chen, J. Liu, J. Liang, A. Du, W. Zhang, Z. Zhu, S.C. Smith, M. Jaroniec, G.Q. Lu, S.Z. Qiao, Nanoporous Graphitic-C_3N_4@Carbon Metal-Free Electrocatalysts for Highly Efficient Oxygen Reduction, Journal of the American Chemical Society, 133 (2011) 20116-20119.

[15] X. Zhang, X. Xie, H. Wang, J. Zhang, B. Pan, Y. Xie, Enhanced Photoresponsive Ultrathin Graphitic-Phase C3N4 Nanosheets for Bioimaging, Journal of the American Chemical Society, 135 (2013) 18-21.

[16] J. Du, X. Lai, N. Yang, J. Zhai, D. Kisailus, F. Su, D. Wang, L. Jiang, Hierarchically ordered macro− mesoporous TiO_2− graphene composite films: Improved mass transfer, reduced charge recombination, and their enhanced photocatalytic activities, Acs Nano, 5 (2010) 590-596.

[17] J. Liu, H. Bai, Y. Wang, Z. Liu, X. Zhang, D.D. Sun, Self-Assembling TiO_2 Nanorods on Large Graphene Oxide Sheets at a Two-Phase Interface and Their Anti-Recombination in Photocatalytic Applications, Advanced Functional Materials, 20 (2010) 4175-4181.

[18] X. Ma, Y. Lv, J. Xu, Y. Liu, R. Zhang, Y. Zhu, A Strategy of Enhancing the Photoactivity of g-C_3N_4 via Doping of Nonmetal Elements: A First-Principles Study, The Journal of Physical Chemistry C, 116 (2012) 23485-23493.

[19] X. Fan, L. Zhang, R. Cheng, M. Wang, M. Li, Y. Zhou, J. Shi, Construction of Graphitic C_3N_4-Based Intramolecular Donor–Acceptor Conjugated Copolymers for Photocatalytic Hydrogen Evolution, ACS Catalysis, 5 (2015) 5008-5015.

[20] D. Chen, Z. Wang, D. Yue, G. Yang, T. Ren, H. Ding, Synthesis and Visible Photodegradation Enhancement of CdS/mpg-C_3N_4 Photocatalyst, Journal of nanoscience and nanotechnology, 16 (2016) 471-479.

[21] G. Dong, Z. Ai, L. Zhang, Efficient anoxic pollutant removal with oxygen functionalized graphitic carbon nitride under visible light, RSC Advances, 4 (2014) 5553-5560.

[22] L. Ming, H. Yue, L. Xu, F. Chen, Hydrothermal Synthesis of Oxidized g-C_3N_4 and Its Photocatalytic Activity Regulation, Journal of Materials Chemistry A, (2014).

[23] Z.-F. Huang, J. Song, L. Pan, Z. Wang, X. Zhang, J.-J. Zou, W. Mi, X. Zhang, L. Wang, Carbon nitride with simultaneous porous network and O-doping for efficient solar-energy-driven hydrogen evolution, Nano Energy, 12 (2015) 646-656.

[24] J. Li, B. Shen, Z. Hong, B. Lin, B. Gao, Y. Chen, A facile approach to synthesize novel oxygen-doped g-C_3N_4 with superior visible-light photoreactivity, Chemical Communications, 48 (2012) 12017-12019.

[25] M.R. Narayan, Review: Dye sensitized solar cells based on natural photosensitizers, Renewable and Sustainable Energy Reviews, 16 (2012) 208-215.

[26] B. O'Regan, M. Gratzel, A low-cost, high-efficiency solar cell based on dye-sensitized colloidal TiO_2 films, Nature, 353 (1991) 737-740.

[27] Y.-C. Chang, C.-L. Wang, T.-Y. Pan, S.-H. Hong, C.-M. Lan, H.-H. Kuo, C.-F. Lo, H.-Y. Hsu, C.-Y. Lin, E.W.-G. Diau, A strategy to design highly efficient porphyrin sensitizers for dye-sensitized solar cells, Chemical Communications, 47 (2011) 8910-8912.

[28] C.-L. Wang, C.-M. Lan, S.-H. Hong, Y.-F. Wang, T.-Y. Pan, C.-W. Chang, H.-H. Kuo, M.-Y. Kuo, E.W.-G. Diau, C.-Y. Lin, Enveloping porphyrins for efficient dye-sensitized solar cells, Energy & Environmental Science, 5 (2012) 6933-6940.

[29] C.-H. Wu, T.-Y. Pan, S.-H. Hong, C.-L. Wang, H.-H. Kuo, Y.-Y. Chu, E.W.-G. Diau, C.-Y. Lin, A fluorene-modified porphyrin for efficient dye-sensitized solar cells, Chemical Communications, 48 (2012) 4329-4331.

[30] X. Li, S. Cui, D. Wang, Y. Zhou, H. Zhou, Y. Hu, J.g. Liu, Y. Long, W. Wu, J. Hua, New Organic Donor–Acceptor–π–Acceptor Sensitizers for Efficient Dye-Sensitized Solar Cells and Photocatalytic Hydrogen Evolution under Visible-Light Irradiation, ChemSusChem, 7 (2014) 2879-2888.

[31] Y. Wang, J. Hong, W. Zhang, R. Xu, Carbon nitride nanosheets for photocatalytic hydrogen evolution: remarkably enhanced activity by dye sensitization, Catalysis Science & Technology, 3 (2013) 1703-1711.

[32] J. Xu, Y. Li, S. Peng, G. Lu, S. Li, Eosin Y-sensitized graphitic carbon nitride fabricated by heating urea for visible light photocatalytic hydrogen evolution: the effect of the pyrolysis temperature of urea, Physical Chemistry Chemical Physics, 15 (2013) 7657-7665.

[33] J. Xu, Y. Li, S. Peng, Photocatalytic hydrogen evolution over Erythrosin B-sensitized graphitic carbon nitride with in situ grown molybdenum sulfide cocatalyst, International Journal of Hydrogen Energy, 40 (2015) 353-362.

[34] K. Mori, T. Itoh, H. Kakudo, T. Iwamoto, Y. Masui, M. Onaka, H. Yamashita, Nickel-supported carbon nitride photocatalyst combined with organic dye for visible-light-driven hydrogen evolution from water, Physical Chemistry Chemical Physics, 17 (2015) 24086-24091.

[35] X. Li, J. Zhang, L. Shen, Y. Ma, W. Lei, Q. Cui, G. Zou, Preparation and characterization of graphitic carbon nitride through pyrolysis of melamine, Applied Physics A, 94 (2009) 387-392.

[36] X. Wang, K. Maeda, A. Thomas, K. Takanabe, G. Xin, J.M. Carlsson, K. Domen, M. Antonietti, A metal-free polymeric photocatalyst for hydrogen production from water under visible light, Nat Mater, 8 (2009) 76-80.

[37] K. Gnanaguru, N. Ramasubbu, K. Venkatesan, V. Ramamurthy, A study on the photochemical dimerization of coumarins in the solid state, The Journal of Organic Chemistry, 50 (1985) 2337-2346.

[38] M. Xu, L. Han, S. Dong, Facile Fabrication of Highly Efficient g-C_3N_4/Ag_2O Heterostructured Photocatalysts with Enhanced Visible-Light Photocatalytic Activity, ACS Applied Materials & Interfaces, 5 (2013) 12533-12540.

[39] Y. Li, H. Zhang, P. Liu, D. Wang, Y. Li, H. Zhao, Cross-Linked g-C_3N_4/rGO Nanocomposites with Tunable Band Structure and Enhanced Visible Light Photocatalytic Activity, Small, 9 (2013) 3336-3344.

[40] V.N. Khabashesku, J.L. Zimmerman, J.L. Margrave, Powder Synthesis and Characterization of Amorphous Carbon Nitride, Chemistry of materials, 12 (2000) 3264-3270.

[41] B.D. Wagner, The use of coumarins as environmentally-sensitive fluorescent probes of heterogeneous inclusion systems, Molecules, 14 (2009) 210-237.

[42] Y.-F. Sun, S.-H. Xu, R.-T. Wu, Z.-Y. Wang, Z.-B. Zheng, J.-K. Li, Y.-P. Cui, The synthesis, structure and photoluminescence of coumarin-based chromophores, Dyes and Pigments, 87 (2010) 109-118.

[43] A. Wojcik, P.V. Kamat, Reduced Graphene Oxide and Porphyrin. An Interactive Affair in 2-D, Acs Nano, 4 (2010) 6697-6706.

[44] A. Pockett, G.E. Eperon, T. Peltola, H.J. Snaith, A. Walker, L.M. Peter, P.J. Cameron, Characterization of Planar Lead Halide Perovskite Solar Cells by Impedance Spectroscopy, Open-Circuit Photovoltage Decay, and Intensity-Modulated Photovoltage/Photocurrent Spectroscopy, The Journal of Physical Chemistry C, 119 (2015) 3456-3465.

[45] P. Ruankham, C. Sae-kung, N. Mangkorntong, P. Mangkorntong, S. Choopun, Photoelectrochemical Characteristic of ZnO Dye-sensitized Solar Cell with Platinum Nanoparticle as a Counterelectrode, CMU. J. Nat. Sci. Special Issue on Nanotechnology, 7 (2008) 177.

[46] Y.T. Tao, C.W. Ko, E. Balasubramaniam, Energy transfer vs. carrier trapping: emission mechanism in dye-doped organic light emitting diodes, Thin solid films, 417 (2002) 61-66.

[47] G. He, S.-C. Chang, F.-C. Chen, Y. Li, Y. Yang, Highly efficient polymer light-emitting devices using a phosphorescent sensitizer, Applied Physics Letters, 81 (2002) 1509-1511.

[48] N. Sato, K. Seki, H. Inokuchi, Polarization energies of organic solids determined by ultraviolet photoelectron spectroscopy, Journal of the Chemical Society, Faraday Transactions 2: Molecular and Chemical Physics, 77 (1981) 1621-1633.

[49] T. Dong, J. Hu, M. Ueda, Y. Wu, X. Zhang, L. Wang, Enhanced proton conductivity of multiblock poly(phenylene ether ketone)s via pendant sulfoalkoxyl side chains with excellent H_2/air fuel cell performance, Journal of Materials Chemistry A, 4 (2016) 2321-2331.

[50] C.M. Krauter, J. Mohring, T. Buckup, M. Pernpointner, M. Motzkus, Ultrafast branching in the excited state of coumarin and umbelliferone, Physical Chemistry Chemical Physics, 15 (2013) 17846-17861.

[51] X. Wang, K. Maeda, A. Thomas, K. Takanabe, G. Xin, J.M. Carlsson, K. Domen, M. Antonietti, A metal-free polymeric photocatalyst for hydrogen production from water under visible light, Nature materials, 8 (2009) 76-80.

[52] H. Zhang, S. Li, R. Lu, A. Yu, Time-Resolved Study on Xanthene Dye-Sensitized Carbon Nitride Photocatalytic Systems, ACS Applied Materials & Interfaces, 7 (2015) 21868-21874.

[53] S. Anandan, M. Yoon, Photoinduced electron transfer studies of Nile red in the presence of TiO_2 colloidal nanoparticles, Spectrochimica Acta Part A: Molecular and Biomolecular Spectroscopy, 60 (2004) 885-888.

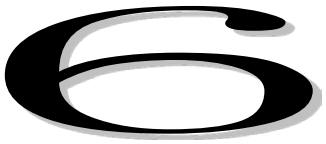

6 Size dependence of uniformed carbon spheres for promoting graphitic carbon nitride toward enhanced photocatalysis

6.1 Abstract

Recently, graphitic carbon nitride (GCN) is increasingly employed as a non-metal/visible light sensitive photocatalyst, whereas the strong recombination of photo-electronic pair limits its wide applications. In this study several nano-carbon spheres (CS) in a uniform size were synthesized from resorcinol-formaldehyde resin via different surfactants and loaded on GCN via a hydrothermal treatment. It was found that the size of CS influenced the properties of CS/GCN and photocatalytic performance. All the CS/GCN catalysts exhibited high photocatalytic activities in degradation of water contaminants, antibiotic sulfachloropyridazine and methylene blue. PL spectra and photocurrent analysis indicated the carbon sphere at 200-500 nm with GCN will significantly reduce the electrocarrier recombination and increase photocurrent intensity, resulting in much better photocatalysis.

6.2 Introduction

The Paris Climate Change Conference (COP21) indicates, during 1990 to 2012, CO_2 emission was dramatically increased in a global wide scale and this tendency in some developing countries (such as China, India, and Brazil) is incredibly high as four times as before[1], which threats people health and ecosystem safety. The main source of CO_2 emission is fossil fuel combustion. Solar energy has been considered as the feasible candidate to fossil fuels in future for its global distribution and low-cost. To extract solar energy in photovoltaic derives, a photo-sensitive semiconductor has been found to be the key, which can convert the light radiation into electrical energy. However, until now there is no effective photo-sensitive material that

can balance the economic cost, high radiation harvest, high efficiency, chemical/physical stability and environmental friendliness[2].

Recent researches exhibited a bright horizon of solar energy applications by an organic semiconductor, graphitic carbon nitride (GCN), which is based on polymeric tri-s-triazine building blocks as a layer-stacked metal-free visible light sensitive photocatalyst[3]. Up to date, GCN is primarily used in water splitting[4], environmental remediation[5], and electronic devices[6-8] because of its unique properties, such as highly chemical/thermal stability and premium electronic properties[9]. GCN is generally regarded as a photosensitive semiconductor because it has tuneable band gap energy from 2.6 to 3.5 eV which can cover visible (~477 nm) to ultraviolet spectrum [10, 11]. But pristine GCN presents low electrical conduction and rapid photo-electron depletion, exhibiting inefficient photon harvesting and low photocatalytic activity [12-14]. Therefore, hybridized GCN photocatalyts have been extensively studied[15].

Carbonaceous materials such as graphene oxide (GO) [16], carbon nanotubes (CNTs) [17], and fullerene[18] can enhance migration of photo-generated electron/hole, which will increase the production of active species in the redox reaction [19, 20]. With polar functional groups or long chain molecules, carbonaceous materials grafting over GCN could enlarge the surface area of the catalyst, transform the electron distribution of the particle surface, enhance carrier mobility and weaken the recombination[21-25].

A new carbonaceous material, resorcinol-formaldehyde carbon sphere (RFCS), exhibits strong environmental compatibility and electric capacity with low impedance for electron drafting [26-28]. In addition, the dimension of RFCS could be controlled during synthesis and produced by different surfactants[29]. Glucose-based amorphous carbon was successfully loaded on GCN by a hydrothermal method, showing enhanced photocatalysis[30, 31]. However, the

dimension of carbon spheres will influence the surface, electronic and optical properties and not such an investigation has been reported.

Hereupon, we present an investigation on synthesis of RFCS-GCN heterojunction materials for photocatalysis. The uniform size controlled RFCS has been successfully synthesised through varying surfactants and impregnated on GCN. The effects of CS on the electronic and optical properties as well as photocatalytic behaviour of the GCN materials were evaluated and discussed.

6.3 Experimental

Materials

All chemicals used are in analytical grade. Melamine powder (99.9%), resorcinol (≥99.0%), formaldehyde (37 wt.% in H_2O), cysteine (≥99.0%), hexadecyltrimethyl ammonium bromide (CTAB) were provided by Sigma-Aldrich. Pluronic F-127 surfactant, ammonia (25%, in water), and ethanol (≥99.9%) were purchased from BASF.

Preparation of graphitic carbon nitride

Graphitic carbon nitride was prepared through condensation of melamine. Typically, 10 g of melamine were placed in a 20 mL alumina crucible and well mixed with 10 mL of methanol. This crucible was then moved into an oven to remove methanol at 60 ℃ for 24 h. After that, the white powder was placed in a muffle furnace for annealing treatment, which was firstly heated to 400 ^{o}C at a heating rate of $5℃/min$ and kept at this temperature for 2 h, followed by heating to 520 ^{o}C with a heating rate of 10 ^{o}C/min and keeping for 2 h. Finally, the yellow product was well ground as GCN.

Preparation of resorcinol-formaldehyde carbon spheres

The preparation of homogeneous resorcinol-formaldehyde (RF) spheres at different sizes follows a similar procedure except the varying precursor solutions [29, 32]. For 500 nm spheres, 16 mL of pure ethanol and 40 mL of deionized water were mixed in an 80 mL Pyrex bottle in a water bath at 30 ℃. Then 0.2 mL of 25% ammonia solution was added into the above solution with stirring for 2 h. And then 0.4 g of resorcinol powder was added in at constantly stirring in air tight, until colour of the solution changed to slightly brown. Then 0.48 mL of formaldehyde solution was gradually added into the solution and sealed well for 24 h. A dark brown RF resins suspension was transferred into an 80 mL Teflon-lined autoclave and treated at 100 °C for 24 h. The dark brown RF resin sphere was collected by centrifugation and purified using deionized water for three times and dried at 100 °C in air. The product was referred to as 500 RF.

For the preparation of 60 nm RF spheres, a surfactant Pluronic F-127 solution (1.476 mmol/L, water/ethanol) was added with stirring into the water/ethanol/ammonia solution before 0.4 g of resorcinol powder was added. The rest of the preparation procedure is the same.

For the preparation of 200 nm RF spheres, three surfactants (F127 0.2 g; CTAB 0.26 g and cysteine 0.4 g) were mixed into the water/ethanol/ammonia solution before the resorcinol powder was added in.

For the preparation of 1000 nm RF spheres, 0.4 mL of 25% ammonia solution was used instead of 0.2 mL to get the water/ethanol/ammonia solution.

In a carbonization procedure, RF spheres were put in a furnace tube and heated to 350 °C at a heating rate of 1 °C/min and kept the temperature for 2 h in nitrogen environment, followed by raising the temperature to 600 °C at the same heating rate, maintaining further for 4 h.

Preparation for CS-GCN **(GCS) photocatalysts**

The CS-GCN photocatalysts were prepared using the prepared carbon sphere and GCN by a hydrothermal treatment (Fig. 39). Typically, 1 wt% carbon sphere was mixed with 1 g of the pure GCN in 50 mL of deionization water. After 3-h ultrasonic treatment, the mixed solution was stirred for 3 h at room temperature to generate a homogenous suspension. Then the suspension was moved into a 100 mL Teflon-lined autoclave for a hydrothermal treatment at 150 ℃ for 12 h. The product was dried at 60 ºC. According to the diameter of carbon sphere, the obtained four samples were referred to GCS-60, GCS-200, GCS-500 and GCS-1000, respectively.

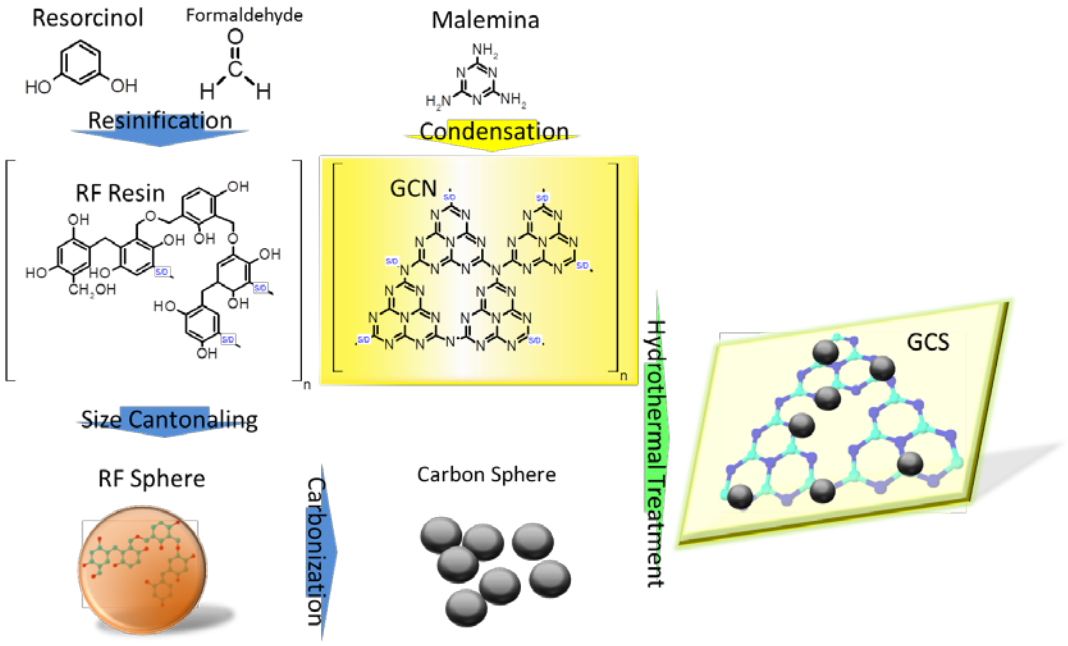

Fig. 39.Schematic illustration of the synthesis processes of the GCS samples.

Characterisation

The crystalline structure of the as-prepared samples were analysed using powder X-ray diffraction (XRD) technology on a D8-advance X-ray diffractometer using a Cu Kα with 40 kV voltage and 40 mA current. FTIR spectrum was performed on a Perkin-Elmer FTIR-100 with a MIR detector. UV-vis diffuse reflectance spectra (DRS) of samples were recorded on a JASCO V670 spectrophotometer with Ø60 mm integrating sphere and $BaSO_4$ as a reference material. Field emission scanning electron microscopy (FE-SEM) performed on Zeiss Neon 40EsB was used to determine the morphology, size and texture of the samples. Raman spectroscopy was processed in RFS100 Raman with 1064 nm laser source at 400 μW operation. The Brunauer-Emmett-Teller (BET) surface area and pore size distribution were evaluated by using a Quantachrome Autosorb AS-1. The Mott–Schottky plots and photocurrent tests were proceeded on Zennium electrochemical workstation in a conventional three-electrode cell, Hg/Hg_2Cl_2 was applied as the reference electrode, a platinum wire was used as the auxiliary electrode, and Na_2SO_4 solution (0.2 M) was used as electrolyte. Five cycles were applied and the intermission for turning on/off light was 30 s.

Photocatalytic activity testing

Photocatalytic performances of CS-GCN photocatalysts were conducted by degradation of an antibiotic, sulfachloropyridazine (SCP, 30 ppm 200 mL) and methylene blue (MB, 10 mg/L, 200 mL) in water solution under artificial sunlight irradiation. In a typical procedure, SCP or MB solution and 100 mg photocatalyst were put into a 1 L glass double-jacket cylindrical reactor with water cycling at 25 ^oC. This reaction vessel was positioned 30 cm away from the light source, a metal halide lamp with intensities at 2.31 $\mu W/cm^2$ (220-280 nm), 6.94 mW/cm^2 (315-400 nm), and 129.3 mW/cm^2 (400-1050 nm). The photocatalytic reaction was triggered by turning on the light. At regular intervals, 3 mL of suspension liquid was collected by a 5 mL

syringe to a centrifuge tube. After 10-min centrifugation, the clear solution was collected. MB solution was measured by a JASCO UV-vis spectrophotometer while SCP was analysed by a high performance liquid chromatography (HPLC, Thermal).

6.4 Results and discussion

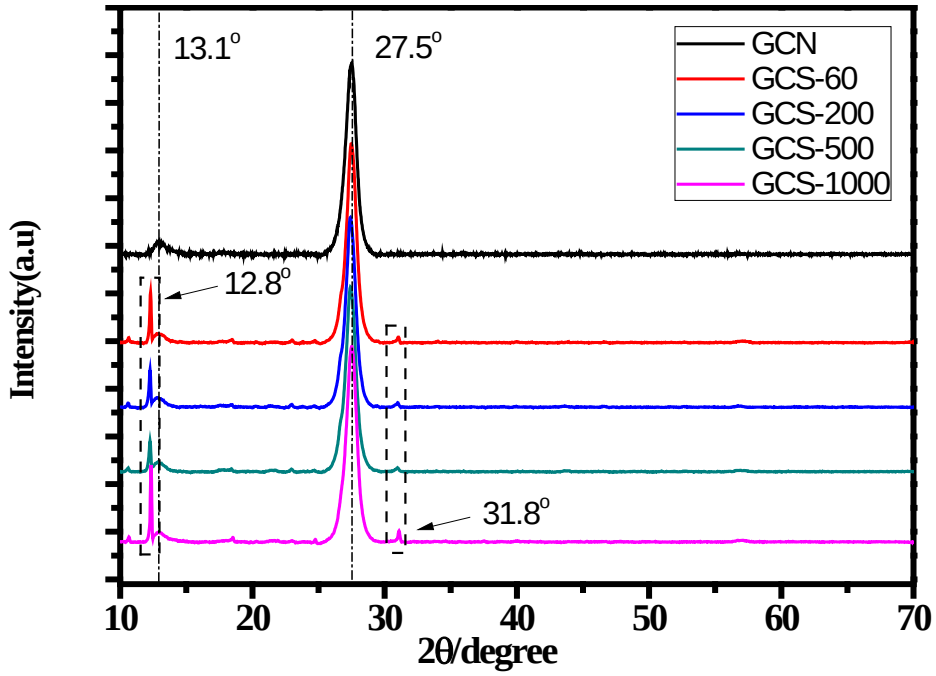

Fig. 40. XRD patterns of GCN, GCS-60, GCS-200, GCS-500 and GCS-1000.

The crystalline properties of GCN and various GCS photocatalysts were investigated by XRD (Fig.40). Two distinct peaks appeared in all samples, which are implied as the phase (002) at 27.5° and the phase (100) at 13.1° of GCN. The two peaks are contributed by the stacking fused aromatic ring and an in-planar structure of GCN. For carbon sphere loaded GCN samples, two extra peaks were appearing at 12.8° and 31.8°, respectively, Those two peaks represented "melon", the hydrolysis compounds of GCN at 150 ℃ [33]. Above results approve stack-layer structure of GCN could remain after hydrothermal treatment[14]. The chemical composition of GCS catalysts was investigated by FTIR (Fig. 49s), GCN and GCS samples have similar

vibration band distributions. The absorption bands at 1571 and 1630 cm^{-1} were attributed to C=N stretching, while the three bands at 1255, 1323 and 1428 cm^{-1} were referred to aromatic C-N stretching. The peak at 809 cm^{-1} belongs to triazin ring mode, which corresponds to condensed CN heterocycles. The band at 3150 to 3500 cm^{-1} corresponds to the stretching modes of $-NH^2$ / $=$ NH groups, all above bands belong to the GCN material[34].

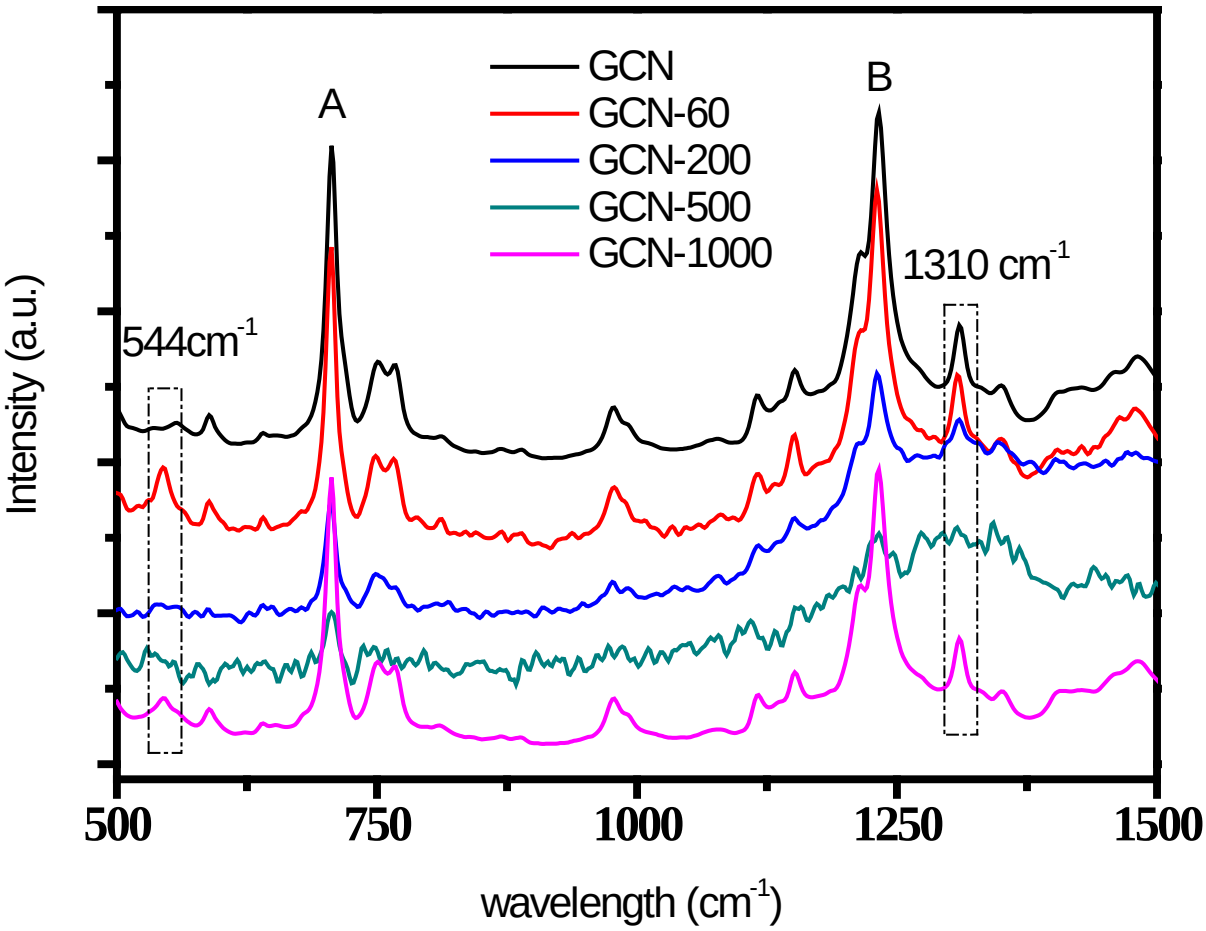

Fig. 41. FT-Raman spectra of GCN, GCS-60, GCS-200, GCS-500 and GCS-1000.

Fig.41 shows FT-Raman spectra of GCN and four size-controlled carbon sphere loaded GCN catalysts (GCS-60, GCS-200, GCS-500 and GCS-1000). A Raman shift at 544 cm^{-1} can be obviously seen in carbon sphere loaded GCN samples, which indicate the new bond between GCN and carbon spheres. The intensity ratio between peaks B (1230 cm^{-1}) and A (706.2 cm^{-1})

in GCN, GCS-60, GCS-200, GCS-500 and GCS-1000 are 1.05, 1.12, 1.48, 1.52 and 1.03, respectively. This value has been increasing with CS dimension size up to 500 nm but decreased at GCN-1000, indicating higher interaction between GCN and small size CS. The intensity of peaks at 544 and 1310 cm^{-1} decreased as the CS diameter increased except GCS-1000, however, those two peaks represent the bond of bending ring and stretch ring in GCN[35], which may be caused by CS covering.

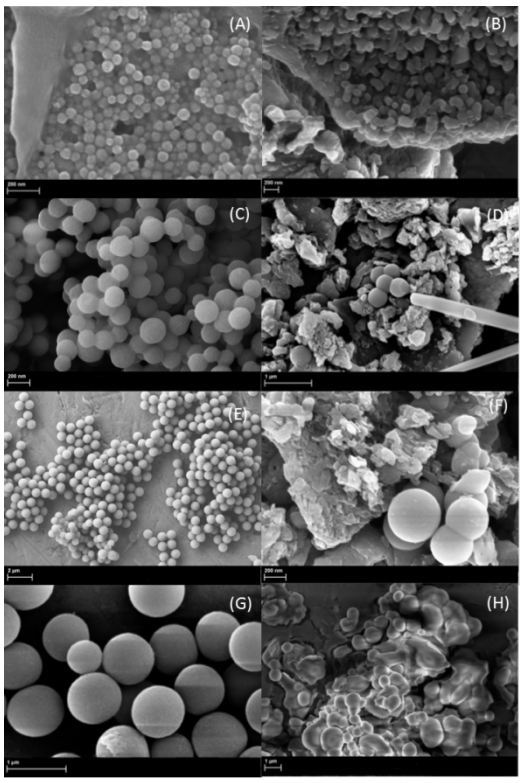

Fig. 42. SEM images of 60(A), 200(C), 500(E) and 1000(G) nm R-F spheres and GCS-60(B), GCS-200(D), GCS-500(F) and GCS-1000(H).

Field emission scanning electron microscopy (SEM) was used for studying the morphology of the resorcinol-formaldehyde sphere (RFS) and sized controlled carbon sphere loaded GCN samples. In Fig.42, images of (A), (C), (E) and (G) represent 60, 200, 500 and 1000 nm RFS, respectively. The RFS presents in good uniformed spherical particles. After carbonization and hydrothermal treatment with GCN, the texture of GCS-60, GCS-200, GCS-500 and GCS-1000

catalysts are displayed in (B), (D), (F) and (H), respectively. The carbon spheres covered the surface of layered GCN (Fig 48s, supplementary information) and aggregated tightly to decrease the surface energy [36]. The surface-covering of CS decreased with increasing CS size.

The nitrogen adsorption/desorption isotherms (Fig. 50s) indicate that the BET surface areas of GCN, GCS-60, GCS-200, GCS-500 and GCS-1000 are 9.2, 8.9, 8.2, 7.9 and 5.2 m^2/g, respectively, showing decreasing surface areas with increasing CS size.

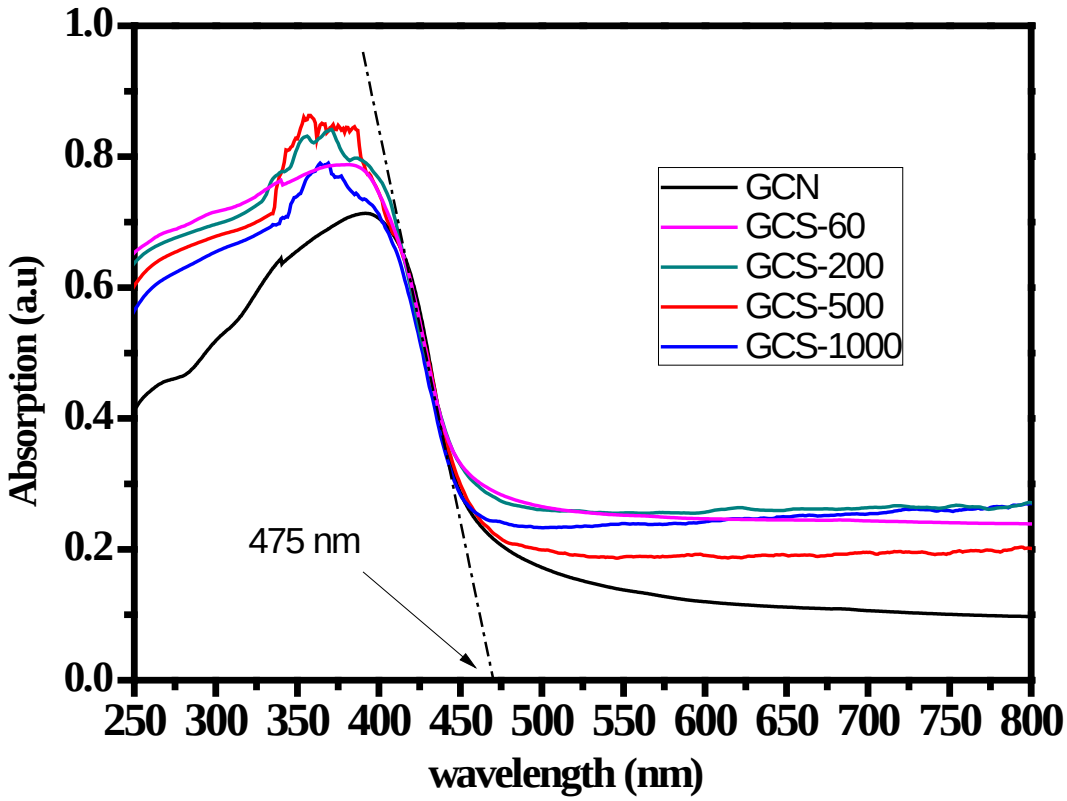

Fig. 43. UV – visible diffuse reflectance absorption of GCN, GCS-60, GCS-200, GCS-500 and GCS-1000.

The optical properties significantly affect photosensitive capacity of semiconductors. Here upon, UV-vis diffuse reflection spectra (DRS) were investigated for radiation absorption of CS

loaded GCN catalysts (Fig. 43). GCN possesses typical photosensitive semiconductor performance via band gap structures [37]. GCN could strongly absorb radiation at wavelength less than 475 nm, corresponding to 2.7 eV bang gap energy for photo-excited electron[4]. All carbon sphere loaded samples (GCS-60, GCS-200, GCS-500 and GCS-1000) had similar absorption as GCN with negligible band gap variation, which is attributed to the lone pair electrons of nitrogen atom in valance band jumping into the π bonding electronic conductive band [38]. Furthermore, the GCS samples present stronger light absorption in whole spectrum. In this study, the conductive band energy of CS loaded GCN samples were evaluated by the Mott–Schottky method (Fig.63s) by an electrochemical method under 500 Mz AC voltage, which indicates all GCS particles possess the energy potential of conductive band at around –1.0 eV (vs Hg_2Cl_2). After hydrothermal treatment with CS at 150℃ , GCN remained its optical properties.

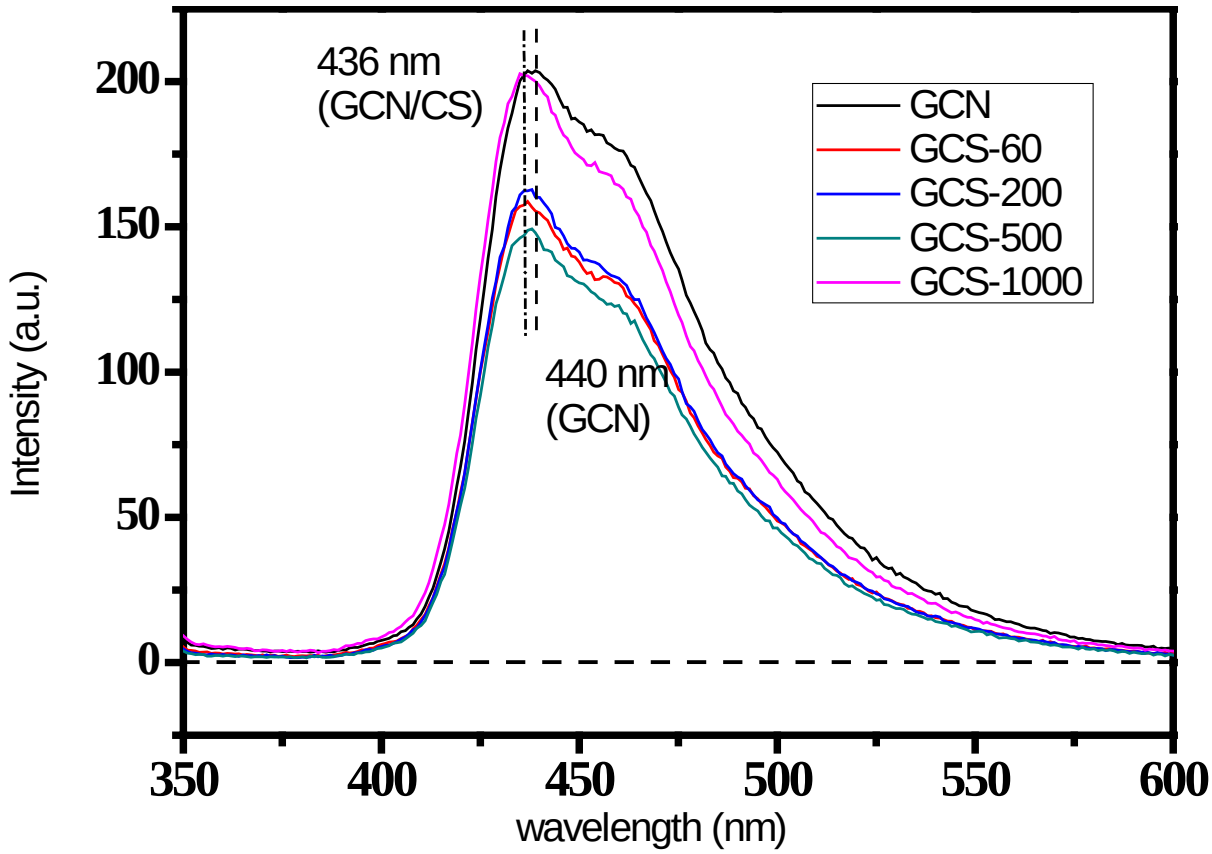

Fig. 43. Photoluminescence emission spectra of GCN, GCS-60, GCS-200, GCS-500, GCS-1000 at 320 nm exciting radiation.

The photoluminescence (PL) emission could reflect the photoelectron transit between interfaces in fluorescent materials, which also indicates the efficiency of recombination of photocarriers in photocatalysts [39]. Fig.44 elucidates the PL-emission of pristine GCN, GCS-60, GCS-200, GCS-500 and GCS-1000 under 320 nm exciting radiation. GCN and GCS-1000 possessed the strongest emission peaks. The intensity of emission in GCS-60, GCS-200 and GCS-500 was obviously decreased after CS impregnation. In particular, GCS-500 had the lowest emission intensity in the five samples, which indicates CS could remarkably weaken the electron-hole recombination of GCN due to size effect [30, 40]. In addition, PL-spectra of GCS has a peak shift from 440 nm into 436 nm. The dislocation represents an interaction between CS and GCN.

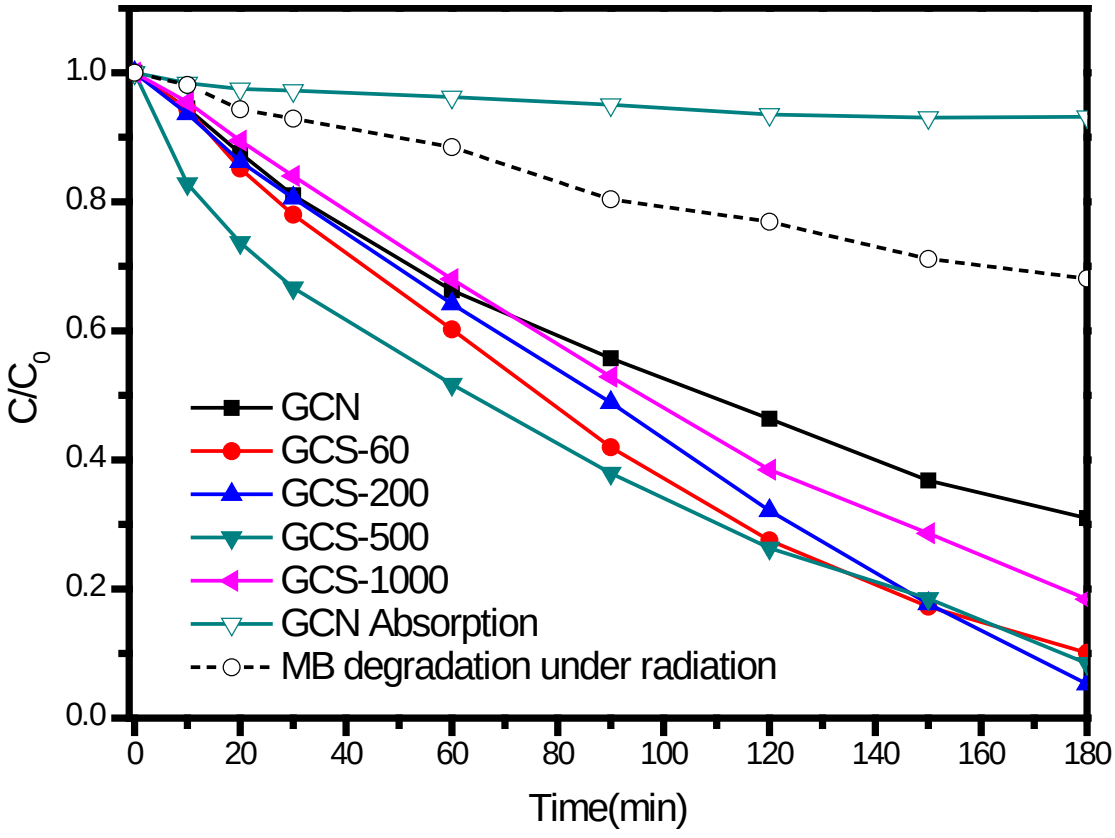

Fig. 44. GCN adsorption and photocatalytic activity of GCN, GCS-60, GCS-200, GCS-500 and GCS-1000 in MB degradation under artificial solar radiation.

Photocatalytic activation of CS loaded GCN photocatalysts were evaluated through MB decomposition under artificial solar illumination (Fig.45). All CS loaded samples have a better activity than GCN, the pristine GCN could decompose about 60% MB at the end of three hours. In contrast, GCS-200 could decompose 98% MB solution after three hours, presenting the best activity in all samples. GCS-60 and GCS-500 had the similar efficiency of 95%. GCS-1000 could remove about 70% MB. The degradation of MB can follow a pseudo-first order kinetics. The reaction rate constant (Fig.62s) of GCS-200 is $0.0125\ h^{-1}$, which is two times higher than that of GCN($k = 0.0066 h^{-1}$). Furthermore, a series of GCS-500 samples at a controlled CS loading of 0.1, 1, 5 and 10 wt% were prepared. It was found that 5% CS content on GCN sample produced the better activity of MB degradation (Fig. 51s).

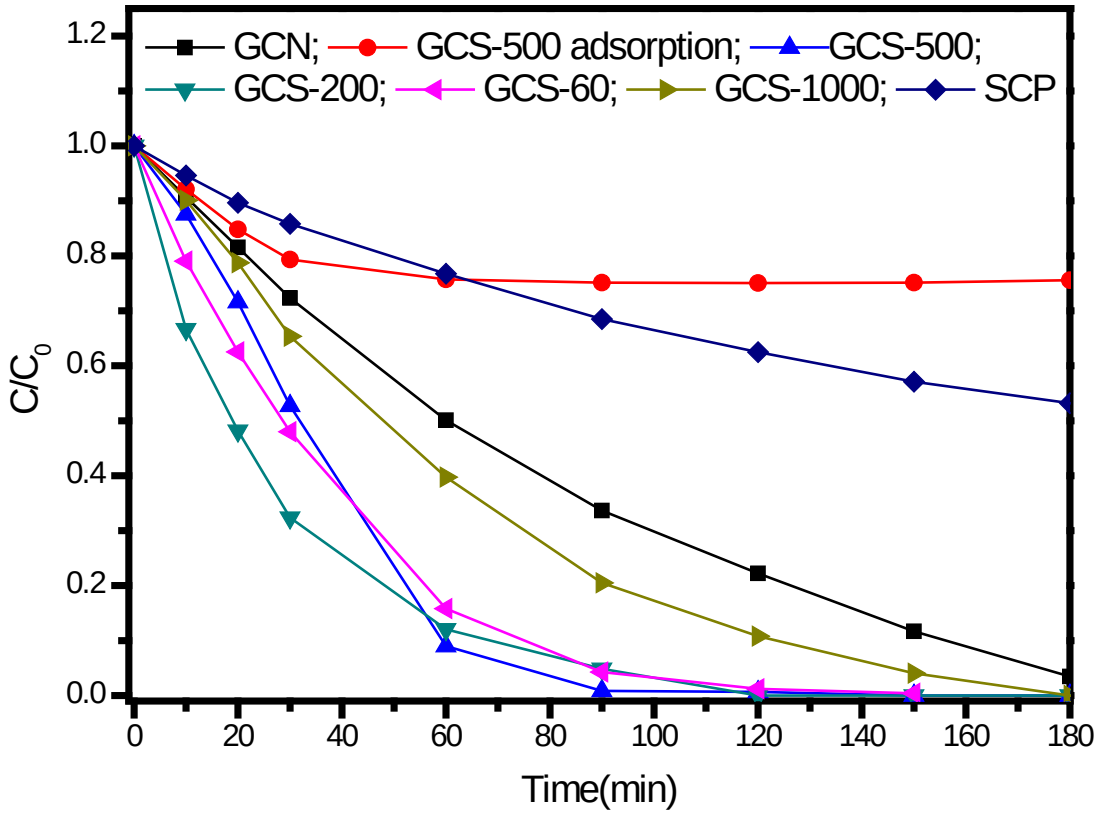

Fig. 45. Photocatalytic activity of GCN, GCS-60, GCS-200, GCS-500 and GCS-1000 in SCP degradation under artificial solar radiation.

In multiple evaluation, antibiotic of sulfachloropyridazine (SCP, 30 ppm 200mL) was subjected to test photocatalytic activity of CS loaded GCN catalysts under artificial solar radiation. In Fig. 46, catalysts could enhance the SCP decomposition, All CS coupled particle occurred a better activity than GCN, which could remove about 90% SCP in 3 hours. GCS-60, GCS-200 and GCS-500 could decompose all SCP within 120 min.

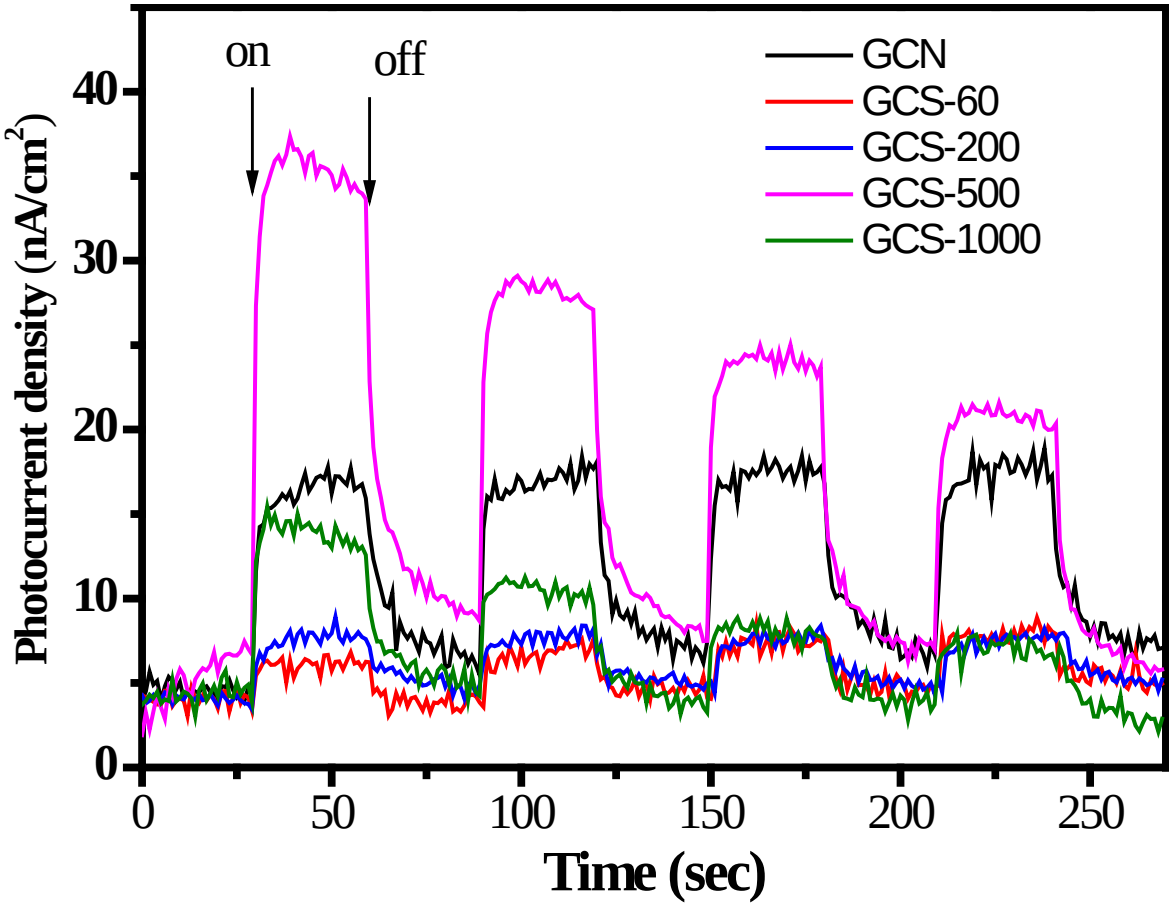

Fig. 46. Transient photocurrent curves of GCN, GCS-60, GCS-200, GCS-500 and GCS-1000 in 0.1 M $\mathbf{Na_2SO_4}$ solution.

In Fig.47 photocurrents of the CS loaded GCN was studied by photoelectrochemical experiments. GCN based samples produced a clear transient photocurrent via irradiation on–off, five cycles unbiased photocurrents were observed in all samples. GCN produced a stable density of ca. 15 nA/cm^2 photocurrent; 500 nm CS assistance enlarged photocurrent into ca. 35 nA/cm^2 while the photocurrent declined gradually in 5 cycles. Photocurrent of GCS-60, GCS-200, GCS-1000 were in a similar intensity and lower than GCN, about 8 nA/cm^2 photocurrent was generated under radiation. GCS-1000 initially had 15 nA/cm^2 photocurrent but decreased into 8 nA/cm^2 at fifth cycle. The phenomenal clearly reveals that CS accepted the photo-electron from GCN, which accelerate the splitting of electron/hole, it also confirms the result of PL-spectra, photo-electron transit led to a weak fluorescence emission in GCS.

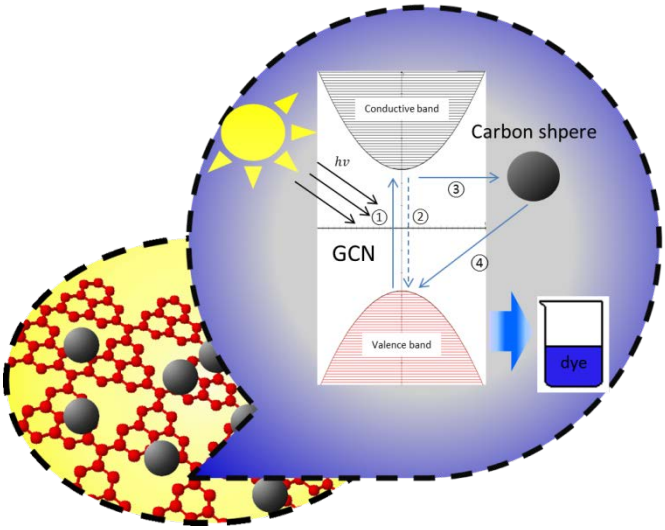

Fig. 47. Mechanism schematic of CS loaded GCN in methylene blue degradation.

In photocatalysis, two radicals, superoxide radical ($\cdot O_2^-$) and hydroxide radical ($\cdot OH$), are believed to dominate photocatalysis in an aqueous system for organic decomposition. Two radical scavengers, tert-butyl alcohol and p-benzoquinone, were then used at a level of 1 mM to quench $\cdot OH$ and $\cdot O_2^-$ radicals, respectively (Fig.52s). Addition of tert-butyl alcohol did not show any reduction to the catalytic performance while addition of p-benzoquinone effectively

reduced SCP degradation. Therefore, $\cdot O_2^-$ generation is the key for GCS photocatalysis and $\cdot$ OH will not be produced during activation of GCS by light radiation.

A mechanism based on the characterisation results and the quenching tests is thus proposed and described in Fig. 47. Carbon sphere modified GCN photocatalysts have a 2.7 eV band-gap which could absorb 475 nm visible light, resulting in the photogenerated electron/hole pairs (step I). After that, the photogenerated electrons are likely to move back to the valence band, recombining with the holes and emitting energy in thermal way (step II), which can be proved by a lower photoluminescence motion. At the same time, higher photocurrent generation indicates carbon sphere plays a role as electron tunnel, the photoelectron is easily transited in GCS particles. Thereby carbon sphere enables the electrons to depart from the surface of GCN (step III), thus reducing the possibility of charge carrier recombination. When the holes and electrons reach the surface of nanomaterials, the Mott–Schottky tests reveal GCS photocatalyst have about -1.0 V conductive band, which is higher enough to generate superoxide radical ($\cdot O_2^-$, -0.25 V) over GCN/CS hybrid particles, the $\cdot O_2^-$ could decompose MB and SCP from water, which was supported by the radical quenching experiments. The dimeter dependence of GCS samples can be explained by the electron drifting speed in CS, The PL results indicate the electron translation between GCN and CS, the 500 nm dimeter CS has best tolerant toward photoelectron, when the size of CS is smaller than it (60, 200 nm), this capability had a weak tendency, in contract 1000nm CS likely impeded electronic pair motivation for recombination. In photocurrent evaluation, GCS-500 sample show best photo-exciting sensitive, the smaller size CS could not pass electron into electrolyte system, which leaded a low photosensitive in photocatalytic reaction.

6.5 Conclusion

Uniformed carbon sphere with varying particle sizes as an electron tunnel were prepared and used for tailoring graphitic carbon nitride to be a new metal-free photocatalyst. Different size carbon spheres possess ability of electron capture, which could contribute to the separation of electron-hole pairs on the surface of GCN. The GCS-200 sample exhibits enhanced photocatalytic activity two times higher than that of the pristine GCN over MB. We envision GCN-CS could be developed to be a new class of metal-free nanomaterials in wastewater treatment, water splitting and energy storage.

6.6 Support information

Preparation of working electrodes

An ITO conductive glass (Sigma-Aldrich) with 8 ohm resistance was cut into 2×1 cm^2 dimension as a working electrode substrate. Before coating samples, the ITO surface was cleaned by ethanol, acetone and isopropanol, successively, and then dried by argon flush. One side of ITO slice (1×1 cm^2) was covered with copper wire and heat conductive and electrical insulated adhesive, and the other side was coated with catalyst particle suspensions. The suspension was obtained from 40 mg particle sample, 5 mL Nafion, and 200 mL ethanol with 2 h sonication treatment. The slurry suspension was gradually dropped on the 1 cm^2 substrate and dried at 110 ℃ for 3 h.

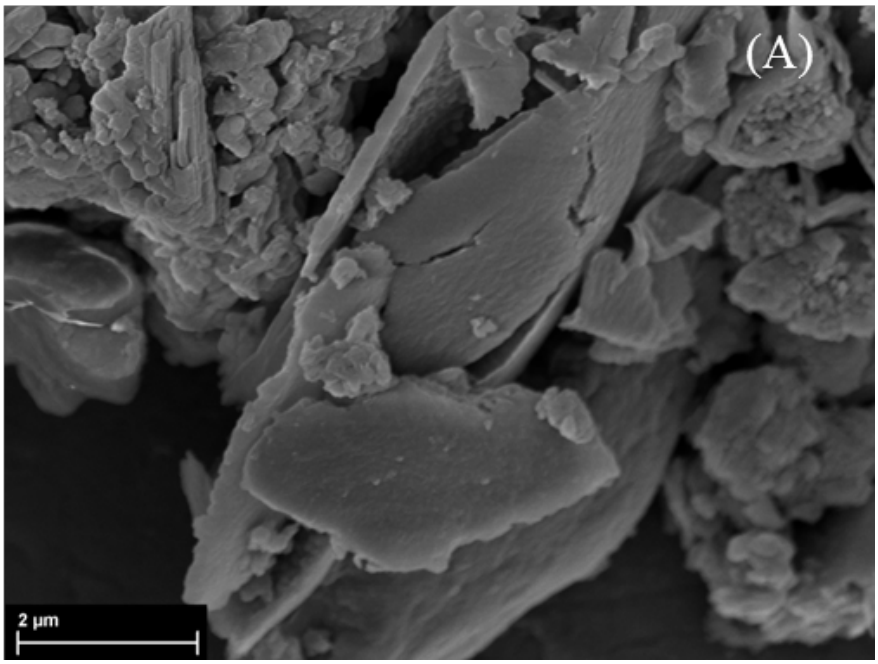

Fig. 48s. SEM image of the pure GCN sample.

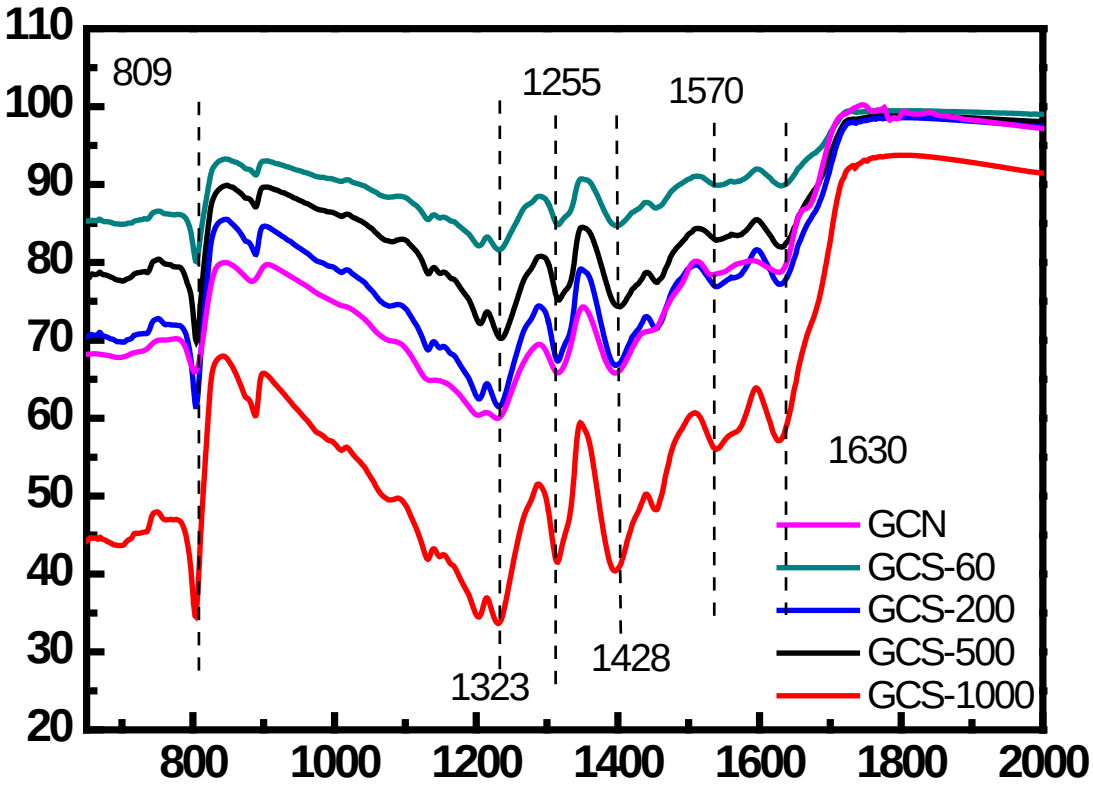

Fig. 49s. FTIR analysis of GCN, GCS-60, GCS-200, GCS-500 and GCS-1000.

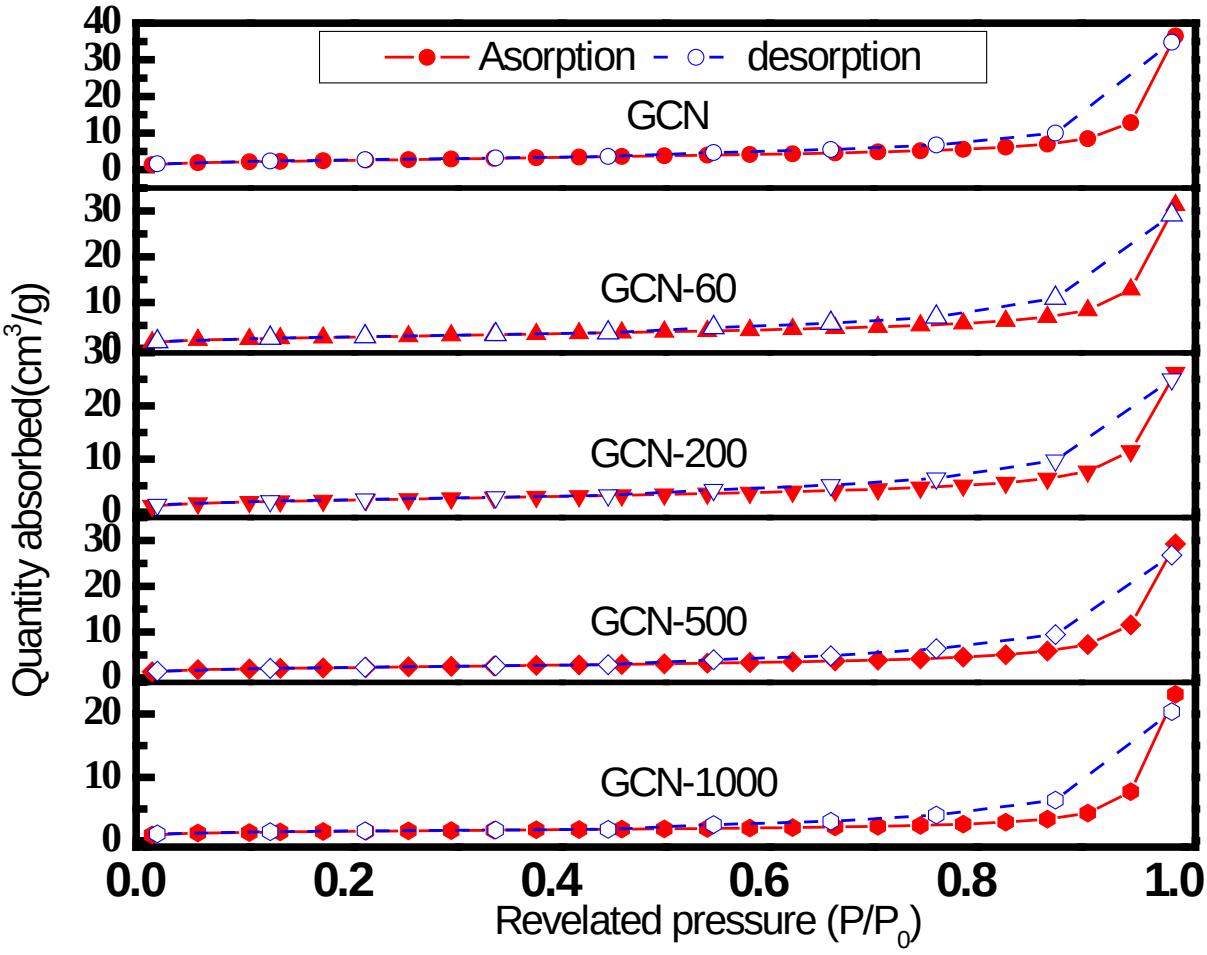

Fig. 50s. Nitrogen adsorption/desorption isotherms of GCN, GCS-60, GCS-200, GCS-500 and GCS-1000.

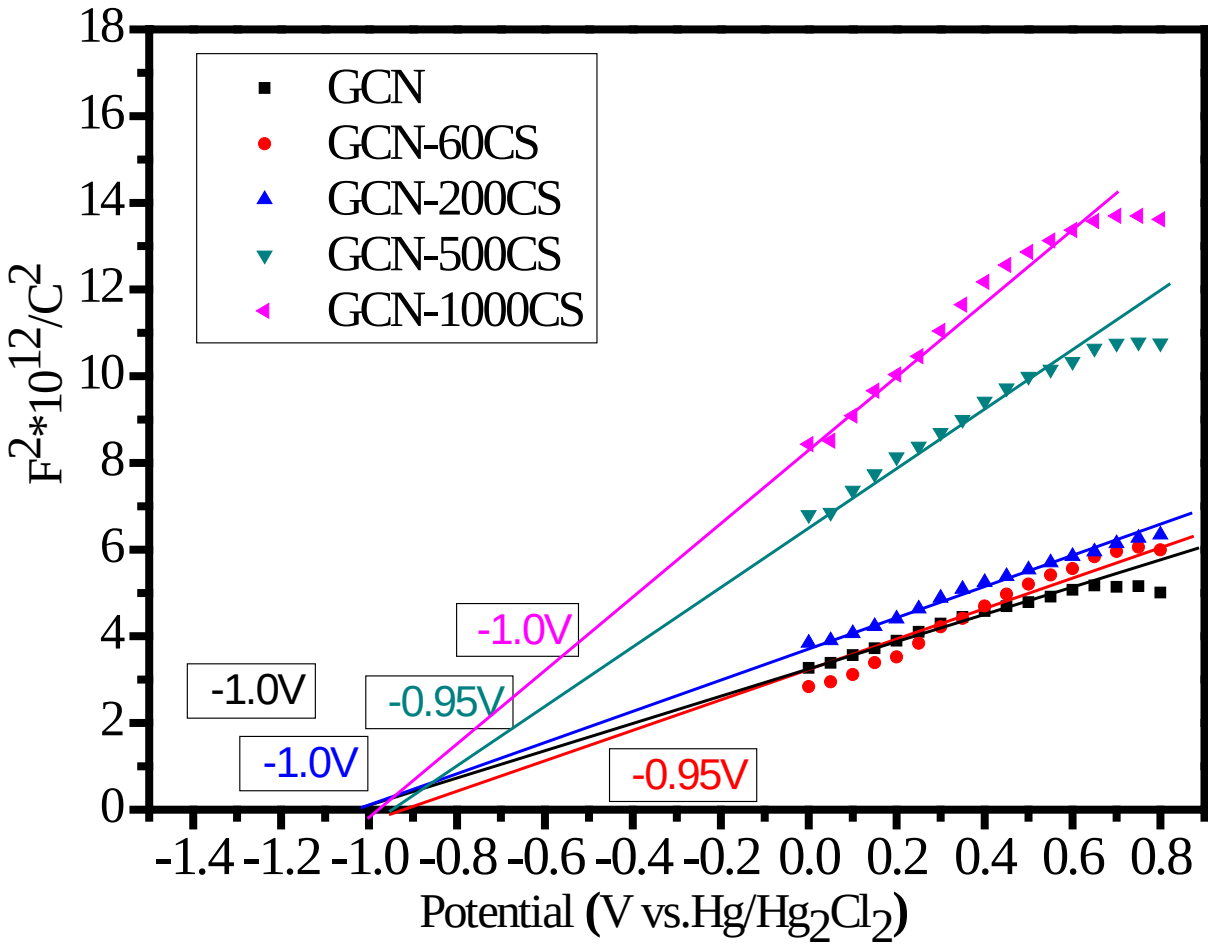

Fig. 51s. Mott–Schottky plots of GCS-60, GCS-200, GCS-500 and GCS-1000.

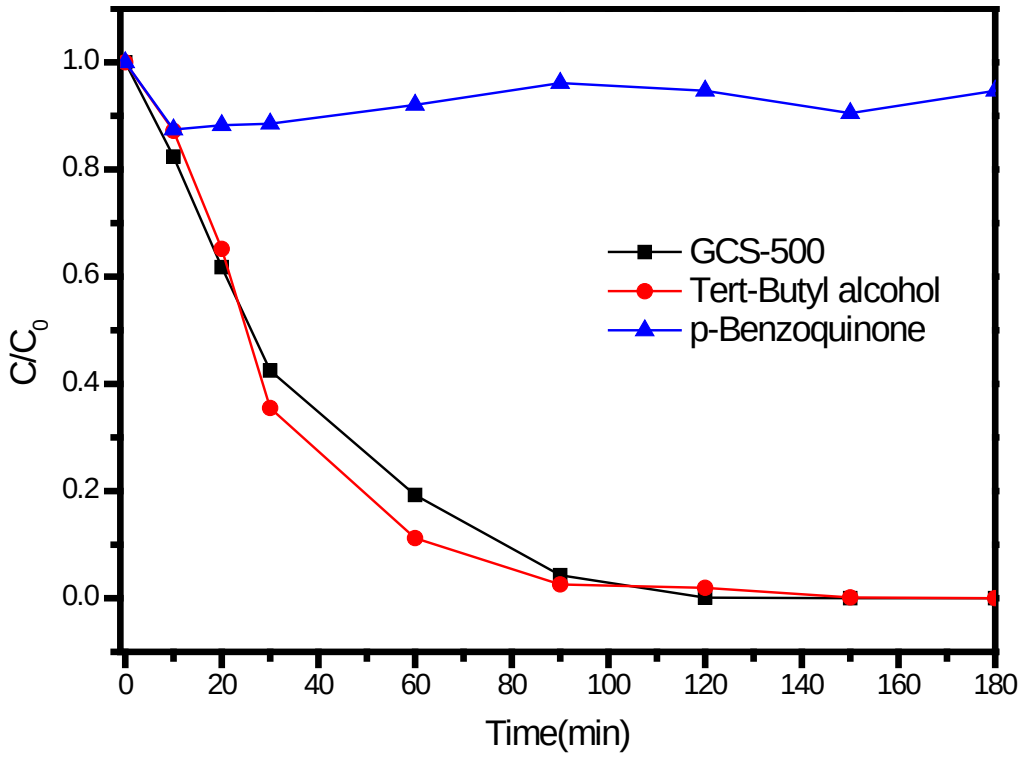

Fig. 52s. Photocatalytic activity of GCS-500 photocatalyst for SCP degradation with radical scavengers (Ter-Butyl alcohol and p-benzoquinone) under visible radiation.

6.7 References

[1] W. Obergassel, C. Arens, L. Hermwille, N. Kreibich, F. Mersmann, H.E. Ott, H. Wang-Helmreich, Phoenix from the Ashes–An Analysis of the Paris Agreement to the United Nations Framework Convention on Climate Change, Wuppertal: Wuppertal Institute. wupperinst. org/uploads/tx_wupperinst/Paris_Results. pdf (accessed February 18, 2016), (2016).

[2] A.R. Bhatti, Z. Salam, M.J.B.A. Aziz, K.P. Yee, R.H. Ashique, Electric vehicles charging using photovoltaic: Status and technological review, Renewable and Sustainable Energy Reviews, 54 (2016) 34-47.

[3] X. Wang, X. Chen, A. Thomas, X. Fu, M. Antonietti, Metal-Containing Carbon Nitride Compounds: A New Functional Organic–Metal Hybrid Material, Advanced Materials, 21 (2009) 1609-1612.

[4] X. Wang, K. Maeda, A. Thomas, K. Takanabe, G. Xin, J.M. Carlsson, K. Domen, M. Antonietti, A metal-free polymeric photocatalyst for hydrogen production from water under visible light, Nature materials, 8 (2009) 76-80.

[5] S.C. Yan, Z.S. Li, Z.G. Zou, Photodegradation Performance of g-C_3N_4 Fabricated by Directly Heating Melamine, Langmuir, 25 (2009) 10397-10401.

[6] G. Liu, P. Niu, C. Sun, S.C. Smith, Z. Chen, G.Q. Lu, H.-M. Cheng, Unique electronic structure induced high photoreactivity of sulfur-doped graphitic C_3N_4, Journal of the American Chemical Society, 132 (2010) 11642-11648.

[7] Y. Zheng, Y. Jiao, J. Chen, J. Liu, J. Liang, A. Du, W. Zhang, Z. Zhu, S.C. Smith, M. Jaroniec, Nanoporous graphitic-C_3N_4@ carbon metal-free electrocatalysts for highly efficient oxygen reduction, Journal of the American Chemical Society, 133 (2011) 20116-20119.

[8] X. Zhang, X. Xie, H. Wang, J. Zhang, B. Pan, Y. Xie, Enhanced photoresponsive ultrathin graphitic-phase C_3N_4 nanosheets for bioimaging, Journal of the American Chemical Society, 135 (2012) 18-21.

[9] A. Du, S. Sanvito, Z. Li, D. Wang, Y. Jiao, T. Liao, Q. Sun, Y.H. Ng, Z. Zhu, R. Amal, Hybrid graphene and graphitic carbon nitride nanocomposite: gap opening, electron–hole puddle, interfacial charge transfer, and enhanced visible light response, Journal of the American Chemical Society, 134 (2012) 4393-4397.

[10] A.Y. Liu, M.L. Cohen, Structural properties and electronic structure of low-compressibility materials: β-Si_3N_4 and hypothetical β-C_3N_4, Physical Review B, 41 (1990) 10727-10734.

[11] A. Thomas, A. Fischer, F. Goettmann, M. Antonietti, J.-O. Müller, R. Schlögl, J.M. Carlsson, Graphitic carbon nitride materials: variation of structure and morphology and their use as metal-free catalysts, Journal of Materials Chemistry, 18 (2008) 4893-4908.

[12] L. Ge, F. Zuo, J. Liu, Q. Ma, C. Wang, D. Sun, L. Bartels, P. Feng, Synthesis and efficient visible light photocatalytic hydrogen evolution of polymeric g-C_3N_4 coupled with CdS quantum dots, The Journal of Physical Chemistry C, 116 (2012) 13708-13714.

[13] J.-X. Sun, Y.-P. Yuan, L.-G. Qiu, X. Jiang, A.-J. Xie, Y.-H. Shen, J.-F. Zhu, Fabrication of composite photocatalyst g-C_3N_4–ZnO and enhancement of photocatalytic activity under visible light, Dalton Transactions, 41 (2012) 6756-6763.

[14] X. Wang, K. Maeda, A. Thomas, K. Takanabe, G. Xin, J.M. Carlsson, K. Domen, M. Antonietti, A metal-free polymeric photocatalyst for hydrogen production from water under visible light, Nature materials, 8 (2008) 76-80.

[15] S. Yin, J. Han, T. Zhou, R. Xu, Recent progress in g-C_3N_4 based low cost photocatalytic system: activity enhancement and emerging applications, Catalysis Science & Technology, 5 (2015) 5048-5061.

[16] Q. Xiang, J. Yu, M. Jaroniec, Preparation and Enhanced Visible-Light Photocatalytic H_2-Production Activity of Graphene/C_3N_4 Composites, The Journal of Physical Chemistry C, 115 (2011) 7355-7363.

[17] Y. Xu, H. Xu, L. Wang, J. Yan, H. Li, Y. Song, L. Huang, G. Cai, The CNT modified white C_3N_4 composite photocatalyst with enhanced visible-light response photoactivity, Dalton Transactions, 42 (2013) 7604-7613.

[18] B. Chai, X. Liao, F. Song, H. Zhou, Fullerene modified C_3N_4 composites with enhanced photocatalytic activity under visible light irradiation, Dalton Transactions, 43 (2014) 982-989.

[19] Y.H. Ng, S. Ikeda, T. Harada, S. Higashida, T. Sakata, H. Mori, M. Matsumura, Fabrication of hollow carbon nanospheres encapsulating platinum nanoparticles using a photocatalytic reaction, Advanced Materials, 19 (2007) 597-601.

[20] Y. Sun, C. Li, Y. Xu, H. Bai, Z. Yao, G. Shi, Chemically converted graphene as substrate for immobilizing and enhancing the activity of a polymeric catalyst, Chemical Communications, 46 (2010) 4740-4742.

[21] Y. Bu, Z. Chen, Effect of oxygen-doped C_3N_4 on the separation capability of the photoinduced electron-hole pairs generated by O-C_3N_4@TiO_2 with quasi-shell-core nanostructure, Electrochimica Acta, 144 (2014) 42-49.

[22] C.D. Dimitrakopoulos, D.J. Mascaro, Organic thin-film transistors: A review of recent advances, IBM Journal of Research and Development, 45 (2001) 11-27.

[23] H. Sirringhaus, Device physics of solution-processed organic field-effect transistors, Advanced Materials, 17 (2005) 2411-2425.

[24] J.E. Anthony, Functionalized acenes and heteroacenes for organic electronics, Chemical Reviews, 106 (2006) 5028-5048.

[25] L. Ming, H. Yue, L. Xu, F. Chen, Hydrothermal synthesis of oxidized g-C_3N_4 and its regulation of photocatalytic activity, Journal of Materials Chemistry A, 2 (2014) 19145-19149.

[26] S.A. Al-Muhtaseb, J.A. Ritter, Preparation and properties of resorcinol–formaldehyde organic and carbon gels, Advanced Materials, 15 (2003) 101-114.

[27] A.B. Fuertes, P. Valle-Vigon, M. Sevilla, One-step synthesis of silica@resorcinol-formaldehyde spheres and their application for the fabrication of polymer and carbon capsules, Chemical Communications, 48 (2012) 6124-6126.

[28] R. Alcántara, P. Lavela, G.F. Ortiz, J.L. Tirado, Carbon Microspheres Obtained from Resorcinol-Formaldehyde as High-Capacity Electrodes for Sodium-Ion Batteries, Electrochemical and Solid-State Letters, 8 (2005) A222-A225.

[29] T. Horikawa, J.i. Hayashi, K. Muroyama, Size control and characterization of spherical carbon aerogel particles from resorcinol–formaldehyde resin, Carbon, 42 (2004) 169-175.

[30] H. Sun, G. Zhou, Y. Wang, A. Suvorova, S. Wang, A New Metal-Free Carbon Hybrid for Enhanced Photocatalysis, ACS Applied Materials & Interfaces, 6 (2014) 16745-16754.

[31] Y. Li, S. Wu, L. Huang, J. Wang, H. Xu, H. Li, Synthesis of carbon-doped g-C_3N_4 composites with enhanced visible-light photocatalytic activity, Materials Letters, 137 (2014) 281-284.

[32] J. Liu, S.Z. Qiao, H. Liu, J. Chen, A. Orpe, D. Zhao, G.Q. Lu, Extension of The Stöber Method to the Preparation of Monodisperse Resorcinol–Formaldehyde Resin Polymer and Carbon Spheres, Angewandte Chemie International Edition, 50 (2011) 5947-5951.

[33] S. Liu, H. Sun, K. O'Donnell, H.M. Ang, M.O. Tade, S. Wang, Metal-free melem/g-C_3N_4 hybrid photocatalysts for water treatment, Journal of Colloid and Interface Science, 464 (2016) 10-17.

[34] C.-B. Cao, Q. Lv, H.-S. Zhu, Carbon nitride prepared by solvothermal method, Diamond and Related Materials, 12 (2003) 1070-1074.

[35] P.V. Zinin, L.-C. Ming, S.K. Sharma, V.N. Khabashesku, X. Liu, S. Hong, S. Endo, T. Acosta, Ultraviolet and near-infrared Raman spectroscopy of graphitic C_3N_4 phase, Chemical physics letters, 472 (2009) 69-73.

[36] T. Sano, S. Tsutsui, K. Koike, T. Hirakawa, Y. Teramoto, N. Negishi, K. Takeuchi, Activation of graphitic carbon nitride (g-C_3N_4) by alkaline hydrothermal treatment for photocatalytic NO oxidation in gas phase, Journal of Materials Chemistry A, 1 (2013) 6489-6496.

[37] R. Leary, A. Westwood, Carbonaceous nanomaterials for the enhancement of TiO_2 photocatalysis, Carbon, 49 (2011) 741-772.

[38] G. Fanchini, A. Tagliaferro, N.M.J. Conway, C. Godet, Role of lone-pair interactions and local disorder in determining the interdependency of optical constants of a-CN: H thin films, Physical Review B, 66 (2002) 195415.

[39] G. Liao, S. Chen, X. Quan, H. Yu, H. Zhao, Graphene oxide modified g-C_3N_4 hybrid with enhanced photocatalytic capability under visible light irradiation, Journal of Materials Chemistry, 22 (2012) 2721-2726.

[40] F. He, G. Chen, Y. Yu, S. Hao, Y. Zhou, Y. Zheng, Facile Approach to Synthesize g-PAN/g-C_3N_4 Composites with Enhanced Photocatalytic H_2 Evolution Activity, ACS Applied Materials & Interfaces, 6 (2014) 7171-7179.

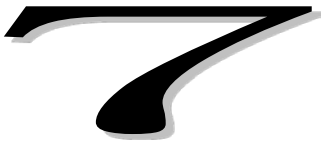

7 Research Conclusions

7.1 Concluding remarks

Graphitic carbon nitride ($g-C_3N_4$) showed a good photocatalytic performance for water remediation. The non-metal $g-C_3N_4$ particles possess very high thermal and chemical stabilities as well as interesting electronic properties, which make them as valuable materials for photocatalysis-driven applications. In summary, the graphitic carbon nitride ($g-C_3N_4$), was synthesized by thermal treatment of melamine. Four different modification technologies were adopted to enhance the photocatalytic efficiency of organic pollutants (methylene blue, phenol, sulfachloropyridazine) degradation under artificial solar radiation, 420 nm visible light, and 480 nm visible light. All modified $g-C_3N_4$ presented a better activity than pristine $g-C_3N_4$. Totally speaking, modification of $g-C_3N_4$ can enlarge absorption spectrum, increase surface area, and suppress electronic pair recombination, increase the quantity of free electron, accelerate photoelectron drifting, enhance the capacity to generate superoxide and hydroxide radicals in water, therefor $g-C_3N_4$ modification presented a better activity in organic pollutant decomposition.

7.2 Melem impregnation $g-C_3N_4$

Polymeric $g-C_3N_4$ is a single layer compound, similar to graphene. Its skeleton is based on a periodic tri-s-triazine aromatic block. During the thermal condensation toward $g-C_3N_4$ formation, the layer structure unit "Melem" is an intermediate with the unique electronic state, able to react with electrophiles to form various Melem derivatives. Melem has special band-gap structure and surface properties. Melem/ $g-C_3N_4$ heterojunction photocatalysts had been generated by hydrothermal treatment of $g-C_3N_4$ in DI water. Photocatalytic methylene blue degradation on the samples indicated MGCN-180 presented much better photocatalytic

performance comparing with other $g - C_3N_4$ catalysts under artificial solar radiation. Melem fibre was identified by XRD and SEM. Optical properties of Melem/$g - C_3N_4$ hybrids showed a synergistic effect of heterojunction. Melem in $g - C_3N_4$ catalyst support provides a new energy level to $g - C_3N_4$ for effectively weaken inset recombination by electron dislocation from $g - C_3N_4$ in to melem cocatalyst, therefore increasing photo generated electron to reaction.

7.3 Oxygen doping/grafting over $\mathbf{g - C_3N_4}$

Heterogeneous atomic doping technologies are able to manipulate multiple defects and distortion into a semiconductor system, and the dopant could become a positive or negative centre in original cloud, which would restrain the electronic motivation. Oxygen modified graphitic carbon nitride photocatalysts were prepared by hydrothermal treatment of GCN and hydrogen peroxide at controlled temperatures. The oxygen functional groups incorporated into GCN structure have induced a positive photoelectronic effect in dye degradation. UV-vis DRS and the band gap energies and band gap positions were manipulated by the oxygen functional groups. All modified GCN performed better degradation of methylene blue under visible light (wavelength more than 420 nm) and sunlight irradiations than pristine GCN. The electrochemical study reveals the multiple roles of oxygen functional groups on GCN in electrocatalysis for increased electron and hole activities. It has been believed that the oxygen-bearing groups suppress the recombination of electron-hole pairs, increase the light radiation absorption and pollutant adsorption on GCN.

7.4 Organic dye photosensitive oxygen modified $\mathbf{g - C_3N_4}$

Dye photosensitization can extend the light absorption range, enhance photon harvesting efficiency, provide extra excited electronic pairs from a dye and accelerate charge transfer,

leading to a high efficiency of photoelectric conversion. O-doping can promote dye sensitization on GCN and the dyes presented different effects on photocatalytic activity. Eosin-Y and Nile Red produced a better synergistic effects on photocatalysis. Nile-red effectively extends the light absorption and hence giving a good activity in methylene blue degradation. Eosin-Y could balance the absorption and the electron/hole pair recombination, leading to the best activity in phenol decomposition. The photocurrent studies reveal the different effects of the dyes, which are able to inject extra photoelectron into GCNO orbits and reduce the recombination.

7.5 Uniformed carbon sphere promote photocatalytic activity of $\mathbf{g-C_3N_4}$

Carbonaceous materials can enhance migration of photo-generated electron/hole, which will increase the production of active species in the redox reaction. Thereby, uniformed carbon sphere with controlled sizes were prepared and used for tailoring graphitic carbon nitride. Different size carbon spheres possess an ability of electron capture, which could contribute to the separation of electron-hole pairs on the surface of $g-C_3N_4$. The sample with 200 nm diameter carbon sphere exhibits enhanced photocatalytic activity two times higher than that of the pristine GCN for MB degradation.

7.6 Recommendation for future work

This study focused on graphitic carbon nitride modification and we wanted to find a new way to produce economic, environmentally friendly and non-metal photosensitive semiconductors. All the catalysts were tested for aromatic organic water pollutant treatment with UV/Visible illumination, showing good activities. However, a detailed study is further required to

comprehensively investigate the mechanism of photocatalytic efficiency and the role of doping and its electronic property on photocatalysis.

As reported, graphitic carbon nitride possesses a high thermal conductivity (~5000 $W\ m^{-1}K^{-1}$), assuring an excellent mobility of charge carriers (200,000 $cm^2\ V^{-1}\ s^{-1}$), and possessing an extremely high specific surface area (~2600 m^2/g). However in our work, $g - C_3N_4$ has limited light absorption in optical properties, the photolumination properties indicated a strong electronic pair quenching reaction. The most important photocurrent studies reflect a low electron drifting rate in $g - C_3N_4$ molecular skeleton, because of the blurry crystal phases of $g - C_3N_4$, the semiconductor structure of this material is unclear, the electronic carriers are easily contacted in the defect. Thus it is suggested that more investigations focusing on mechanism of generation and combination of electron-hole pairs.

In the future, we will try to find ways to synthesise prefect crystal $\mathrm{g-C_3N_4}$ in a mild environment. More methods to modify $\mathrm{g-C_3N_4}$ are expected to extend the light absorption property. How to induce additional free photo-electron into $\mathrm{g-C_3N_4}$ is a big challenge. To reduce the dimension of $\mathrm{g-C_3N_4}$ and increasing the electron exposing is helpful in increasing photocatalysis efficiency. Finally, how to adjust the energy level of $\mathrm{g-C_3N_4}$ for its compatibility in different reactions will be considered in our future study.

More importantly, industrial application for photocatalytic degradation of water contaminants should be carried out based on laboratory tests.